Space Sciences Laboratory
University of California
Berkeley, California 94720

MARS: VISIBLE AND NEAR INFRARED STUDIES AND THE COMPOSITION OF THE SURFACE

by

Brian T. O'Leary

Technical Report on
NASA Grant NsG 101-61

Space Sciences Laboratory
Series 8, Issue 103

Submitted in partial satisfaction
of the requirements for the degree of

DOCTOR OF PHILOSOPHY

Department of Astronomy
University of California, Berkeley

November 8, 1967

CONTENTS

MARS: VISIBLE AND NEAR-INFRARED STUDIES AND THE COMPOSITION OF THE SURFACE

ABSTRACT

An extensive analysis of polarimetric, photometric, and spectrophotometric measurements of Mars is performed.

First, Dollfus and Focas' polarimetric observations are discussed. It is concluded that because of the uncertainty in the atmospheric brightness and polarization contributions to the observed brightness and polarization of Mars, the range of possible polarizations of the Martian bright areas at a given phase angle and wavelength would encompass the polarizations of many powdered substances measured in the laboratory: e.g., limonites, desert sand, augite, red sandstone, and volcanic ashes. Even if the atmospheric component has been assessed correctly, there is still not the close match in polarization between the Martian surface and various forms of yellow ochre limonite as previously claimed. Many other substances fit the assumed polarization properties of the Martian surface just as well.

In the second chapter, photometric observations of Mars in six colors is described. The interesting feature of these observations is that they encompass very small phase angles attained during the 1967 apparition: a minimum phase angle of 1°.2 was reached. This enabled me to obtain phase curves of Mars to measure its opposition effect, i.e., a non-linear surge in brightness as the planet approaches zero phase. The results were successful, indicating a moderate opposition effect for Mars, but much less pronounced than the lunar opposition effect. Because

of the Martian opposition effect, various parameters of the planet had to be revised: the mean opposition magnitude, the geometric albedo, and the phase integral. Previously, these parameters have been derived from linear extrapolation of the observed linear phase function for phase angles greater than about 10°. The extent of the Martian opposition effect varies inversely with wavelength. A peculiar steepness was observed in the Martian phase function near a phase angle of 6° in the blue and ultraviolet filters. Aerosols in the Martian atmosphere are suggested as the cause of this anomaly. A report of the results of these observations is published in the Astrophysical Journal Letters to the Editor, September 1967.

In the third chapter, opposition effects and phase functions of various sample substances of interest for the Martian surface were measured with a reflectometer-polarimeter designed and constructed as part of this thesis. Also, visible and near infrared spectrophotometry was performed on these same substances. It is concluded that, although the limonite, goethite, and hematite samples match the Martian opposition effects reasonably well, the lack of the 0.87-μ iron oxide band in the Martian spectrum makes it very difficult to explain any of these samples as the predominant surface substance on Mars. In addition, the limb darkening of all these samples is much less than that observed on Mars; this appears to be another strong argument against the widespread presence of these iron oxides on the Martian surface. The probable thermodynamic instability of goethite under conditions at the Martian surface offers an additional argument.

On the other hand, siderite and/or other carbonates remain as interesting candidates. The case of siderite is intriguing in view of a

broad feature at 1.05 μ found both in laboratory spectra of siderite and reported in a spectrum of Mars obtained by Tull. Although this feature is much weaker on Mars than for the siderite samples, a small fractional concentration of siderite on the Martian surface is suggested. There is the additional 3.45-μ band, marginally found in the Martian spectrum by Sinton, which could be due to siderite or some other carbonate.

It is generally concluded that all samples so far investigated might be present on Mars in small quantities but cannot be the predominant covering for the Martian surface. An emphatic warning is given to those who continue to assert limonite is the major constituent of the Martian surface. The question about the composition of the Martian surface is very much an open one. It is suggested that infrared spectrophotometry from space is the best remote-sensing device to find answers, but until a laboratory is landed on the planet, definitive answers will probably not be found.

CHAPTER I. INTRODUCTION

1.1 Scope of the Problem

The aim of this thesis is to present new observational and experimental data along with an analysis of existing data to clarify our thinking about the composition of the Martian surface. The work deals with two fundamental optical parameters: reflectivity and polarization. The physical meaning of these parameters and the importance of their dependence on other parameters will be described mathematically in Section 1.2. The two most significant relations which emerge from this research are: (1) polarization-vs.-phase angle at all angles, and (2) reflectivity-vs.-phase near opposition where the shape and extent of the brightness surge when Mars approaches very small phase angles provides a further description of the surface material. As this second relation has yet to be exploited, it will be given special attention herein.

Conversely, the polarization-vs.-phase angle relation (hereafter called $P(\alpha)$), has been explored extensively since Dollfus (1955) first interpreted the data as being indicative of finely pulverized limonite covering the Martian bright areas. This identification was based upon a similarity between $P(\alpha)$ observed for the bright areas and corrected for an 85 mb atmosphere and $P(\alpha)$ of a laboratory sample of powdered yellow-ochre limonite (Fig. 1). Such an association did not occur with any other substance he investigated in the laboratory.

What has followed in the literature has been a barrage of papers either questioning or reinforcing the limonite hypothesis. Rather than going into a detailed review of the literature--since this has been done recently by Wells (1967), Egan and Foreman (1967), Younkin (1966), Rea (1966), and Cann *et al.* (1965)--I shall review only briefly in

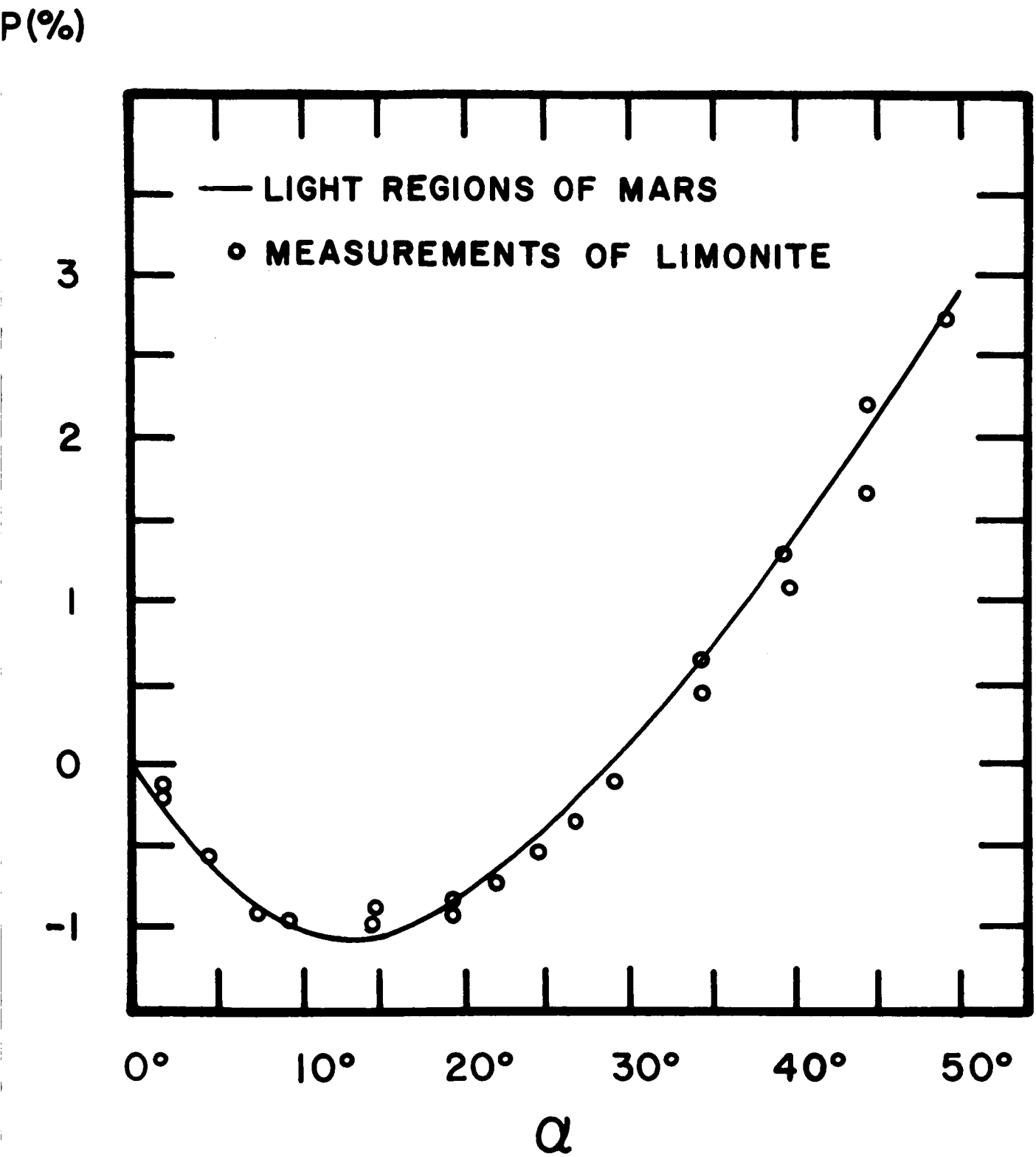

Fig. 1. Polarization versus phase angle of powdered limonite and of the bright regions of Mars corrected for an atmosphere of dry air with a surface pressure of 85 mb (after Dollfus 1955, 1961).

Section 1.3 the most important contributions to the field since Dollfus' pioneering work. However, considerable effort is devoted to critically evaluating previous interpretations. In the concluding chapter, some of these works are reviewed in the context of my results, to be described in the next two chapters.

1.2 Definitions and Physical Bases

The electromagnetic properties of sunlight reflected from a planet can be described by the four Stokes parameters. Chandrasekhar (1950) has thoroughly discussed the theory of the parameters. Coulson, Bouricius, and Gray (1964) have given a useful summary of the parameters and their application to reflection measurements of natural materials.

Two of these parameters may be defined as I_{max} and I_{min}, the intensities in the directions of electric vector maximum and minimum of the electromagnetic vibration. The total intensity, $\underline{I}$, and the degree of polarization, P, are defined as

$$\underline{I} = I_{max} + I_{min} \tag{1.2.1}$$

$$P = \frac{I_{max} - I_{min}}{I_{max} + I_{min}} \tag{1.2.2}$$

A third Stokes parameter describes the extent of elliptic polarization. This has been neglected in previous analyses of light reflected from planets. Since its effect is expected to be very small, and there are few data available on elliptic polarization of natural surfaces (Coulson et al. 1964), I have also neglected this parameter. Furthermore, elliptic polarization of Mars has not yet been measured.

The fourth parameter, χ, can be described as the angle between the plane of polarization (i.e., the plane containing the direction of propagation of the radiation and the direction of I_{max}) and the normal to the plane of vision (i.e., the plane containing the source, reflecting surface, and observer). By convention (Lyot 1929) if $\chi = 0°$, the polarization is considered as positive and if $\chi = 90°$, the polarization is considered as negative.

There are conflicting observations as to whether χ assumes values other than 0° or 90° for natural surfaces. Kohan (1962) and Clarke (1965) have noted a rotation of the plane of polarization, i.e., a steady variation of χ between 0° and 90°, of light reflected from the Moon at small phase angles. In the same paper Clarke has reported similar behavior for Mars, although his error scatter is large. A'hearn (1966) has also reported this effect for Venus. On the other hand, Lyot (1929) and Dollfus (1955, 1961), have observed no such rotation for any planet or satellite, i.e., $\chi = 0°$ or 90° only. Likewise, Coulson *et al.* (1964) have noted no rotation in their laboratory studies. This troublesome conflict is most probably due to instrumental error on the part of one or the other set of observers. Unfortunately, it cannot be resolved until further observations are made. I shall not go into the problem in this work, since such observations are not available to me.

The measurable optical parameters to be considered are thus *I*, P, and χ. In order that these parameters be indicative of the surface under investigation, it is first necessary to consider the optical properties of the incident light: sunlight incident on a planet is essentially unpolarized, so the measured values of P and χ depend on properties of the planet's surface and atmosphere. However, in the laboratory any

residual polarization in the incident light must be calibrated out of the measurements.

Secondly, it is necessary to relate the measured flux to that of a standard surface. For parallel light incident on a surface element dA at angle θ_0 from the surface normal, and reflected at nadir and azimuth angle of observation, θ and ϕ, respectively, into solid angle $d\omega$, the measured flux is

$$\text{Flux} = I_0 \rho(\theta_0, \theta, \phi) \cos \theta_0 \cos \theta \, dA \, d\omega \qquad (1.2.3)$$

where I_0 is the incident intensity and $\rho(\theta_0, \theta, \phi)$ is the directional reflectivity. A Lambert surface is defined as the perfect diffuser, i.e., ρ is independent of θ_0, θ, and ϕ. The most convenient reference surface is a non-absorbing Lambert surface (i.e., albedo of unity) of the same size and at the same distance from the source as the surface to be measured. In the case of a planet the quantity ρ can be calculated from the planet's brightness, the knowledge of the solar brightness and size of the planet. In the laboratory the intensity of a standard surface such as heavily smoked magnesium oxide (MgO) is measured as a reference to calculate ρ for a surface sample. Details of these calibrations will be discussed in Chapters II and III.

The values for ρ, P, and χ are measured with respect to the angles θ_0, θ, and ϕ. The geometry of these three angles is shown in the planetary and laboratory cases in Fig. 2. In the former, the planetary disk is shown with a spherical triangle drawn to illustrate the values of θ_0, θ, and ϕ for the point P, on the planet, where S is the sub-solar point and E the sub-earth point. The three angles are similarly depicted in the laboratory case in Fig. 2, from which the correspondences between light

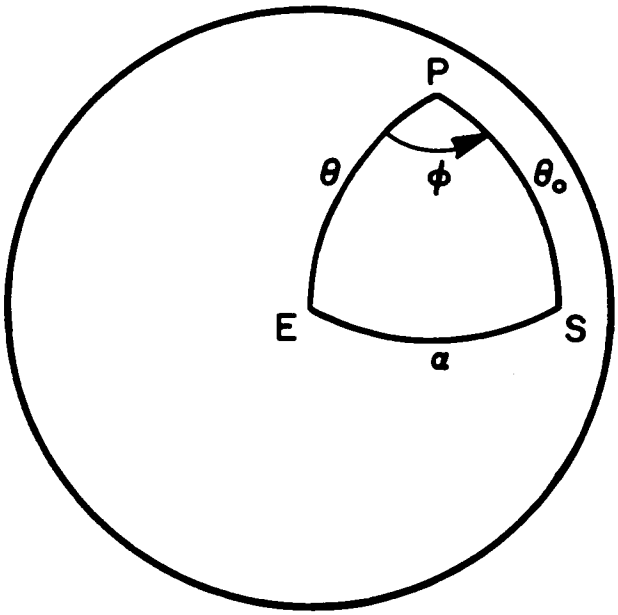

PLANET

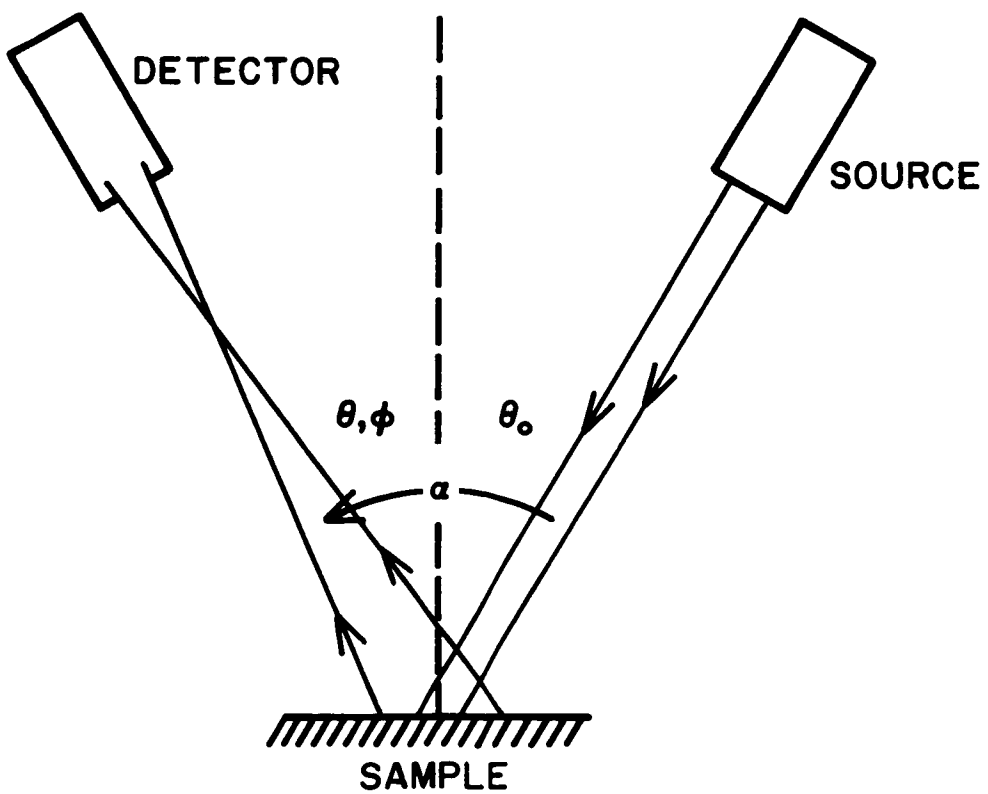

LABORATORY

Fig. 2. The geometry of light reflected from a point, P, on a planet and from sample in the laboratory.

source - Sun, sample - point P on the planet, and detector - Earth can be easily deduced.

Also shown in Fig. 2 is the phase angle, α, whose value from spherical trigonometry is

$$\alpha = \cos^{-1} (\cos \theta \cos \theta_0 + \sin \theta \sin \theta_0 \cos \phi) \qquad (1.2.4)$$

In other words, α is that angle formed at the planet (or sample) between the source of illumination and the observer. Observational experience has shown α to be a very important parameter in studying the optical properties of a planet (e.g., see Dollfus 1955, 1961; de Voucouleurs 1964). This is especially true in the case of $P(\alpha)$ for all α and $\rho(\alpha)$ for small α, relations which are sensitive to the composition, particle size and shape of a sample surface or atmosphere. There is the possibility of the additional parameters of roughness and packing density of the surface.

There is finally an important dependence of the optical parameters on the wavelength, λ, of observation. This fact is obvious from observational and laboratory experience. Thus, we can establish the most significant relations to be $\rho(\alpha, \lambda)$, $P(\alpha, \lambda)$ and $\chi(\alpha, \lambda)$. Although it is true that there are weaker dependences on other parameters, the vast majority of the work herein reported is an empirical and interpretational study of only $\rho(\alpha, \lambda)$, $P(\alpha, \lambda)$, and $\chi(\alpha, \lambda)$.

1.3 Polarization and Limonite: Previous Work and Motivation

Laboratory studies (Dollfus 1955, 1961; Coulson *et al.* 1964, 1965; Wright *et al.* 1963; Egan and Foreman 1967) have shown that the $P(\alpha, \lambda)$ relation is very sensitive to composition and particle size. A third variable, packing density, should also be considered.

The compositional variable must unfortunately be divided into a number of sub-variables in the case of natural mineral samples. A prime example of this problem is limonite, the substance whose match in $P(\alpha)$ with the observed Martian $P(\alpha)$ at $\lambda = 0.61$ (cf. Fig. 1) was reported by Dollfus (1955) in the following manner: "...hydrated samples of goethite, $Fe_2O_3 \cdot H_2O$, as yellow, or yellow ochre powder, and especially limonite, $Fe_2O_3 \cdot 3H_2O$, yellowish-brown with an albedo of 0.20 reproduce the Martian polarization in all its details." However, no mineralogical details were presented, e.g., the relative abundances of iron oxide minerals and other minerals present in his sample, manner of preparation, and packing density. Coulson et al. (1964, 1965) and Egan and Foreman (1967) investigated $P(\alpha)$ for some other samples of limonite, but they, too, did not completely characterize their composition (although they did consider particle sizes).

A more thorough attempt to characterize samples was made by Dollfus and Focas (1966). Although they claimed to have found a good fit in $P(\alpha)$ for a limonite-goethite sample they called D_0, there were objections to D_0 as the composition of the bright areas: the lack of a match in spectral variation of reflectivity and geological arguments. However, they were able to reproduce the Martian $P(\alpha)$ with D_0 combined in a mosaic with a sample prepared by Adamcik, consisting of "grains of silica and kaolin coated by a superficial deposit of limonite." Dollfus and Focas (1966) concluded, "The surface of the soil of the ochre coloured desertic bright areas of Mars is similar to a mixture of fine grains of any size, wrapping (sic) each other and forming a sufficiently aerated deposit of a low roughness. The grains consist of limonite, or a pulverized absorbent (sic) and opaque material with the surface of the grains coated by a deposit

of hydrated iron oxide of the 'limonite' type."

Dollfus and Focas' arguments for making the identification of a limonite mixture on the Martian bright areas are: (1) the crossover point in $P(\alpha)$ from negative to positive values of P--hereafter called the "inversion point"--is at very large α, and (2) $P(\alpha)$ in the negative branch is independent of λ.

There are still many difficulties in this identification, the most fundamental one being, can one definitely say a certain material must be present in great quantities on the Martian bright areas from the relationship $P(\alpha, \lambda)$, when not all of an infinitely possible number of materials have been tested in the laboratory? Furthermore, between what limits is $P(\alpha, \lambda)$ for the Martian bright areas known and do other materials besides limonite fall into these limits? In what way does the Martian atmosphere affect the observed $P(\alpha, \lambda)$? Finally, what other types of observations and geological arguments can be made to test the limonite hypothesis? We shall address ourselves to these fundamental questions throughout this work, and operate under the assumption that the positive identification of limonite covering the Martian bright areas is premature.

Before going into the empirical work of the next two chapters, it is useful to answer the questions raised above from information provided in the recent literature.

We first look at the question about the effect of the Martian atmosphere on $P(\alpha, \lambda)$. This question has been discussed extensively, yet a satisfactory answer has not been found. The most important results are as follows.

Using four different methods based on polarization and brightness measures of Mars, Dollfus (1955, 1961) derived for λ 0.61 μ a ratio of

the atmospheric to the surface brightness, $B_a/B_s = 0.028$, for the bright areas at the center of the Martian disk at zero phase. (Here I am using B as the brightness, i.e., I/cos θ.) Applying the expression for Rayleigh scattering, and assuming that the scattering properties of the atmospheric gases of Mars and Earth are similar, he arrived at a surface pressure of 90 mb.

Rea and O'Leary (1965) suggested the presence of aerosols in the Martian atmosphere to explain the discrepancy between Dollfus' 90 mb and the more recent spectrographic determination by Kaplan, Munch, and Spinrad (1964) of 25 mb. They adopted Kuiper's (1964) suggestion of submicron spherical ice particles for the aerosols, and computed the polarization of reflected light from several sample mixtures. Using the formula

$$P_{OBS}(\alpha, \lambda) = \frac{P_s B_s + P_m B_m + P_p B_p}{B_s + B_m + B_p}(\alpha, \lambda)$$

where subscripts s, m, and p refer to surface, atmospheric molecules, and atmospheric particles (aerosols), respectively, Rea and O'Leary computed $P_s(\alpha)$ at λ 0.61 μ, finding polarization curves quite different from that of limonite. In particular, the inversion points were less than that for Dollfus' limonite, thus presenting many other candidates for Martian surface material.

Meanwhile, the Dollfus' determination of B_a/B_s was re-analyzed by Cann et al. (1965) and Chamberlain and Hunten (1965), who found the results to be in considerable question. Cann et al. derived $B_a/B_s = 0.01^{+0.010}_{-0.007}$ s.e. at 0.61 μ, but recommended caution in the use of these figures. This point cannot be disputed in view of the fact that there are many possible sources for Martian brightness and polarization other

than surface-reflected radiation and Rayleigh backscattering by atmospheric molecules: there is also Rayleigh backscattering by small aerosols, Mie backscattering by aerosols whose sizes approximately equal a wavelength of light, the forward Mie and Rayleigh scattering by the atmosphere radiation reflected from the Martian surface, and multiply-scattered radiation. There is also the possibility of atmospheric absorption.

Since the Martian surface albedos are generally low, the atmosphere is tenuous, and no reasonable source of absorption has been postulated or unambiguously detected, it is expected that all these additional components are small except for Rayleigh and Mie backscattering by aerosols. This aerosol question has occupied much attention in the literature.

In a recent, more elaborate study, Dollfus and Focas (1966) have analyzed 5,200 polarimetric data points obtained over the past 18 years. They were careful to select only those points in which the Martian atmosphere was particularly transparent. They have concluded that $B_a/B_s = 0.01$ at λ 0.61 μ, and deduce from this value a surface pressure of 30 mb, if the scattering properties are the same as molecules in dry air.

The modern value of the Martian surface pressure is in the range of ~ 4 to 9 mb from the Mariner IV occultation experiment (Kliore et al. 1965) and recent spectroscopic determinations (Gray 1966; Schorn and Gray 1967; Owen 1967), with a nearly pure CO_2 atmosphere. Since the scattering power of dry air is 0.8 times that of CO_2, a pure CO_2 atmosphere would give 24 mb from the polarimetric results. The discrepancy between the determinations might be still large enough to resort to the aerosol interpretation, just as Rea and O'Leary (1965) had done in the situation of 85 mb versus 25 mb.

There is other evidence that B_a is not entirely due to molecules: Evans' (1965) ultraviolet rocket spectra indicate a pressure of 12 ± 5 mb, where the Martian atmospheric reflectivity follows a λ^{-4} law from 0.24 to 0.35 μ. Furthermore, a high layer of haze is suspected to appear on some of the Mariner IV photographs.

From the above discussion it is probable that aerosols contribute appreciably to scattering in the Martian atmosphere, although this statement is not unequivocal. But the evidence for aerosols is strong enough to devote considerable effort in attempting a more detailed description than heretofore possible.

As to whether these postulated aerosols are Rayleigh or Mie scatterers is also a perplexing question. It should be emphasized that this is an important question: in the case of Mie aerosols, the Rea and O'Leary (1965) analysis of non-uniqueness of $P_s(\alpha)$ would apply, whereas in the case of Rayleigh aerosols, a unique $P_s(\alpha)$ can be derived (at least to the accuracy to which B_a/B_s is known--since B_a/B_s is presumed to be very small for $\lambda > 0.61$ μ, $P_s(\alpha)$ should be well known at these wavelengths in the case of Rayleigh scattering).

If we accept the value $B_a/B_s = 0.01$ (Dollfus and Focas 1966) at λ 0.61 μ, the non-molecular component, B_p, to the total atmospheric brightness, B_a, immediately follows from the discrepancy between the recent value of the Martian surface pressure (~ 6 mb pure CO_2) and the polarimetric surface pressure (~ 24 mb pure CO_2): $B_p/B_s = 0.007$ at 0.61 μ and 0.05 at 0.47 μ.

In their analysis Dollfus and Focas assume that B_p is caused by Rayleigh scattering aerosols alone, and in their determination of B_a/B_s they use the Rayleigh phase functions of both polarization and brightness.

They then justify this assumption by showing that the change in B_a from λ 0.61 to 0.47 μ follows closely the Rayleigh λ^{-4} law. However, as we shall see in Sec. 2.4, Mie scatterers of ice with mean particle radii $\bar{r} \sim 0.3\ \mu$ follow the λ^{-4} law in the visible, even though $P(\alpha)$ and $B(\alpha)$ are very different from the Rayleigh case. Cann et al. (1965) have shown that $P(\alpha)$ in the visible deviates from the Rayleigh case for ice particles with $\bar{r} > 0.2\ \mu$.

Furthermore, there are certain observations which suggest Mie scattering is playing a significant role in the Martian atmosphere. The results of my measurements of the Martian phase function near opposition to be described in Chapter II suggest $\bar{r} \sim 0.3\ \mu$ for ice. Kuiper's (1964) analyses of the unusual ultraviolet polarizations of Mars observed by Gehrels and Teska (1962) and of the photometric and polarimetric properties of the Martian blue haze suggest the presence of submicron aerosols. Rea and O'Leary (1965) proposed that the strong polarization component of submicron aerosols, combined with an albedo difference between the Martian dark areas during and not during passage of the darkening wave, can explain the observed polarization differences between the two areas (i.e., there is no need to hypothesize different intrinsic polarizations between the dark areas before and during the darkening wave). From these investigations, $\bar{r} \sim 0.2$ to $0.5\ \mu$.

To summarize what has been discussed so far, there appears to be a strong case for the presence of submicron aerosols in the Martian atmosphere. It is possible that these aerosols obey the Rayleigh law in $P(\alpha)$ and $B(\alpha)$ in the visible, as suggested by Dollfus and Focas (1966), but their justification for asserting this is very weak. On the contrary there is more evidence for Mie-scattering aerosols ($\bar{r} \sim 0.2$ to $0.5\ \mu$)

in which case it is possible for $P_s(\alpha)$ to be altered. However, the alteration in $P_s(\alpha)$ would probably not be as great as those alterations predicted by Rea and O'Leary (1965), since $B_p/B_s \sim 0.007$ at 0.61 μ from the recent Dollfus and Focas analysis, rather than the older value of $B_p/B_s \sim 0.020$ used by Rea and O'Leary. The end result from Rea and O'Leary's particle mixtures (see their Fig. 2) is for the inversion point to be 1° to 2° less, the negative branch to be 0.0 to 0.1% less, and $P_s(\alpha = 40°)$ to be up to ± 0.2% different from those values derivable from a 30 mb Rayleigh atmosphere.

The situation might not be as simple as that described in the above paragraph. In spite of these small alterations in $P_s(\alpha)$, there are still doubts about the value of B_a/B_s itself, even beyond the error limits discussed by Cann et al. (1964). These doubts arise from assumptions made in Dollfus and Focas' derivation of B_a/B_s.

A general form of their derivation is as follows: For a given value of α the brightness distribution of the Martian atmosphere from center to limb is:

$$B_a(\alpha, \theta) = \frac{B_a(\alpha, 0)}{\cos \theta} \qquad (1.3.1)$$

where the first quantity in parentheses represents the value of α and the second quantity the value of θ, the inclination of the Martian surface along the equator to the direction of the Earth.

The polarization of the soil and atmosphere are combined to give

$$P(\alpha, \theta) = P_s(\alpha, \theta) + \frac{B_a(\alpha, \theta)}{B_s(\alpha, \theta)} P_a(\alpha)$$

$$= P_s(\alpha, \theta) + \frac{B_a(\alpha)}{B_s(\alpha, \theta) \cos \theta} P_a(\alpha) \qquad (1.3.2)$$

The differences between the measures taken at the limb and the center of the disk gives:

$$P(\alpha, \theta) - P(\alpha, 0) = P_s(\alpha, \theta) + \frac{B_a(\alpha)}{B_s(\alpha, \theta) \cos \theta} P_a(\alpha)$$

$$- P_s(\alpha, 0) - \frac{B_a(\alpha)}{B_s(\alpha, 0)} P_a(\alpha) \qquad (1.3.3)$$

Then

$$P(\alpha, \theta) - P(\alpha, 0) - P_s(\alpha, \theta) + P_s(\alpha, 0)$$

$$= B_a(\alpha)P_a(\alpha)\left[\frac{1}{B_s(\alpha, \theta) \cos \theta} - \frac{1}{B_s(\alpha, 0)}\right]$$

$$= \frac{B_a(\alpha)P_a(\alpha)}{B_s(0, 0)} \left[\frac{B_s(0, 0)}{B_s(\alpha, \theta) \cos \theta} - \frac{B_s(0, 0)}{B_s(\alpha, 0)}\right]$$

(1.3.4)

If we assume that

$$P_s(\alpha, \theta) = P_s(\alpha, 0) + P_s(0, \theta) \qquad (1.3.5)$$

and

$$P_s(0, 0) = 0 \quad , \qquad (1.3.6)$$

then the left-hand side of Eq. (1.3.4)

$$P(\alpha, \theta) - P(\alpha, 0) - [P_s(\alpha, 0) + P_s(0, \theta)] + [P_s(\alpha, 0) + P_s(0, 0)]$$

$$= P(\alpha, \theta) - P(\alpha, 0) - P_s(0, \theta) \quad .$$

(1.3.7)

The final expression is thus

$$P(\alpha, \theta) - P(\alpha, 0) - P_s(0, \theta)$$

$$= \frac{B_a(0, 0)}{B_s(0, 0)} \frac{B_a(\alpha)P_a(\alpha)}{B_a(0)} \left[\frac{B_s(0, 0)}{B_s(\alpha, \theta)} \frac{1}{\cos \theta} - \frac{B_s(0, 0)}{B_s(\alpha, 0)}\right] . \tag{1.3.8}$$

In equation (1.3.8) we define

$$X = \frac{B_a(\alpha)P_a(\alpha)s}{B_a(0)} \tag{1.3.9}$$

where

$$s = \left[\frac{B_s(0, 0)}{B_s(\alpha, 0)} \frac{1}{\cos \theta} - \frac{B_s(0, 0)}{B_s(\alpha, 0)}\right] \tag{1.3.10}$$

and

$$Y = P(\alpha, \theta) - P(\alpha, 0) - P_s(0, \theta) \tag{1.3.11}$$

Dropping subscripts, where B_a/B_s equals $B_a(0, 0)/B_s(0, 0)$, we have

$$Y = \frac{B_a}{B_s} X \tag{1.3.12}$$

Implicit in their derivation is the assumption that $P_s(\theta)$ is known and is independent of α [equation (1.3.5)]. Fig. 3 shows the $P_s(\theta)$ dependence they used. This dependence was deduced from "measurements carried out in the laboratory on samples having the same properties (as) the soil of Mars." However, if we take the laboratory data of Coulson et al. (1965) shown in Table I, we see that $P_s(\theta)$ is different from the Dollfus and Focas sample and that $P_s(\theta)$ is not independent of α. The most important fact is that if the Coulson et al. values of $P_s(\theta)$ were

TABLE I

Limb-to-center variation in polarization of laboratory samples of limonite.

	$\frac{\alpha = 53°}{P_s(\theta=53°)-P_s(\theta=0°)}$	$\frac{\alpha = 10°}{P_s(\theta=43°)-P_s(\theta=0°)}$
Coulson et al. (1964):		
λ 0.64 μ:		
Coarse limonite	+0.2%	-0.3%
Fine limonite	-0.2	-0.6
λ 0.49 μ:		
Coarse limonite	+0.6	+0.6
Fine limonite	-0.8	+0.2
Dollfus and Focas (1966):		
λ 0.61 μ:		
Fine limonite	---	~ -0.1

used, then the resulting values of Y in Fig. 1 would change enormously (in some cases by a factor of more than 5) resulting in a correspondingly large change in B_a/B_s, since X depends upon $\sin^2 \alpha$. Although Dollfus and Focas found the $P_s(\theta)$ dependence shown in Fig. 4 to be independent of α for their limonite sample, the laboratory data of Coulson et al. show that such a dependence is not unique for all limonites, and certainly cannot be relied upon to derive a value of B_a/B_s. Furthermore laboratory data on opaque emery powder, sand, glass, etc., presented by Dollfus (1961) show $P_s(\theta)$ to vary considerably with α.

The other assumption implicit in the derivation of B_a/B_s is that $B_a(\alpha)$ and $P_a(\alpha)$ obey the Rayleigh law:

$$B_a(\alpha) = B_a(0)\left(\frac{1 + \cos^2 \alpha}{2}\right) \tag{1.3.13}$$

and

$$P_a(\alpha) = \frac{\sin^2 \alpha}{1 + \cos^2 \alpha} \tag{1.3.14}$$

Combining (1.3.13) with (1.3.14) we have

$$\frac{B_a(\alpha)P_a(\alpha)}{B_a(0)} = \frac{\sin^2 \alpha}{2} \tag{1.3.15}$$

Dollfus and Focas have used $\sin^2 \alpha/2$ as a factor in Eqs. (1.3.8) and (1.3.9). This would be true in the case of Rayleigh scattering only. Values of X and Y for the Rayleigh case were plotted by Dollfus and Focas, and are shown in Fig. 4. From (1.3.12), the slope of the plot is B_a/B_s.

However, if Mie aerosol scatterers were present as a significant component in the Martian atmosphere, then $B_a(\alpha)$ and $P_a(\alpha)$ would change

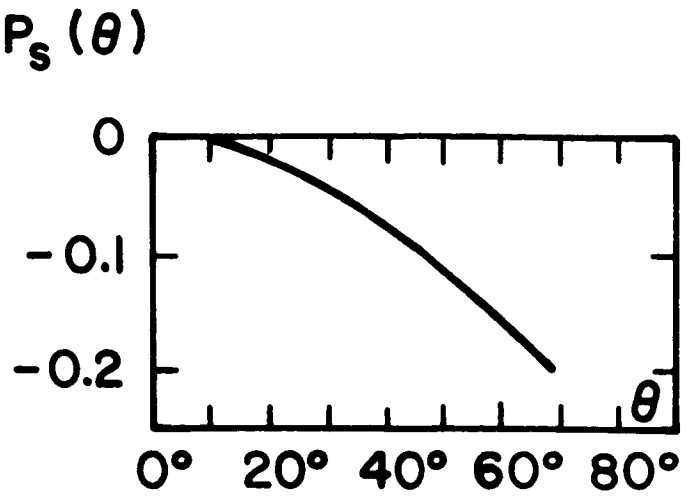

Fig. 3. Assumed center-to-limb variation in the surface polarization of Mars at $\lambda = 0.61\ \mu$ (after Dollfus and Focas 1966).

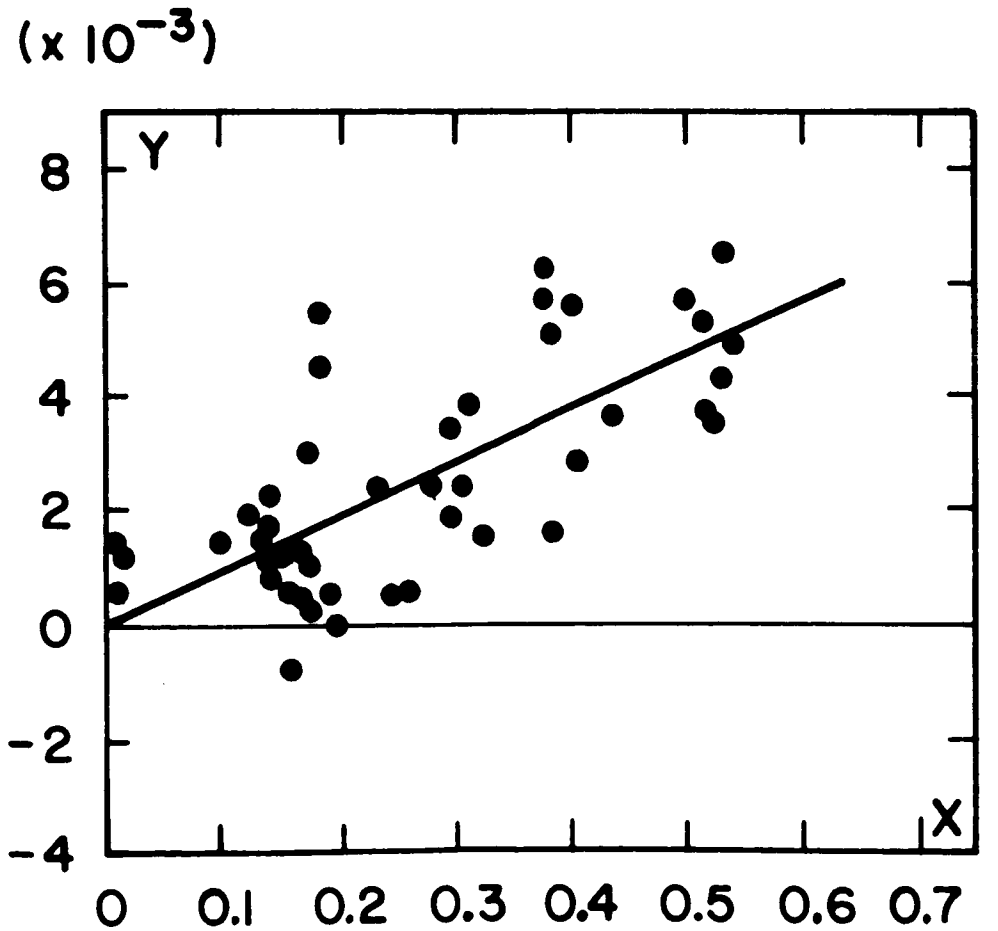

Fig. 4. The X-Y plot for a Rayleigh atmosphere at 0.61 μ (after Dollfus and Focas 1966; see text for definitions and derivation of X and Y).

considerably. Consider a mixture of aerosols discussed by Kuiper (1964): Mixture A", where $\bar{r} \sim 0.3\ \mu$ for observations at 0.61 μ, and neither integral nor half-integral values of $x = 2\pi r/\lambda$ is favored. In that case

$$B_a(\alpha) = 0.98^{\alpha}\ B_a(0) \qquad (1.3.16)$$

and $P_a(\alpha)$ has a complex relation perhaps including a negative branch. In this case, substitution of (1.3.16) into (1.3.9) would give

$$X = 0.98^{\alpha}\ P_a(\alpha)s \qquad (1.3.17)$$

in contrast to the values of X in the Rayleigh case. These new values of $B_a(\alpha)$ in (1.3.16) would alone change the value of X, and thus of B_a/B_s, by a factor of ~ 2. The polarizations, $P_a(\alpha)$, could have an even more drastic effect on B_a/B_s, and might even yield negative values for X in the negative branch phase. But since X does not take on negative values in the Dollfus and Focas (1966) report, this might be an argument against the existence of a negative branch due to atmospheric aerosols. However, a negative branch cannot be excluded because of the possible invalidity of the $P_s(\theta)$ assumption mentioned in the above paragraph.

Let us summarize what can be said so far about the atmospheric contribution to the observed brightness and polarization of Mars. Dollfus and Focas (1966) have performed a careful analysis of many good observations. There is considerable evidence, however, that their assumptions about $P_s(\theta)$, $B_a(\alpha)$, and $P_a(\alpha)$, are wrong to such an extent that their value of B_a/B_s cannot be used in deriving certain surface and atmospheric properties of Mars. Their value of B_a/B_s could well be in error by a factor of 10. This complicates any attempt to make quantitative analyses

such as those of Rea and O'Leary (1965), Dollfus and Focas (1966), and Pollack (1967).

There are other observations which might add some information about Rayleigh versus Mie scattering in the Martian atmosphere. As mentioned earlier, Evans (1965) derived a surface pressure of ~ 12 ± 5 mb from ultraviolet reflectivities measured from a rocket. The apparent discrepancy between this value and the value of ~ 6 ± 2 mb derived from (1) the Mariner IV occultation data (Kliore et al. 1965) and (2) the infrared spectroscopic data (Gray 1966, Schorn and Gray 1967, and Owen 1967) can be explained by aerosols. Although the error bars are rather large, the discrepancy between the two values is ~ 6 mb, i.e., the contribution by aerosols to the ultraviolet reflectivity of Mars might equal that by molecules (Evans made the assumption that the surface reflectivity of Mars is zero, an assumption which is probably quite accurate).

I have also mentioned that Evans found a good fit of reflectivity from 0.24 to 0.35 μ with the λ^{-4} law. Thus it would appear that aerosols as well as molecules obey the λ^{-4} law in the ultraviolet. It would seem, then, that the λ^{-4} law should be obeyed in the visible region as well, since the aerosol particles in the visible are smaller relative to λ than they are in the ultraviolet, i.e., we are further approaching the Rayleigh limit in the visible. Such correspondence between aerosols and molecules would imply small B_p/B_s (~ 0.002) at 0.61 μ.

D. G. Rea pointed out to me a possible fallacy in this reasoning. For example, let us say there is a small quantity of aerosols with $r \gtrsim 0.8$ μ in the Martian atmosphere. Such particles do not obey the λ^{-4} law from the ultraviolet to the visible, whereas those particles for which $r \lesssim 0.3$ μ do (e.g., see Kuiper, 1964; Deirmendjian and Clasen, 1962). The

dependence on λ for these larger particles becomes very small. Table II lists an example of what might happen in a simple case: say the scattered intensity for molecules and those aerosols obeying the λ^{-4} law at 0.3 μ were 100 (arbitrary units) and those aerosols exhibiting no dependence on λ were 10. The situation at $\lambda = 0.6\ \mu$ is very clear: larger sized aerosols ($r \gtrsim 0.5\ \mu$) can dominate atmospheric scattering in the visible but might not be detected in the ultraviolet. Although this simple example is probably far from the truth, it is not difficult to imagine a reasonable aerosol particle size distribution and abundance which would make Mie scattering dominate in the visible and Rayleigh scattering dominate in the ultraviolet. Note that there are at least three different sources for the aerosols: dust, H_2O, and CO_2. Thus a bimodal distribution can be readily explained.

However, it might be argued that λ^{-4} is in fact obeyed in the visible, as I have mentioned that Dollfus and Focas (1966) found that $B_a(0.61\ \mu)/B_a(0.47\ \mu) = (0.61/0.47)^{-4}$. But we have just found that little reliance can be put on any determination of B_a/B_s, and thus of B_a.

It is clear from this discussion that very little can be said about the scattering processes in the Martian atmosphere. Previous investigators have overinterpreted without regarding all the facts, and we must now face the possibility that the atmosphere is altering the optical parameters previously attributable to the surface. Particularly significant is the relation $P(\alpha)$: because of the great uncertainties in B_a/B_s, we simply do not know what $P_s(\alpha)$ actually is. There are some arguments favoring the Mie-scattering aerosol and some favoring a Rayleigh-scattering aerosol. We simply do not know the extent of their participation in the scattering.

TABLE II

A simple example of possible scattering components in the Martian atmosphere (see text).

	Intensity (relative units)		
$\lambda(\mu)$	Molecules and aerosols obeying the λ^{-4} law	Aerosols, $\bar{r} \gtrsim 0.8\ \mu$	Total (observed)
0.3	100	10	110
0.6	6	10	16

However, I have mentioned that in the event B_a/B_s is small (e.g., $B_a/B_s \sim 0.01$ at λ 0.61 μ), the uncertainties in $P_s(\alpha)$ are small regardless of the scattering mechanisms in the Martian atmosphere. For example, I have earlier stated that <u>provided</u> $B_a/B_s \lesssim 0.01$, then the uncertainty in inversion points is $\sim \pm 2°$ and the value of P at $\alpha = 40°$ is uncertain by $\pm$ 0.2% because of Mie-scattering aerosols. This small uncertainty arising from a small value of B_a/B_s is the situation one would hope for but might not necessarily get.

It is next worthwhile to check the correspondence between Martian $P_s(\alpha)$ under a hypothetically tenuous atmosphere and $P_s(\alpha)$ of laboratory samples of limonite. Two observational situations are presented in Table III: one in which the Martian atmosphere adds no component to the scattering so that the observed $P(\alpha)$ equals $P_s(\alpha)$, and the other in which $B_a/B_s = 0.01$ at 0.61 μ and the scattering is entirely Rayleigh, equivalent to 30 mb of dry air (Dollfus and Focas 1966). In the latter case I assumed $B_a(\lambda) \propto \lambda^{-4}$ and that $B_s(\lambda)$ corresponds to the observed spectral reflectivity curve of Mars (Dollfus 1957). The laboratory values listed in Table III correspond to Dollfus and Focas' limonite sample M_4, which was found to match the suspected Martian $P_s(\alpha)$ so well. Incidentally, Dollfus and Focus' Martian $P(\alpha)$ curves in their Fig. 16 appear to have been overcorrected for the Martian atmosphere. However, the match with M_4 is still fairly good at all wavelengths, when the 30 mb correction is made (see Table III). (But at the shorter wavelengths, the agreement in the 0 mb case is poor.) What is most important is that the correction for the atmosphere for $\lambda \gtrsim 0.60$ μ is small. In spite of this, there are slight disagreements in Table III between Dollfus and Focas' sample mixture M_4 and Martian $P_s(\alpha)$ for $\lambda \gtrsim 0.60$ μ. The disagreement alone (as much as 4°

TABLE III

Polarimetric parameters of Mars observed and corrected for a 30 mb Rayleigh-scattering atmosphere of air

λ	α (inversion point)			P(α = 40°)		
	Mars		Limonite[b]	Mars		Limonite[b]
	observed[a]	corrected		observed[a]	corrected	
0.50 μ	22°	25°	27°	3.3%	2.1%	2.3%
0.53	23°	26°	27°	2.7	1.8	2.1
0.60	25°	26°	27°	1.8	1.6	2.0
0.63	25°	26°	27°	1.6	1.4	1.9
0.83	24°	24°	28°	1.8	1.7	1.6
0.95	25°	25°	28°	1.5	1.5	1.4
1.05	25°	25°	28°	1.5	1.5	1.2

[a]From Figs. 4 and 5 of Dollfus and Focas (1966)

[b]Sample M_4 from Fig. 18 of Dollfus and Focas (1966)

in inversion points and 0.3% in P at $\alpha = 40°$) seems to be sufficient to question a pure limonite composition for the bright areas.

Furthermore, the disagreements in Table III are in such a direction as to consider other candidates for bright-area surface substances. Table IV illustrates the inversion points of various solar system objects and substances in the laboratory for $\lambda \sim 0.60\ \mu$. It has been often noted that the rather large inversion point of Mars is matched only by Dollfus' variety of limonite (the inversion point is probably the most descriptive way of distinguishing materials besides presenting the curves themselves). However, Table IV shows a quite different story: the Martian inversion points are roughly intermediate between those of some limonites and those of desert sand, red sandstone, and augite. The similarity between the Martian inversion points and those of the Moon and some of the asteroids is also interesting: it is apparent that the identification of yellow ochre limonite covering the Martian bright areas from polarization curves has been overplayed too much; materials such as desert sand, red sandstone, augite, and Moon-covering come nearly as close, if not just as close, to the observed or corrected (by a small atmospheric component) Martian polarizations as does yellow ochre limonite. In fact Kohan (1962) has noted that $P(\alpha)$ for the lunar maria matches most closely $P(\alpha)$ for "ocherous limonite." Because of large reflectivity differences between the two, as well as the thermodynamic instability of goethite in a vacuum, the possibility of limonite-covered lunar maria would be quite out of the question.

This fundamental point of non-uniqueness must always be borne in mind in discussing limonite for covering of the Martian surface. On the other hand, if $B_a/B_s \gg 0.01$ at 0.60 and if the aerosols are Rayleigh

TABLE IV

Inversion points from negative and positive polarization for various objects and substances at $\lambda \sim 0.60\ \mu$.

	α (inversion point)
Mars[a,b,c]	24° - 26°
Moon[b]	23°
Asteroids[b]	15° - 27°
red sandstone[d]	22° - 23°
augite[d]	22° - 23°
desert sand ($\lambda \sim 0.49\ \mu$)[e]	25° - 26°
various limonites[e]	25° - 35°
yellow ochre limonite[c]	27° - 28°

[a] corrected for a 0 to 30 mb atmosphere of dry air (see Table III).

[b] from Gehrels *et al.* (1964)

[c] from Dollfus and Focas (1966)

[d] from Dollfus (1955, 1961)

[e] from Coulson *et al.* (1965)

scatterers, then the correction would be such as to make the inversion point in Martian $P_s(\alpha)$ higher, thus approaching the inversion point of the yellow ochre limonite powder. But this sort of additional atmospheric component would go the wrong way in matching the $P(\alpha = 40°)$ correction with limonite between $\lambda\lambda$ 0.50 μ - 0.63 μ (Table III).

Obviously, the parameters of compositional heterogeneity, particle size, and Mie aerosols can be juggled in any of an infinite number of possible ways to obtain a reasonable fit with Martian $P(\alpha, \lambda)$, and it is certainly premature to specify a unique fit at the present time.

There is one final question to ask: to what accuracy is Martian $P(\alpha, \lambda)$ known? Although Dollfus and Focas' data points are reasonably consistent with one another, there is still the possibility of variations in the polarizing properties of the Martian atmosphere and instrumental errors. D. L. Coffeen kindly communicated to me some polarization data of Mars he obtained at the Lunar and Planetary Laboratory in Tucson, Arizona. These data are shown on Fig. 5: the observations were made on June 6, 1967 when Mars was at $\alpha = 34°$. Shown on the same figure are the polarizations at $\alpha = 34°$ from the curves of Dollfus and Focas (1966). It is immediately seen that the two sets of results are significantly discordant. One possible explanation is that Coffeen's observations were made at a time of extensive cloudiness in the Martian atmosphere. Whatever the cause of the discrepancy may be, it is nevertheless large enough to consider many possible Martian surface substances from polarization data, even regardless of what assumptions are made about the polarizing properties of the atmosphere and samples in the laboratory.

In view of the gross uncertainties in the limonite identifications, it is worthwhile to examine more recent analyses. Investigations of

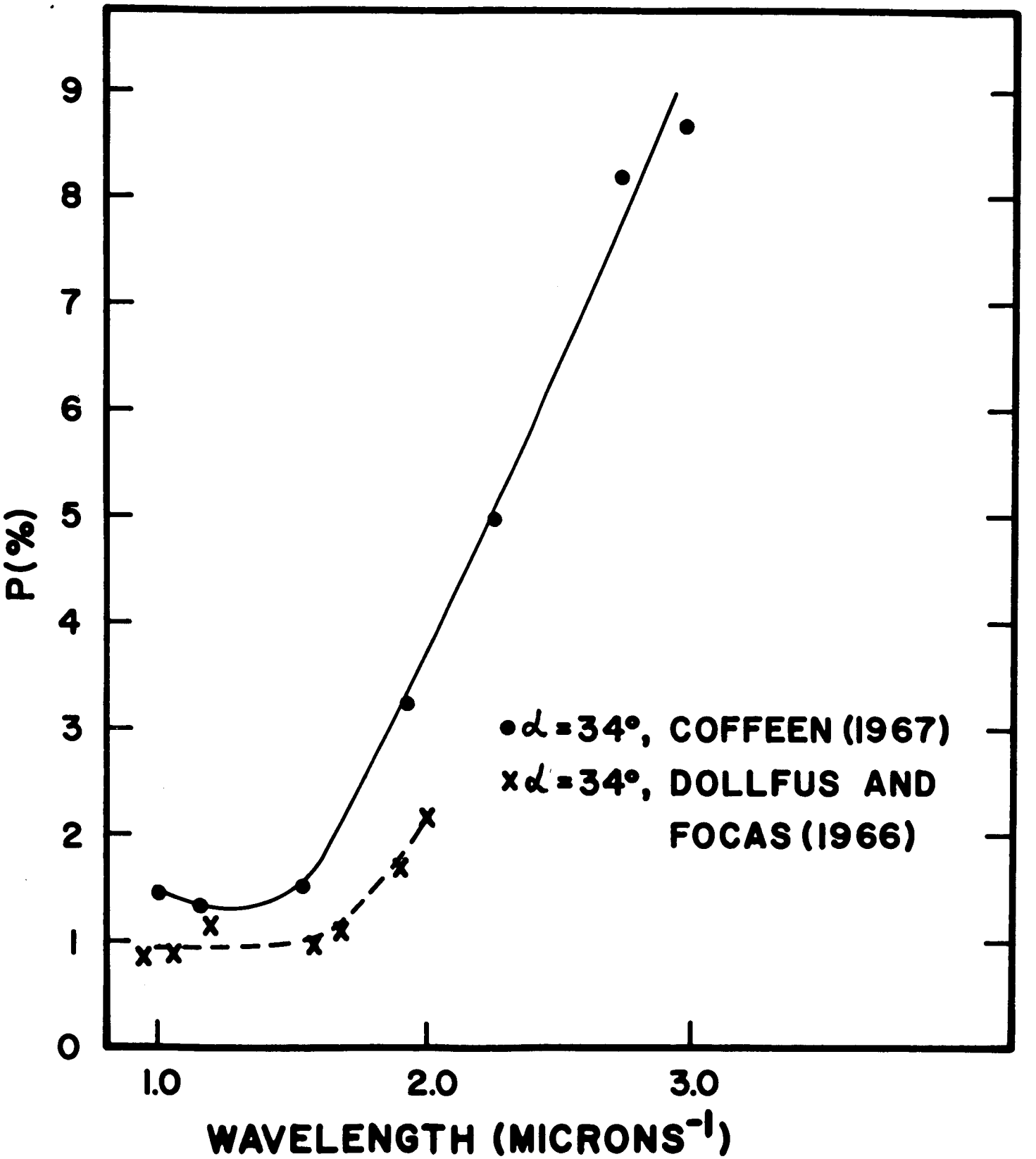

Fig. 5. Comparison of Martian polarization vs. wavelength data.

polarization by laboratory samples of limonite have been carried out by Egan and Foreman (1967) and Egan (1967). They found a good match in $P_s(\alpha)$ of 1 - 2 mm-size limonite particles from Venango County, Pa. with the observed $P(\alpha)$ of Mars, but found a poor match in the case of a limonite powder with particle sizes less than 1 μ. They went on to suggest that because of such large-sized particles, extraordinary wind speeds are required to initiate Martian yellow clouds.

Their curves of $P(\lambda)$ at $\alpha = 40°$ are reproduced in Fig. 6. There is is good match between the Martian data and the 1 - 2 mm-sized particles provided the atmospheric correction to the Martian data is very small, especially for $\lambda > 0.50$ μ (i.e., B_a/B_s at 0.60 μ is essentially zero). However, if $B_a/B_s \sim 0.01$ at λ 0.60 μ and the atmosphere is Rayleigh scattering as assumed by Dollfus and Focas (1966), the match of the corrected Martian data (Table III) with the limonite powder would be much better. Thus, Egan and Foreman's laboratory results corroborate those of Dollfus and Focas. The interpretations as to the particle sizes are different in the two works only because the assumptions about atmospheric scattering are different.

The considerations leading to Egan and Foreman's atmospheric correction are in error, however. They were aware that their interpretation might be subject to alteration if aerosols were to contribute appreciably to the scattering, but the extent to which they show them to operate is miscalculated. They stated that Rayleigh-scattering aerosols and molecules equivalent to a Martian atmospheric pressure of 218 mb is needed to make the derived $P_s(\alpha = 40°)$ correspond to limonite powder, and 95 mb to make $P_s(\alpha = 40°)$ correspond to 1 - 2 mm limonite particles at λ 0.48 μ. They stated that this correction in terms of polarization is $\Delta P = 0.023$ in the

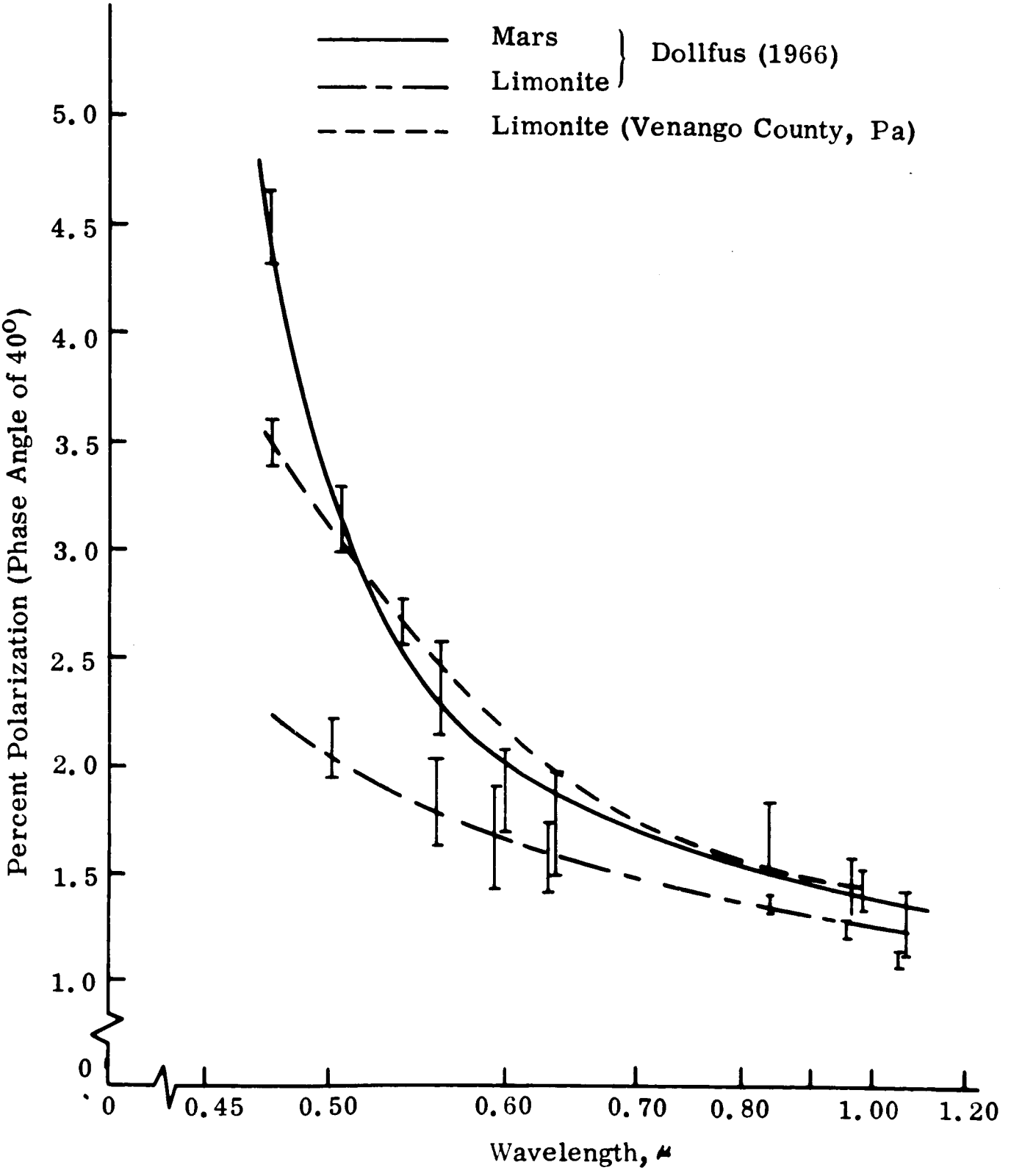

Fig. 6. Spectral comparison of polarimetric properties of Mars with simulated limonite surfaces (after Egan and Foreman 1967, and Egan 1967).

former case and $\Delta P = 0.010$ in the latter case (Fig. 6). However, slight extrapolation of the data in Table III to λ 0.48 μ shows that a 30 mb--not a 218 mb--atmosphere would be nearly enough to give $\Delta P = 0.023$ at 0.48 μ. Evidently Egan and Foreman had neglected the very rapid increase of B_a/B_s with decreasing λ (for a given equivalent atmospheric pressure) because of: (1) the assumed λ^{-4} dependence of B_a, and (2) the observed rapid drop in Martian reflectivity with decreasing λ. In any case, in view of the uncertainties discussed in the last several pages, it would be premature to adopt either Egan and Foreman's particle sizes or their interpretation of yellow cloud phenomena and high Martian winds.

Pollack (1967) has offered two arguments against a non-Rayleigh scattering aerosol in the Martian atmosphere: (1) Evans' (1965) observations of the λ^{-4} dependence of brightness between λ 0.24 and 0.35 μ, and (2) Dollfus and Focas' (1966) demonstration of a λ^{-4} dependence of B_a between λ 0.47 and λ 0.61 μ. He then went on to deduce elevation differences of ~ 10 km with a surface pressure of ~ 20 mb (the polarimetric value he derived for CO_2) over the bright area lowlands, and 5.5 mb at Mariner IV ingress, presumably in a dark area highland. For this interpretation to be valid he assumed a small contribution by aerosols, as deduced from accordance of Evans' ultraviolet data with the spectroscopic data.

However, the discussion presented herein would cast some doubt on such evidences for Rayleigh scattering dominating the B_a component in the visible. Even if the Rayleigh scattering were to dominate the visible B_a component, the fact that $P_s(\theta)$ might be in error and/or be independent of α, as well as the large error bars in B_a/B_s discussed by Cann et al. (1965), would make Pollack's reliance on $B_a/B_s \sim 0.01$ for his later interpretations appear too strong.

For example, let us be extremely optimistic and assume that B_a is due to Rayleigh scattering alone and $B_a/B_s = 0.01^{+0.01}_{-0.005}$ at 0.61 μ. The elevation differences implied between the "highland" at Mariner IV occultation immersion and the bright areas as determined polarimetrically would range from 5 to 28 km at these very conservative error limits on B_a/B_s. Furthermore, the rather close agreement of the most recent infrared spectrographic surface pressures (Gray 1966, Schorn and Gray 1967, and Owen 1967) with the Mariner IV surface pressure would tend to argue that the occultation point of immersion is fairly representative of the mean surface pressure of the planet. Anyway, it is uncertain as to whether Mariner IV ingressed at a highland or not.

The main point of this section was to indicate the great extent to which Martian phenomena have been overinterpreted from photometric and polarimetric data. It is entirely possible that the assumptions these investigators have used are correct, but there is considerable evidence they are not. It is very likely that $P_s(\alpha)$ of Mars is being disguised sufficiently by an uncertain atmospheric component so as to introduce large error bars in the derived $P_s(\alpha)$. In view of our present state of knowledge it is my opinion that these error bars are large enough to encompass $P_s(\alpha)$ of many materials investigated in the laboratory, e.g., desert sand, augite, red sandstone, hematite, lavas, volcanic ashes, etc. (Dollfus 1955). But even if the atmospheric component were very small and/or correctly assessed in a previous analysis, there are still convincing reasons to believe that yellow ochre limonite does not necessarily abound on the Martian bright areas: the fact that a great number of substances (as well as the Moon itself and some asteroids) show a match with derived Martian $P_s(\alpha, \lambda)$ as well as does limonite, and the probable

situation that the Martian surface is heterogeneous in composition, particle size, and roughness.

Unfortunately, $P_s(\alpha)$ has been the major piece of evidence for limonite on Mars. As secondary pieces of evidence, visible and infrared reflectivities have been matched with various types of limonites (e.g., Sharonov 1961; Moroz 1964; Draper, Adamcik, and Gibson 1964, 1965; Sagan, Phaneuf, and Ihnat 1965; Binder and Cruikshank 1966; and Tull 1966). But all these other investigations showed that these properties of Mars are merely consistent with, not diagnostic of, limonite. On the other hand, Younkin (1966) does not find a good correspondence between the reflectivities of limonite and of Mars between 0.5 and 1.1 μ and sets an upper limit of 2% on the strength of limonite spectral features on Mars. Similarly, Sinton (1967) did not detect the λ 0.88 μ limonite band and concluded that iron oxides are not major constituents of the Martian surface.

In the most recent discussion about the stability of limonite on Mars, O'Connor (1967) performed thermodynamic calculations under a range of predicted surface conditions for Mars. He showed that "goethite will be unstable except under the wettest and coldest parts ($p_{H_2O} \sim 10^{-6}$ atm., $T < 200°K$) of this range." It appears, then, that there is difficulty in explaining the widespread presence of limonite over the Martian surface.

But the limonite debate still continues. The next two chapters attempt to present a new method of resolving the debate: the photometric function near opposition. The concluding chapter will coordinate the critical review of this section with my opposition effect results.

1.4 The Opposition Effect: Previous Work and Motivation

Photoelectric and photographic photometry of Mars near opposition has been performed by many observers in great detail. Yet one important question has not been considered: How does the phase function of Mars behave as it passes through very small phase angles? For reasons to be explained below the answer to this and related questions may provide an important clue to the composition of the surface of Mars.

Many workers (originally Barabashev 1922, and more recently Wildey and Pohn 1964; Gehrels, Coffeen, and Owings 1964; and Van Diggelen 1965) have reported a curious phenomenon about the lunar surface: its brightness increases very rapidly as the Moon approaches full phase (or close to $\alpha = 0°$). The lunar phase function is linear at 0.028 (visual) mag./deg. for $\alpha > 5°$, but the slope increases at smaller phase angles, becoming very steep at phase angles less than 2°. At 1° the slope is more than 0.2 mag./deg. (Gehrels et al. 1964). This is called the lunar opposition effect, true for all parts of the Moon, but especially pronounced for the large crater areas, where the reflectivity increases by a factor of 2 from $\alpha = 5°$ to $\alpha = 0°$.

Subsequent to extensive laboratory work, Hapke and Van Horn (1963) found few materials that matched this strong opposition effect, and proposed a lunar model showing a complex surface structure with much shadowing when the phase angle is not near zero. Recently, however, Oetking (1966) reported that the laboratory work to date has not shown the opposition effect simply because of the large spread in phase angles received at the aperture of the laboratory photometer. The effect was thus smeared out. Using a small angle of acceptance and a narrow collimated beam, Oetking found that nearly all materials, including the standard Lambert surface

magnesium oxide, exhibit this opposition effect. Hapke (1966) agrees. The magnitude of the effect varies from sample to sample, thus providing a new test for the surface composition of a planet.

The existence of a Martian opposition effect has been suggested by Gehrels et al. (1964) referring to data reported by Harris (1961, p. 302) at Mt. Stromlo and at McDonald Observatory, May 3-4, 1952, when Mars was at a phase angle of 2°.5. On that night, both observatories reported that at various wavelengths Mars was 0.1 to 0.3 mag. brighter than expected.

Photoelectric photometry of various areas on Mars during the 1956 opposition was reported by Moroz and Kharitonov (1957). They observed on opposition night (September 10-11) and reported both the bright areas and dark areas to be 0.06 V mag. brighter than the following night, and over 0.10 mg. brighter than other nights about one week from opposition. Unfortunately Mars reached only $\alpha = 4°.3$ at opposition, 1956, an extraordinarily high value. Also, the presence of a dust storm near the opposition casts some doubt on the observations. Finally, the dark and bright areas observed on each night were generally different. But, again, there is marginal evidence for the Martian opposition effect.

Extensive visual photometry of Mars has been performed by Muller (1893) from 1877 to 1889. His phase curve, reproduced by de Vaucouleurs (1964), shows a linear curve with three points inside $\alpha = 10°$, a few hundredths of a magnitude above the mean phase curve. The scatter of his points, however, is also a few hundredths of a magnitude, which makes any evidence for or against an opposition effect inconclusive.

After a detailed search of the literature, I have concluded that no other photometric measurements of Mars have been made at $\alpha < 5°$. Fortunately the 1967 apparition provided a rare opportunity for a good

description of a Martian opposition effect. Table V shows the minimum phase angle of Mars at all oppositions since the favorable opposition of 1939. In the 28-year period to follow only four oppositions were within $\alpha = 2°$. The 1967 opposition was one of them: $\alpha = 1.^{\circ}2$. Figure 7 shows the observational opportunities for Mars in the Western U.S., 1967. It is seen that Mars was in the sky over the Western U.S. as the planet passed through the $1.^{\circ}2$ minimum (early morning, April 15). There were four nights in which $\alpha < 2°$ (nights of April 13-16, local time). Thus, there was much justification for an observational program in the 1967 opposition.

My observations were performed at the Kitt Peak No. 2 36-inch telescope and kindly backed by Drs. Sanduleak and MacConnell at Cerro Tololo Inter-American Observatory, Chile. The results were successful and will be described in detail in the next chapter.

In regard to the opposition effect, we cannot make meaningful interpretations from observations alone. An adequate theory or experiment is also needed. Because of the many parameters involved, I would expect that the experimental approach is necessary as any Martian opposition effect theory might be on shaky grounds. Experience has shown this to be true in the case of the Moon, where Oetking (1966) experimentally showed that Hapke's shadowing model (Hapke 1963) is not a unique explanation.

Let us examine what kind of experiment is needed to describe an opposition effect. Oetking (1966) has shown that an experiment whose photometer accepts a large spread of phase angles cannot define a correct opposition effect. Coulson, Bouricius, and Gray (1965) have measured the opposition effects of various materials including limonite, but their photometer aperture received a spread of 5° in phase angle. This naturally

TABLE V

Values of minimum phase angles of Mars for oppositions since 1939.

Interpolated from the American Ephemeris and National Almanac.

Date	Minimum Phase Angle
1939, July 23, 8^h	4°.5
1941, October 10, 13^h	2°.3
1943, December 5, 18^h	1°.3
1946, January 14, 1^h	2°.4
1948, February 17, 16^h	2°.6
1950, March 23, 6^h	2°.0
1952, May 1, 1^h	0°.7
1954, June 24, 17^h	3°.0
1956, September 10, 22^h	4°.3
1958, November 16, 14^h	0°.4
1960, December 30, 10^h	2°.2
1963, February 4, 12^h	2°.6
1965, March 9, 12^h	2°.3
1967, April 15, 12^h	1°.2

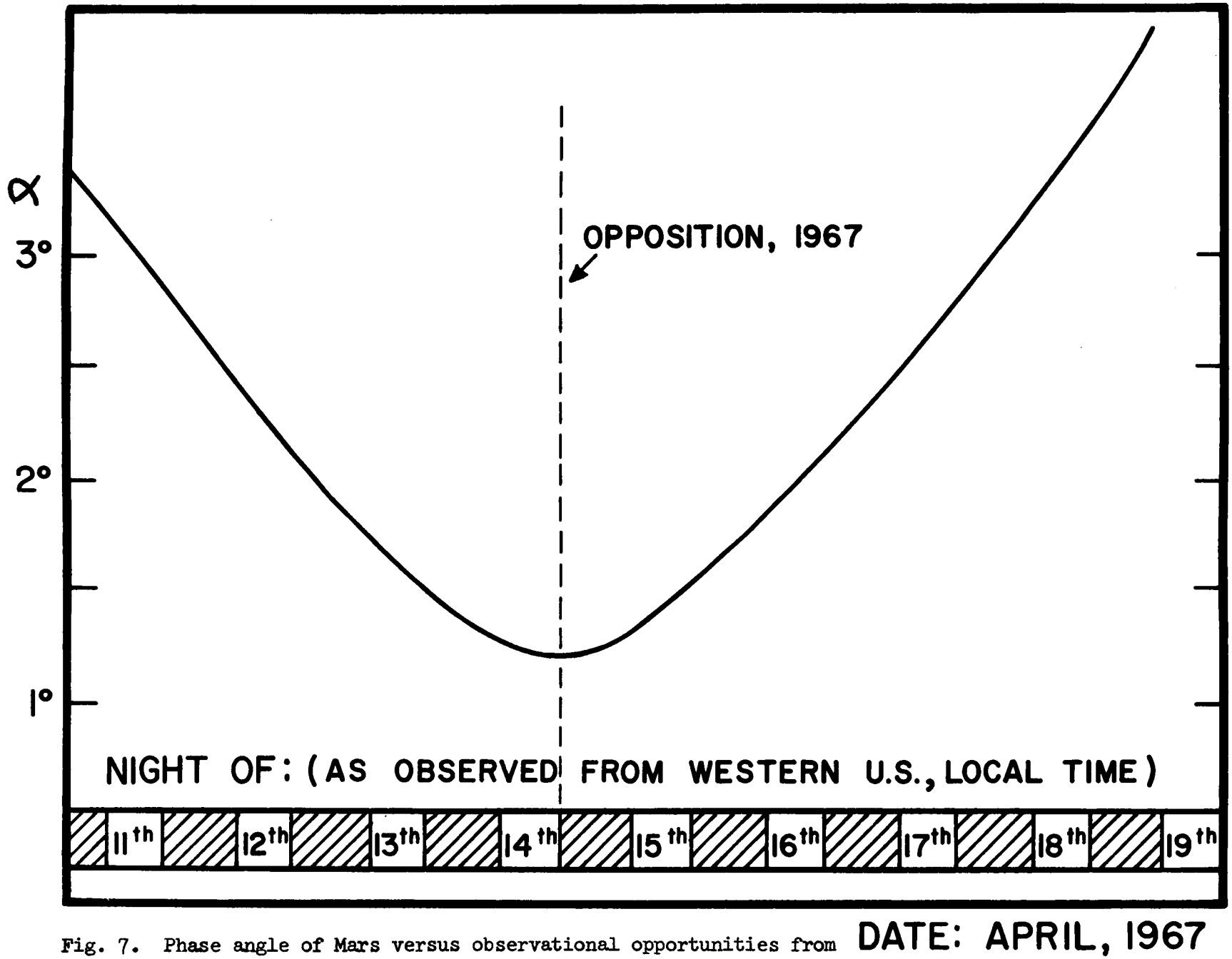

Fig. 7. Phase angle of Mars versus observational opportunities from U.S. Western Observatories, just before and after the 1967 opposition.

gave rise to erroneous phase functions inside ~ 10° (unless they were linear) and partially smeared out the opposition effect. It is interesting, however, that Coulson et al. still found a much stronger opposition effect for limonites than for other substances they investigated (see, for example Fig. 8).

The importance of measuring the opposition effect of Mars and of laboratory substances is obvious: it is a method of selecting or eliminating consideration of various Martian surface materials. For example, if the Martian opposition effect were not strong, then various samples of limonite may be eliminated. The stage is then set: measure the Martian opposition effect and build into the reflectometer design an accurate means of measuring the opposition effect. Both have been accomplished in this research.

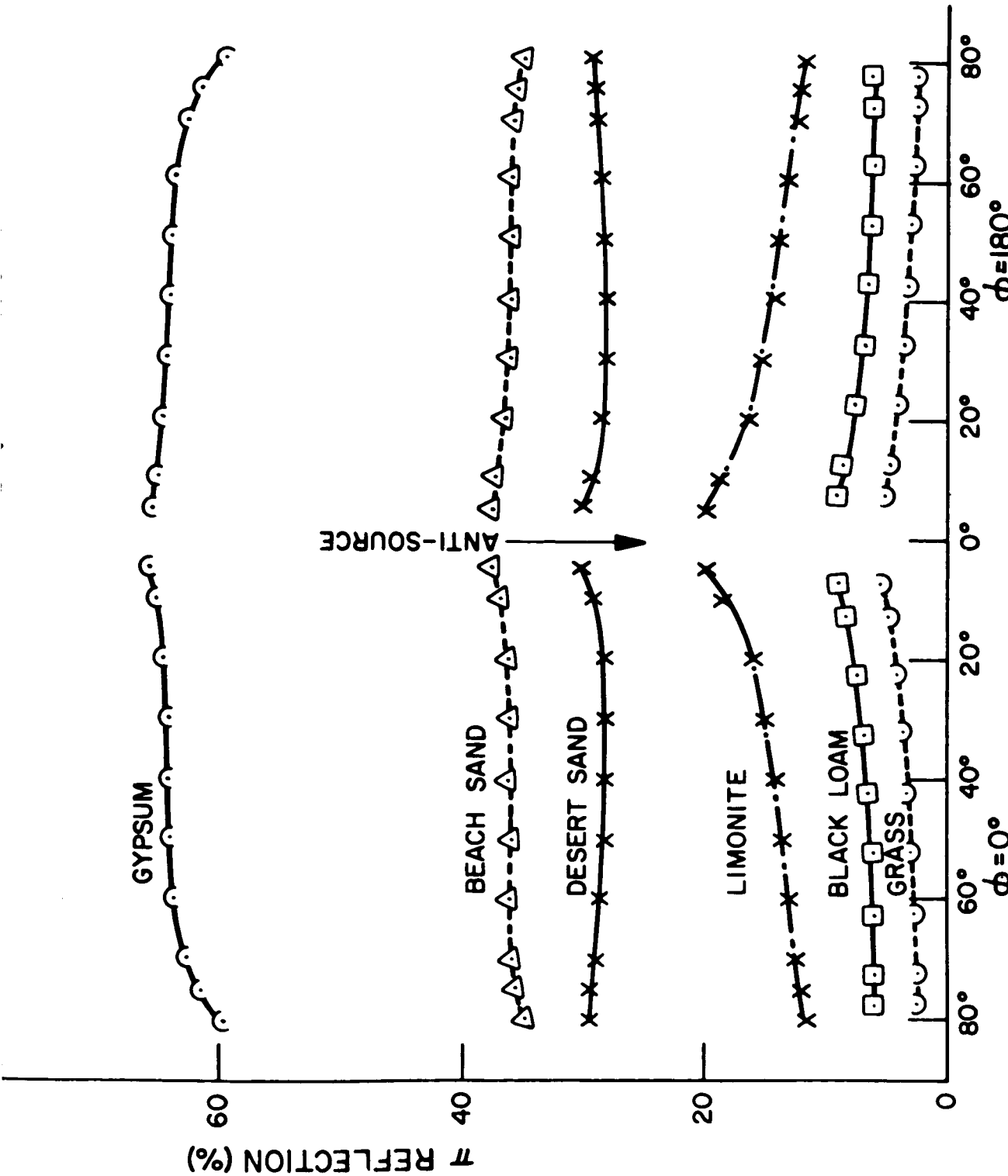

Fig. 8. Directional reflectance of various surfaces, $\lambda = 0.64\ \mu$, $\theta_o = 0°$, $\phi = 0°$ (after Coulson et al. 1965).

CHAPTER II. PHOTOMETRY OF A MARTIAN OPPOSITION EFFECT

2.1 Observational Instrumentation and Procedure

Photoelectric photometry of Mars has been performed in six colors with the Kitt Peak No. 2 36-inch reflector. The results are summarized as a Letter to the Editor of the Astrophysical Journal (O'Leary 1967), and details are presented in this chapter.

In order to provide ample coverage of the anticipated opposition effect, I asked for three weeks' telescope time from April 4-24, 1967, to cover Mars from $\alpha = 8°$ to $1\overset{\circ}{.}2$ to $8°$. This was thought to be a sufficient span, since the lunar opposition effect does not become significant for $\alpha > 5°$. Though the generosity of the Kitt Peak staff I was given all the observing time I requested.

The photometer consisted of a refrigerated RCA 7102 photomultiplier tube, operating at 1400 volts, and a charge-collecting integrator, where the integration time was set at 5 sec. The results were recorded on a strip-chart recorder, and all deflections were repeated at least once.

A special diaphragm slide with apertures of 1" to 35" arc was used so that photometry of the whole Martian disk (about 15" arc) and of small areas was possible. A beamsplitter was built into the photometer head in order that the telescope might be guided or aligned upon certain areas during a series of integrations.

The small-area photometry understandably yielded results with errors as much as a few tenths of a magnitude. Attempts were made to isolate Elysium, Isidis Regio, and Syrtis Major (all are about 2" to 4" arc in diameter) when each area appeared at the sub-Earth point. However, seeing variations even as small as 1" arc were enough to make the results using

a 2"-arc diaphragm too inconsistent to be meaningful. Other factors underlying inconsistencies fron night to night could be centering errors, or possibly the appearance or disappearance of clouds in a given area.

The weather at Kitt Peak was unseasonably cloudy during most of the run, with only two clear nights (α = 4.°5 and 1.°6) in the first 13 nights. Fortunately it was clear at Kitt Peak during the last week (α = 2.°7 to 7.°5) and Drs. N. Sanduleak and D. J. MacConnell at Cerro Tololo, Chile added some valuable points at α = 1.°2, 1.°45, 2.°0, and 2.°3, thanks to their compliance with my last-minute request to them over short-wave radio.

The effective wavelengths, band widths, and components of my filter systems are listed in Table VI. Their wavelengths were designed to approximate as closely as possible Johnson's U, B, V, R, and I in his lists of standard stars (Johnson 1963); and also the U, B, V, R, and I listed by de Vaucouleurs (1964) for previous observations of Mars. I added a filter designated I' at 1.04 μ, where standardization was made from observations of the Martian reflectivity curve between 0.82 μ and 1.04 μ. These observations will be discussed in Section 2.3.

Spica (α Virginis) was used as the comparison star. Its selection was based upon the following considerations: its proximity to Mars during April (within 10° of arc); its high brightness which meant no drastic changes in photomultiplier gain settings between it and Mars; and the fact that it is present on Johnson's list of standard stars. These distinct advantages were offset somewhat by two disadvantages: (1) Spica has a great color difference from Mars, where $(B-V)_{Spica} - (B-V)_{Mars} = 1.6$, and (2) Spica is an eclipsing binary of period 4 days and amplitude of 0.1 magnitude. The first problem was easily corrected by proper evaluation of second order extinction coefficients and by

TABLE VI

Transmission Characteristics of Filters Used in Kitt Peak Mars Observations

	U	B	V	R	I	I'
$\lambda_e(\mu)$	0.36	0.43	0.55	0.67	0.83	1.04
$\Delta\lambda(\mu)$	0.03	0.05	0.04	0.05	0.06	0.15
Filters Used	Schott UG-1, WG-2, BG-18, UG-11	Corning CS5- 74, Schott BG-18	Corning CS4-64, Schott OG-1, BG-18	Corning CS2-64, CS4-94	Optical Coating Lab. N-8300, Neutral Density =1 Filter	2-Corning CS7-56

minimizing filter band widths. The second problem, however, was embarrassing, since I had not been aware of this at observation time (and evidently Johnson had not either), and Spica's light curve is not well known. However, Stebbins (1914) did publish a light curve of normal magnitudes (Fig. 9) in which he derives the light elements:

$$\text{Min. I} = \text{J.D. } 2417957^{d}.094 + 4^{d}.01416\ E \qquad (2.1.1)$$

$$\text{Min.II-Min. I} = 2^{d}.224 = 0^{p}.554 \qquad (2.1.2)$$

where J.D. is Julian Date, Minimum I corresponds closely to zero phase of Fig. 9, and E corresponds to the number of light cycles since the epoch J.D. 2417957.094.

Struve, Sahade, Huang, and Zebergs (1958) discussed the radial velocity curve of Spica. Referring to the spectroscopic data of Luyten and Ebbinghausen (1935) of 1934 and their owd data of 1956, we see that the position of zero velocity shifted + $0^{d}.12$. Also, assuming that zero velocity positions correspond to the light minima, we derive from Struve and Ebbinghausen (1934)

$$\text{Min. I} = \text{J.D. } 2426041^{d}.76 + 4^{d}.01460\ E\ ; \qquad (2.1.3)$$

or the light curve from 1912 to 1934 shifted + $0^{d}.15$. It appears therefore that the light curve advances ~ $0^{d}.0064$ per year, so that a corrected light curve can be better expressed by

$$\text{Min. I} = \text{J.D. } 2417957^{d}.094 + 4^{d}.01423\ E \qquad (2.1.4)$$

The dates U.T. of predicted eclipse in April 1967 during the observation time of Spica are shown in Fig. 9. Two fortuitious events occurred:

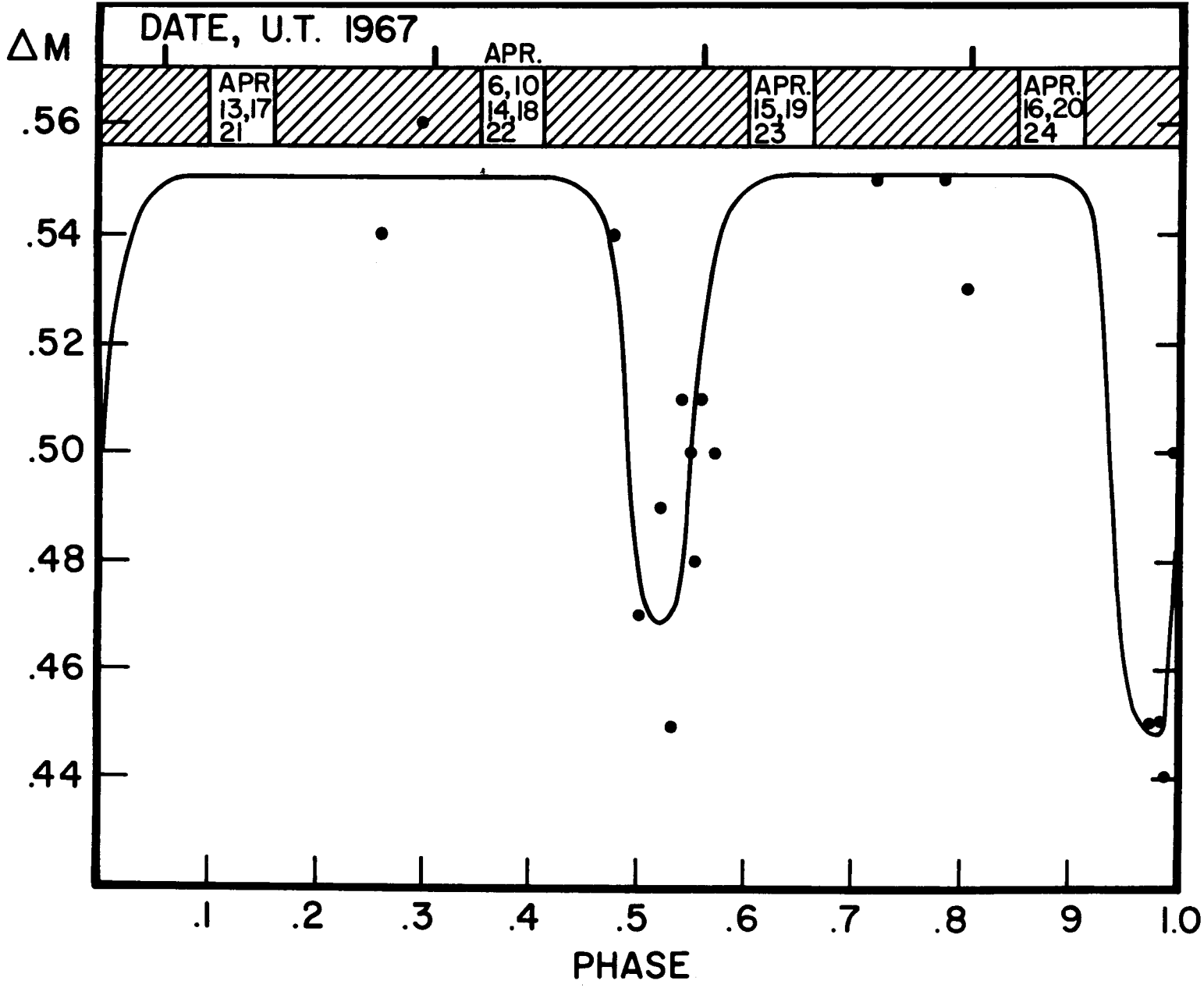

Fig. 9. Approximate curve of light variation of Spica (taken from observations reported by Stebbins, 1914). Those portions of the light curve covered during my observations of Spica are shown at the top of the Figure.

(1) The period of Spica is close enough to 4^d so as to cover essentially the same phase every 4 nights; (2) Eclipses seemed to be avoided at all times. This second point is not entirely certain since the exact locations of the drops toward minima are not well known. It is encouraging, however, that no reduced Mars points at four-day intervals seem to lie anomalously high above its phase curve, an effect that would have occurred had Spica eclipsed during the observations. In any case, the two components of Spica are B2 and B3 stars, so color changes during eclipse would be small.

Incidentally, the variable star catalog (1959) gives for Spica

$$\text{Min. I} = \text{J.D. } 2419530^d.60 + 4^d.014160\ E \qquad (2.1.5)$$

which deviates from the expression (2.1.4) in the April 1967 epoch by $-\ 0^d.06$ in phase shift. This deviation creates an insignificant shift in Fig. 9, and all observations of Spica's light curve and radial velocity curve seem to be consistent within observational error.

The observational procedure, then, was to observe Mars and Spica in rapid succession (within 3 minutes' time) in each color. The observations were timed so that certain prespecified Martian central longitudes, λ_c, spaced at 15° intervals were observed. This was considered helpful in view of the fact that the brightness of Mars varies with rotation (Guthnick and Prager 1918, Johnson and Gardiner 1955, Harris 1961, and de Vaucouleurs 1964), and the variation can be as much as $0^m.05$ for $\Delta\lambda_c = 15°$. It was therefore important to coordinate observations from night to night so that rotation effects could be eliminated from the Martian phase curves. The 15° intervals meant that about one hour separated each series of observations. All Martian observations were made within

10 minutes of the scheduled transits of Earth at Martian λ_c's of 90°, 105°, 120°, ..., 300° for all nights. This usually gave time for two observations of Mars and two of Spica for each hour, totaling about 14 observations of both objects in each color on a clear night.

The Chilean observations were made with the Cerro Tololo No. 2 16-inch reflector, using a refrigerated RCA 1P21 photomultiplier tube and Corning UBV filters. The Martian deflections were barely on-scale through the yellow filter for the lowest gain setting when the voltage was turned down to 600 v. The integration times were 1 second. As a result, there was photomultiplier tube fatigue during exposure to Mars such that the magnitudes of the comparison star, Spica, measured a few minutes after Mars, were 0.03 to 0.06 fainter than those measured a few minutes before Mars. In the reductions the mean between the Spica magnitudes was used, but there remains the uncertainty as to the degree of consistency of the fatigue effect from observation to observation. One observation of Mars and two of Spica were made at two of the prespecified times each night corresponding to Martian λ_c = 210° and 195°. They could thus be coordinated with my results without correcting for rotation effects.

Observations related to deriving extinction and transformation coefficients are described in the next section.

2.2 Data Reduction

The data reduction included many steps in evaluating extinction and transformation coefficients in reducing apparent Martian magnitudes to absolute magnitudes and reflectivities of solar radiation.

First, the second order extinction coefficients were derived by a method outlined by Hardie (1962), where a close optical pair of stars is

observed through a number of differing air masses. Apply his expressions to this case, we have

$$\Delta v_0 = v - k''_v \Delta(B - V)X \quad ,$$

$$\Delta(b - v)_0 = \Delta(b - v) - k''_{bv} \Delta(B - V)X \quad ,$$

$$\Delta(u - v)_0 = \Delta(u - v) - k''_{uv} \Delta(B - V)X \quad ,$$

$$\Delta(v - r)_0 = \Delta(v - r) - k''_{vr} \Delta(B - V)X \quad ,$$

$$\Delta(v - i)_0 = \Delta(v - i) - k''_{vi} \Delta(B - V)X \quad , \text{ and}$$

$$\Delta(v - i')_0 = \Delta(v - i') - k''_{vi'} \Delta(B - V)X \quad . \qquad (2.2.1)$$

where Δ represents the differences in colors and magnitudes between the two stars; u, b, v, r, i, and i' are instrumental magnitudes of each star; u_0, b_0, etc., are these mangitudes with zero air mass, i.e., after extinction corrections (assuming the pair of stars are sufficiently close so as not to give rise to first-order extinction), and B-V is the listed B-V color index of each star (Johnson 1963). Plots of Δv versus $\Delta(B - V)X$, of $\Delta(b - v)$ versus $\Delta(B - V)X$, etc., yield for a slope the second order extinction coefficients k''_v, k''_{bv}, etc. Two groups of stars were observed on different nights: σ Boo and p Boo; and δ Hya, σ Hya, and η Hya. The derived values of k" are listed in Table VII. As Hardie (1962) mentioned, they are expected to be constant from night to night, as they depend primarily upon the bandwidth of the filter system and not on atmospheric fluctuations. Since my bandwidths were fairly narrow (Table VI), my k" values were less than those in standard UBV systems. These values would have to be in considerable error (several thousandths of a magnitude) to

TABLE VII

COEFFICIENTS AND SPICA MAGNITUDES AND COLORS USED IN KITT PEAK REDUCTION PROGRAM

	First Order Extinction Coefficients, k' (mean values)	Second Order Extinction Coefficients, k'	Transformation Coefficients	Spica Magnitudes and Colors[a]
V	0.153	-0.005	$\varepsilon = 0.050$	0.96
U-V	0.353	-0.015	$\psi = 1.099$	-1.17
B-V	0.108	-0.010	$\mu = 1.042$	-0.23
V-R	0.066	-0.003	$\sigma = 0.877$	-0.23
V-I	0.107	-0.003	$\theta = 0.935$	-0.49
V-I'	0.128	-0.003	$\zeta = 0.935$	-0.81[b]

[a] From Johnson (1963)

[b] Extrapolated from Johnson's data (1963)

cause the correction error in this color term to exceed $0^m.01$, even though Spica and Mars have very different colors. This is attributable to the fact that the correction involves the product of k", $\Delta(B - V)$ for Mars minus Spica (~ 1.6 mag.), and mean air mass.

The first-order extinction coefficients, k'_v, k'_{bv}, k'_{uv}, k'_{ur}, k'_{vi}, and k'_{vi} were derived nightly by Hardie's method (Hardie 1962), where pairs of stars of differing air mass, ΔX, were observed:

$$k'_v = \frac{\Delta(v - k'_v(B - V)X) - \Delta v_0}{\Delta X}$$

$$k'_{bv} = \frac{\Delta((b - v) - k''_{bv}(B - V)X) - \Delta v_0}{\Delta X}$$

$$k'_{vr} = \frac{\Delta((v - r) - k''_{vr}(B - V)X) - \Delta v_0}{\Delta X}$$

etc. (2.2.2)

On clear nights at least two pairs of stars were observed: α Leo and γ Gem, and η Boo and β Vir. Mean values of k' are listed in Table VII although the nightly values were used in the reductions. Nightly values of k'_v varied no more than 15 per cent from the mean value, and varied much less for k'_{bv}, k'_{uv}, etc. Since Mars and Spica were rarely more than $\Delta X = 0.2$ apart, first-order extinction corrections are expected to be accurate to better than $0^m.01$.

Finally, there is the derivation of the transformation coefficients to another system. Johnson (1963) has compiled a list of V, B - V, U - B, R, and R - I for many stars. His R and I effective wavelengths are 0.68 and 0.825 μ respectively, very close to mine. I observed about 25 of these stars at small air masses and corrected their instrumental magnitudes and colors for extinction, yielding value for v_0, $(b - v)_0$,

etc. I then derived the transformation coefficients, again by a method outlined by Hardie, in the following manner:

The quantities $V - v_0$ (ordinate) vs. B - V of all stars are plotted on one graph. The slope of the curve was defined as ε, the transformation coefficient in the V-system. Then $(B - V) - (b - v)_0$ vs. B - V of all stars is plotted on another graph. The slope of this curve is equal to $1 - 1/\mu$, where μ is the transformation coefficient in B - V. Likewise, $(U - V) - (u - v)_0$ vs. U - V was plotted to derive ψ, the U - V transformation coefficient. These coefficients for all colors are listed in Table VII. The (V - I') coefficient, ζ, was assumed to equal the (V - I) coefficient, θ, for lack of a standard system in I'.

Unfortunately, the transformation plots showed considerable scatter, making the transformations uncertain. This uncertainty is magnified by the fact that the color of Mars is very different from that of Spica, since the final derivation of Martian magnitude includes a term with the product of the transformation coefficient and the color difference. The troublesome scatter in the transformation plots arose mostly from the fact that the very highest gain settings were necessary and deflections were small in many of these observations, since most stars were about fourth magnitude. As we shall see later, this problem affects only the absolute photometry of Mars (fortunately, the relative photometry--and hence the shape of the phase curve--remains intact).

The final reductions were done on the SDS 930 computer at the University of California, Space Sciences Laboratory. Apparent magnitudes of Mars were derived using the following equations (Hardie 1962), with Δ in the sense of Mars minus Spica:

$$V_{Mars} = V_{Spica} + \Delta v - k'_v X + \varepsilon\Delta(B - V) \quad ,$$

$$(B - V)_{Mars} = (B - V)_{Spica} + \mu[\Delta (b - v) - k'_{bv}\Delta X - k_{bv}\Delta(b - v)X] \quad ,$$

$$(U - V)_{Mars} = (U - V)_{Spica} + \psi[\Delta (u - v) - k'_{uv}\Delta X - k''_{uv}\Delta(u - v)X] \quad ,$$

etc. (2.2.3)

where V_{Spica}, etc., are listed in Table VII and X is the mean of the air masses of Mars and Spica.

The next step is the computation of the absolute magnitudes and colors of Mars. By definition the absolute magnitude of a planet (Harris 1961) is equal to the apparent magnitude of the fully illuminated disk reduced to unit distance from Earth and Sun, or

$$m_0 = m_{Mars} + 5 \log (rd) + \Delta m(\alpha) \qquad (2.2.4)$$

where m_0 is the absolute Martian opposition magnitude, m_{Mars} is the measured apparent magnitude of Mars, r is the planet's distance from the Sun, d is the planet's distance from Earth, and $\Delta m(\alpha)$ is the phase variation of the Martian magnitude. This phase variation is due to two factors: the fraction, f, of the illuminated disk visible from Earth, and the properties of diffuse reflection from the Martian surface and atmosphere.

In evaluating f, we must consider center-to-limb variations in Martian brightness. Limb darkening is in fact observed for Mars in the visible wavelengths (e.g., see Dollfus 1957 and Koval 1964). Lack of consideration of this would make the correction in f too large. Fortunately the derived magnitudes of Mars are virtually unaffected by this correction, since the value of f during the observations was always

greater than 0.996. This gives a maximum difference of only $0^{m}.005$ between the extreme assumptions of no limb darkening on the one hand and complete limb darkening (according to Lambert's Law) on the other hand. I assumed limb darkening according to Lambert's Law, based on previous observations.

Thus the term $\Delta m(\alpha)$ refers only to the phase variation of Martian magnitude attributable to the properties of diffuse reflection by the surface and atmosphere. We define $m_0(\alpha)$ as the phase variation of the Martian absolute magnitude, where $m_0(0°) = m_0$ and $\Delta m(0°) = 0$ so

$$m_0(\alpha) = m_0 + \Delta m(\alpha) \quad , \quad \text{or}$$

$$m_0(\alpha) = m_{Mars} + 5 \log (rd) \qquad (2.2.5)$$

Equation (2.2.5) was used to compute the Martian absolute magnitudes U, B, V, R, I, and I' for each observation.

2.3 Results

The results for the V wavelength are plotted in Fig. 10. Each curve represents the values of V during a night for every 15° in Martian rotation, where λ_c is the central Martian longitude of each observation. The dashed curve indicates the light curve of Martian rotation in the V wavelength from observations in 1954 at Lowell and McDonald Observatories (Harris 1961). Since this dashed curve was taken from observations made at some α different from my observations, its zero point does not play a significant role in Fig. 10. Each symbol represents a different night or α of observation. The effect of change of α during a night is neglected, since such changes were no greater than 0°.1.

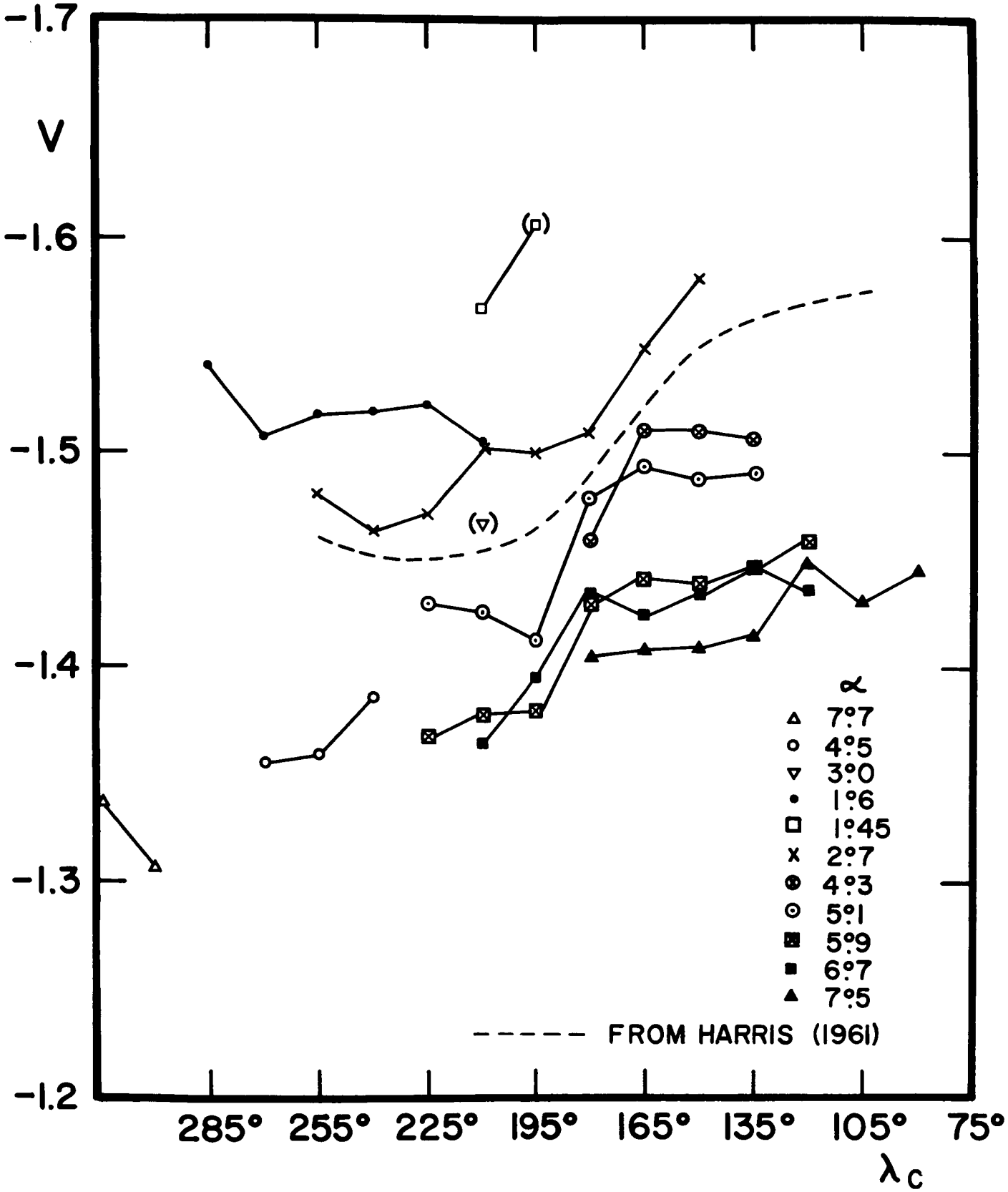

Fig. 10. Variations of the absolute visual magnitude (uncorrected for transformation errors) of the Martian disk with rotation for various phase angles during the 1967 opposition. The symbol λ_c denotes the central Martian longitude for each observation.

Figure 11 shows a phase curve in V plotted for $\lambda_c = 210°$. The best curve drawn through the points definitely shows an opposition effect, where the slope, a, of the phase function is typically 0.035 mag./deg. The rest of the phase function has been reported as linear with a = 0.015 mag./deg. (de Vaucouleurs 1964). The mean residual from the drawn curve is ~ 0.015. This scatter is small in view of the fact that each point represents only one or two observations of Mars and Spica.

The closed circles in the phase curve of Fig. 11 and all phase curves presented thereafter are those Kitt Peak observations before opposition, while the crosses are those Kitt Peak observations after opposition. Points in parentheses are observations made on cloudy nights where the deflections are somewhat inconsistent. Open circles are the results of the Chilean observers, whose point at $\alpha = 1.^{\circ}6$ on April 14th was normalized to my point at $\alpha = 1.^{\circ}6$. This normalization was essential because of large zero-point differences in our two photometric systems. This point will be discussed later in this section. Numbers next to each point represent the U.T. date of observation in April 1967.

A phase curve deduced from several λ_c's is more significant than that deduced from only one λ_c, since we can average many observations made each night. This procedure of averaging over a Martian rotation assumes that the shape of the rotation curve is independent of α in the observed range of α, i.e., that the Martian bright and dark areas exhibit approximately the same phase functions and opposition effects. We shall see in Section 2.4 that this assumption is valid for the whole-disk photometry.

In order to make use of observations at all λ_c for at a given α, the following procedure suggested by Dr. Ivan King, was adopted: take

Fig. 11. Variation of the absolute visual magnitude (uncorrected for transformation errors) of the Martian disk with phase for a central Martian longitude of 210° during the 1967 opposition. The abbreviations K.P. and C.T. represent the Kitt Peak and Cerro Tololo observations, respectively. The U.T. data are indicated beside each point. The point in parentheses represents a marginal observation made on a cloudy night.

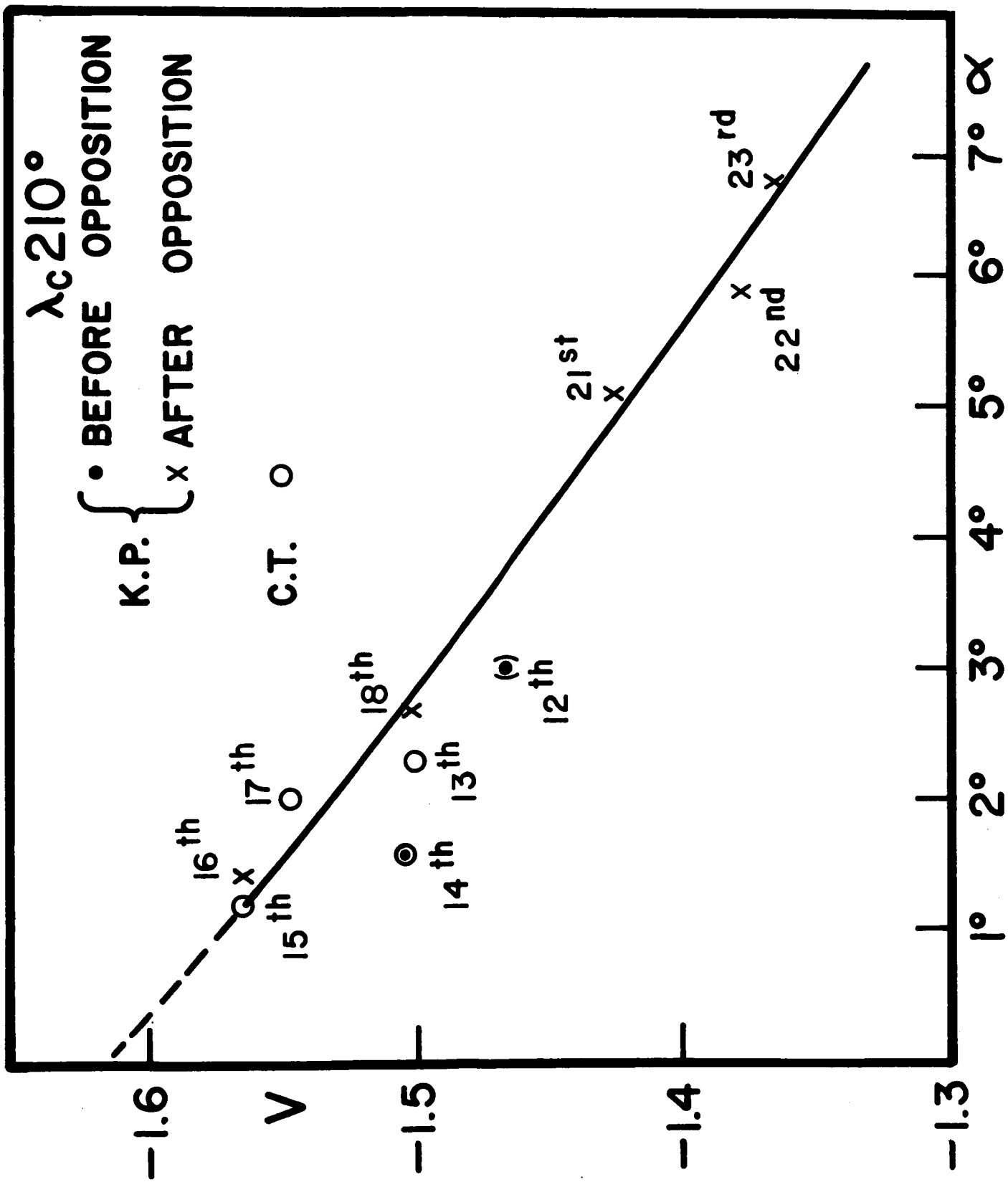
λc 210°
• BEFORE OPPOSITION
x AFTER OPPOSITION
K.P.
C.T.
V
α
−1.6
−1.5
−1.4
−1.3
1°
2°
3°
4°
5°
6°
7°
15th
16th
17th
18th
14th
13th
12th
21st
22nd
23rd

the dashed rotation curve of Fig. 10, trace the points of each night while shifting the zero of the dashed curve to minimize the residuals of each night. With the mean values of points within each λ_c, we can now define a reliable mean rotation light curve of Mars, Fig. 12. So, for a given night the zero shift plus the sum of the night's deviations from this newly defined rotation curve yields a mean magnitude for that night. The resultant phase curve is shown in Fig. 13, where the mean residual from the drawn curve is $0^m.015$.

This error scatter is partly due to the fact that the rotation curve for some longitudes is now well defined, e.g., only one night's observation was made at each of $\lambda_c = 285°$, 105°, and 90°. For this reason it was decided in the final analysis to consider only those points at $\lambda_c =$ 225°, 210°, 195°, 165°, 150°, and 135°. Several observations were made at each of these values of λ_c so that we have a well-defined rotation light curve in this region (most data come from observations at these six values of λ_c). Moreover, the first three longitudes represent consistently low brightness values for Mars because of the presence of the dark areas Syrtis Major, Mare Tyrrhenum, and Mare Cimmerium, while the last three longitudes represent consistently high brightness for Mars because of the presence of the deserts Amazonis, Arcadia, and Nix Olympia. Taking nightly mean deviations from the mean rotation curve for these six λ_c's, we have the values of m_0 tabulated in Table VIII and plotted in Figs. 14 to 19. Figure 16 shows that the mean error from the drawn curve is $0^m.011$, so this procedure of selecting the most-often observed λ_c reduces the error scatter. Furthermore, the actual values of the magnitudes are expected to be close to the average of Mars, since three of the λ_c's emphasize dark areas and the other three λ_c's emphasize bright

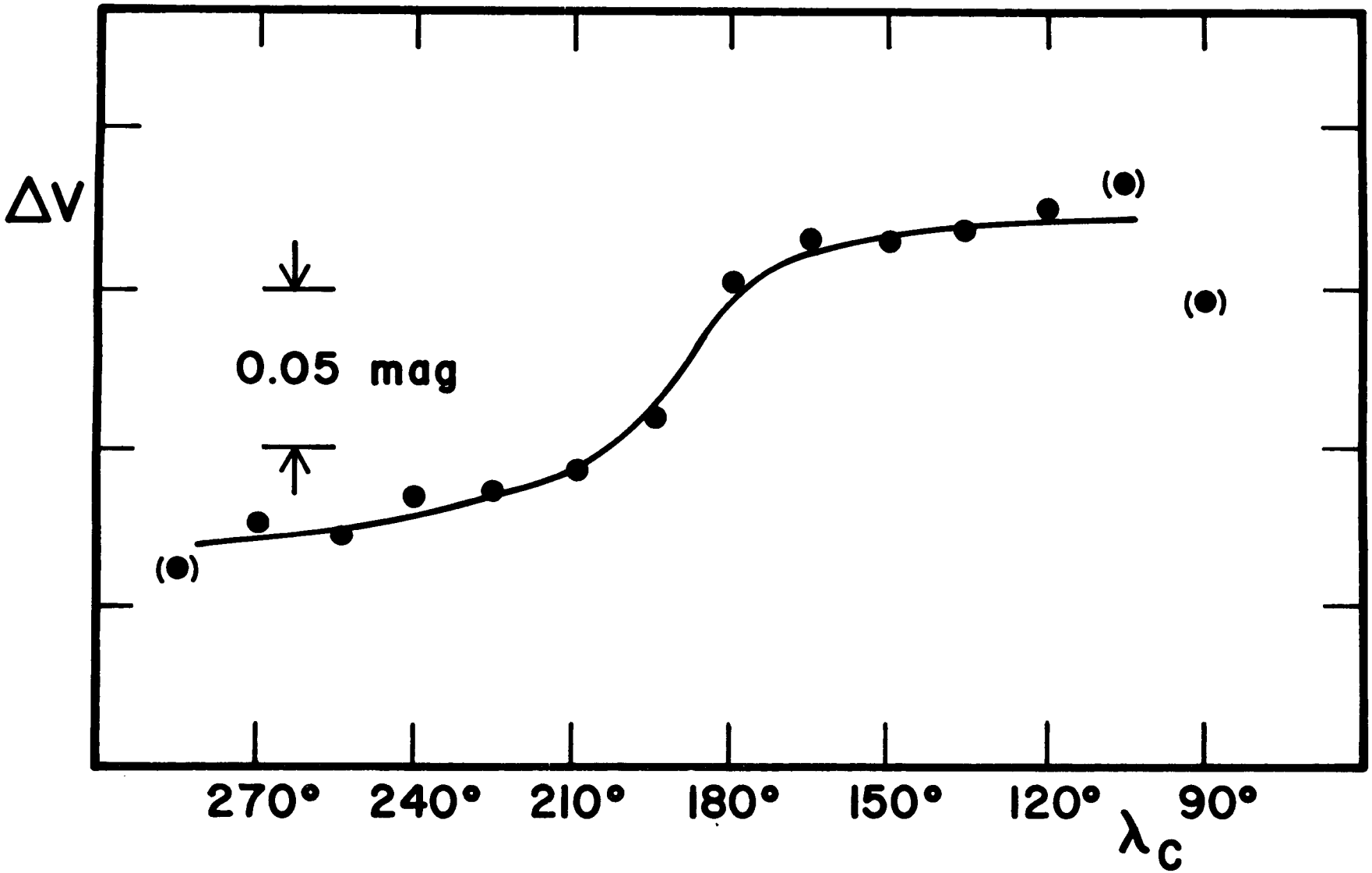

Fig. 12. Variation of the visual magnitude of the Martian disk with rotation during the 1967 opposition. All points, except those in parentheses, represent an average of observations made at two or more phase angles.

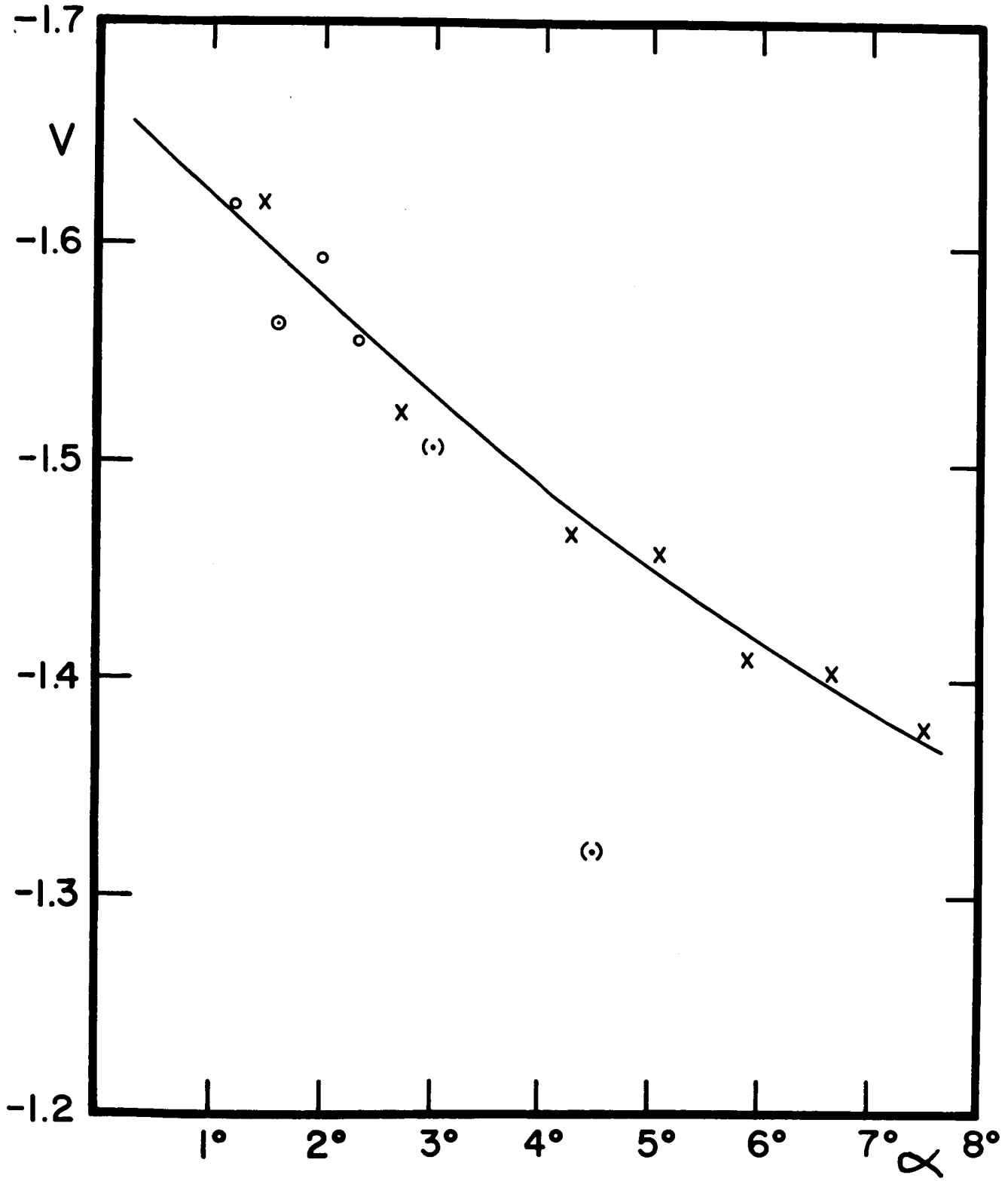

Fig. 13. Variation of the absolute visual magnitude (uncorrected for transformation errors) of the Martian disk with phase during the 1967 opposition. Each point represents an average over all observed position of rotation of Mars (see text). Point symbols follow the nomenclature of Fig. 11.

TABLE VIII

MEAN ABSOLUTE MAGNITUDES OF MARS

(Corrected for rotation effects but uncorrected for Transformation Errors)

Date U.T., 1967	Phase Angle, a	Observatory[a]	U	B	V	R	I	I'
April 10	4°.5	K. P.	.583	-.158	-1.404	-2.067	-2.469	-2.445
12	3°.0	K. P.	.555	-.268	-1.498	-2.199	-2.681	-2.651
13	2°.3	C. T.	.493	-.278	-1.536	---	---	---
14	1°.6	K.P., C.T.	.496	-.275	-1.544	-2.302	-2.612	-2.605
15	1°.2	C. T.	.460	-.327	-1.598	---	---	---
16	1°.45	K. P.	.468	-.307	-1.598	-2.359	-2.666	-2.671
17	2°.0	C. T.	.470	-.299	-1.575	---	---	---
18	2°.7	K. P.	.568	-.252	-1.528	-2.312	-2.622	-2.633
20	4°.3	K. P.	.620	-.201	-1.475	-2.262	-2.588	-2,607
21	5°.1	K. P.	.602	-.181	-1.455	-2.261	-2.590	-2.606
22	5°.9	K. P.	.671	-.115	-1.408	-2.217	-2.542	-2.566
23	6°.7	K. P.	.665	-.112	-1.407	-2.221	-2.571	-2.578
24	7°.5	K. P.	.737	-.087	-1.378	-2.201	-2.508	-2.562

[a] K. P. = Kitt Peak National Observatory, Tucson, Arizona; C. T. = Cerro Tololo Inter-American Observatory, Chile

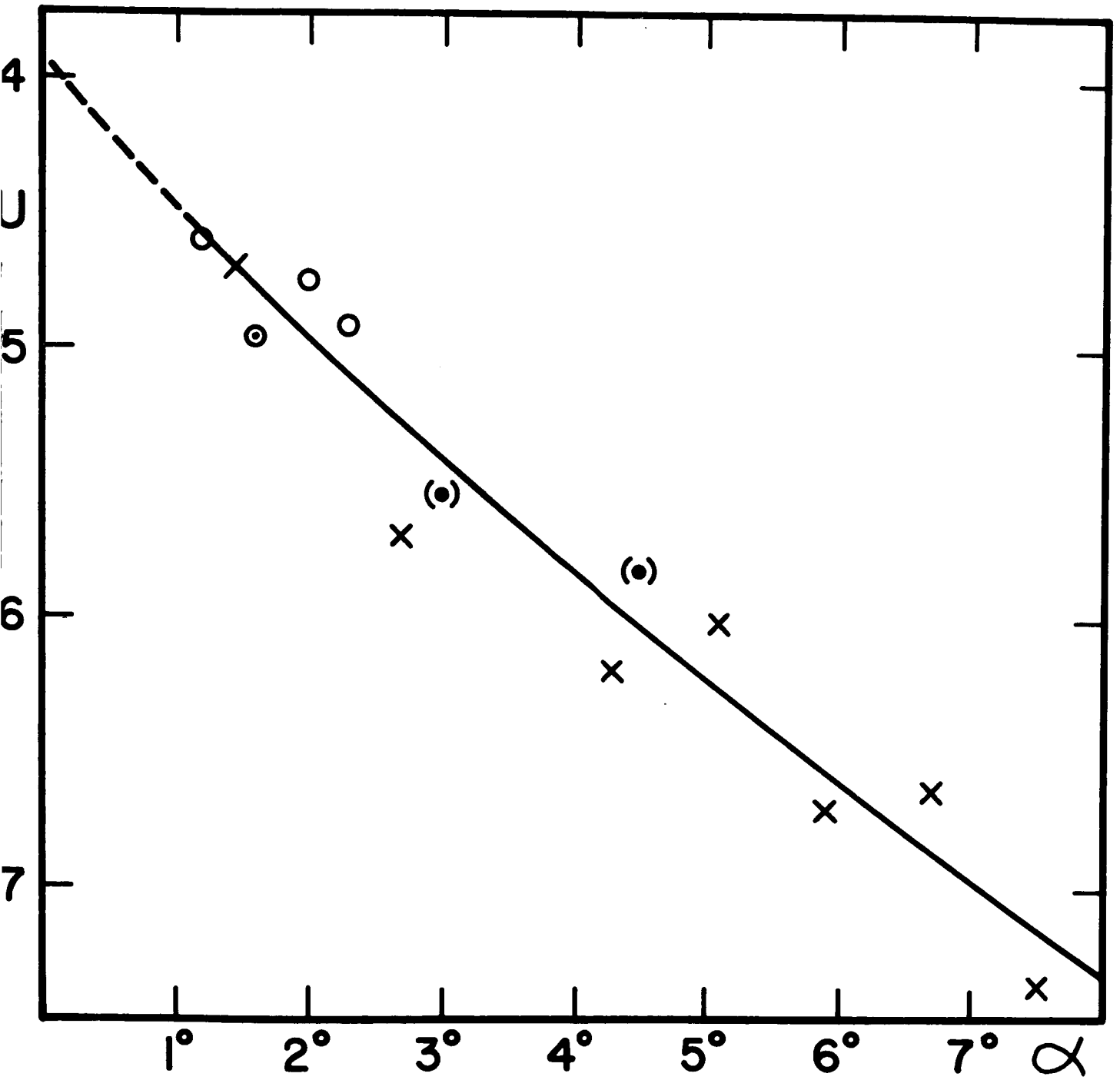

Fig. 14. Variation of the absolute magnitude (uncorrected for transformation errors) of the Martian disk with phase at $\lambda = 0.36\ \mu$ during the 1967 opposition. Each point represents an average of the most-often observed positions of rotation of Mars (see text). Point symbols follow the nomenclature of Fig. 12.

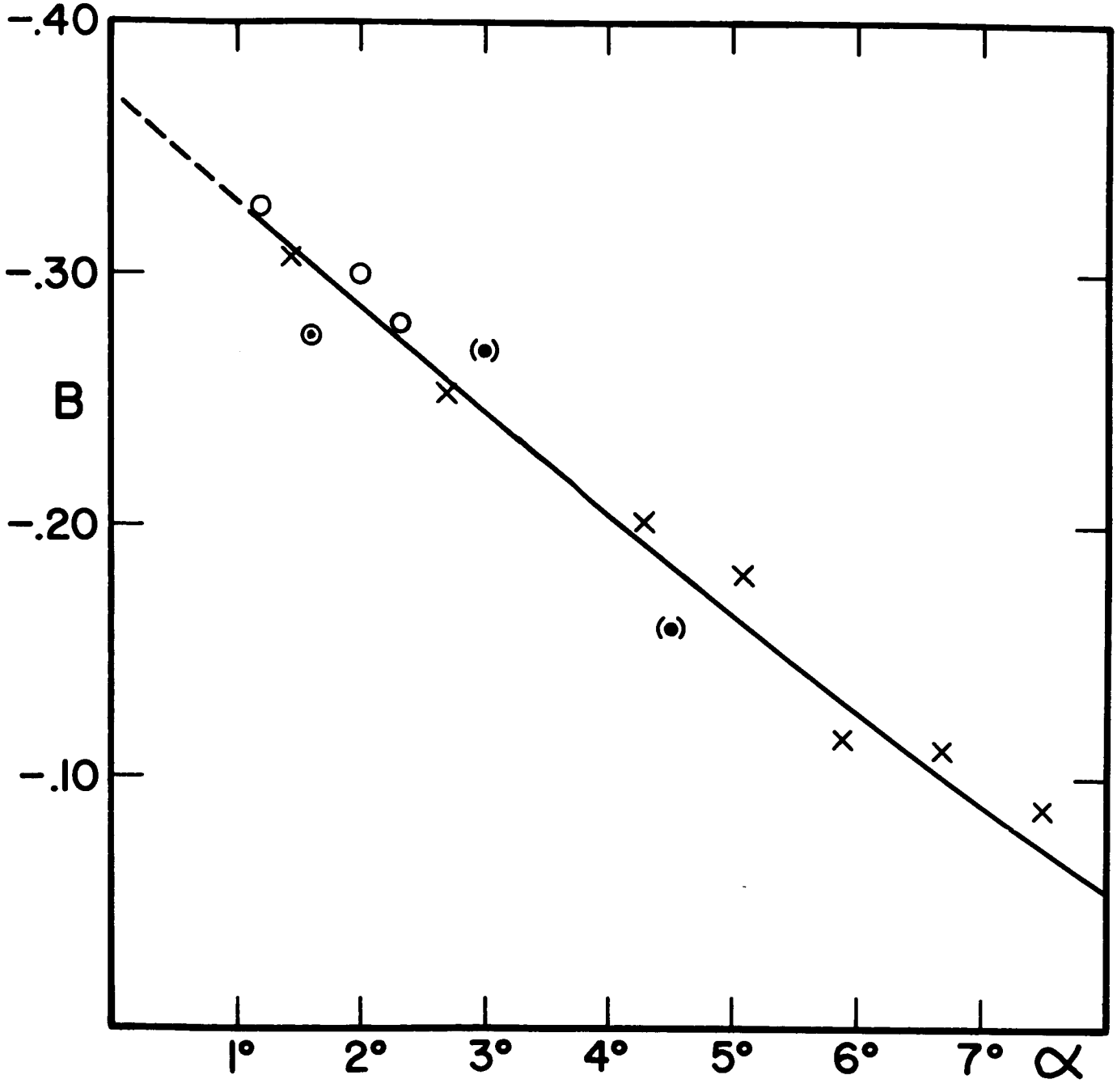

Fig. 15. Same as Fig. 14, except $\lambda = 0.43\ \mu$.

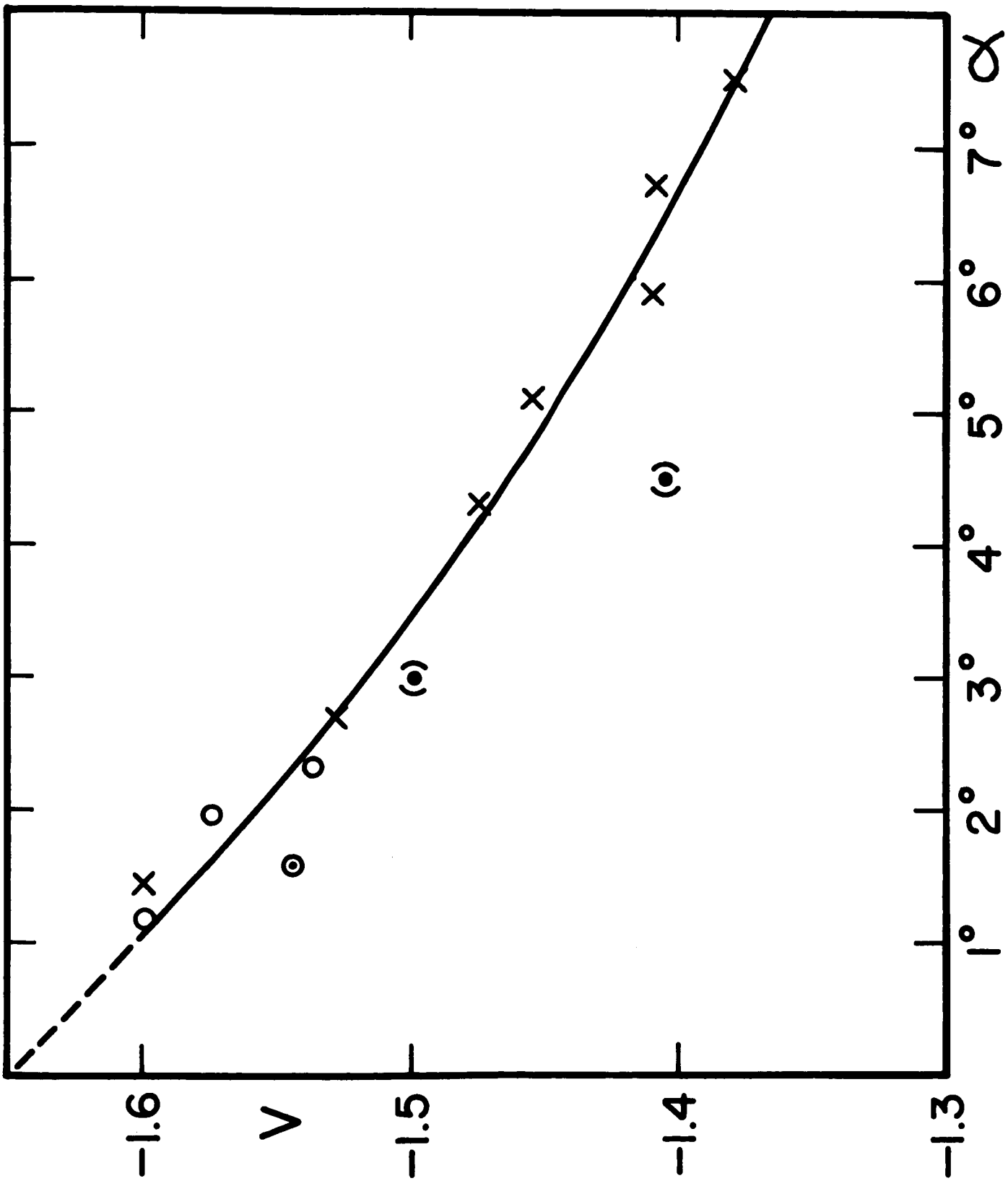

Fig. 16. Same as Fig. 14, except $\lambda = 0.55\ \mu$.

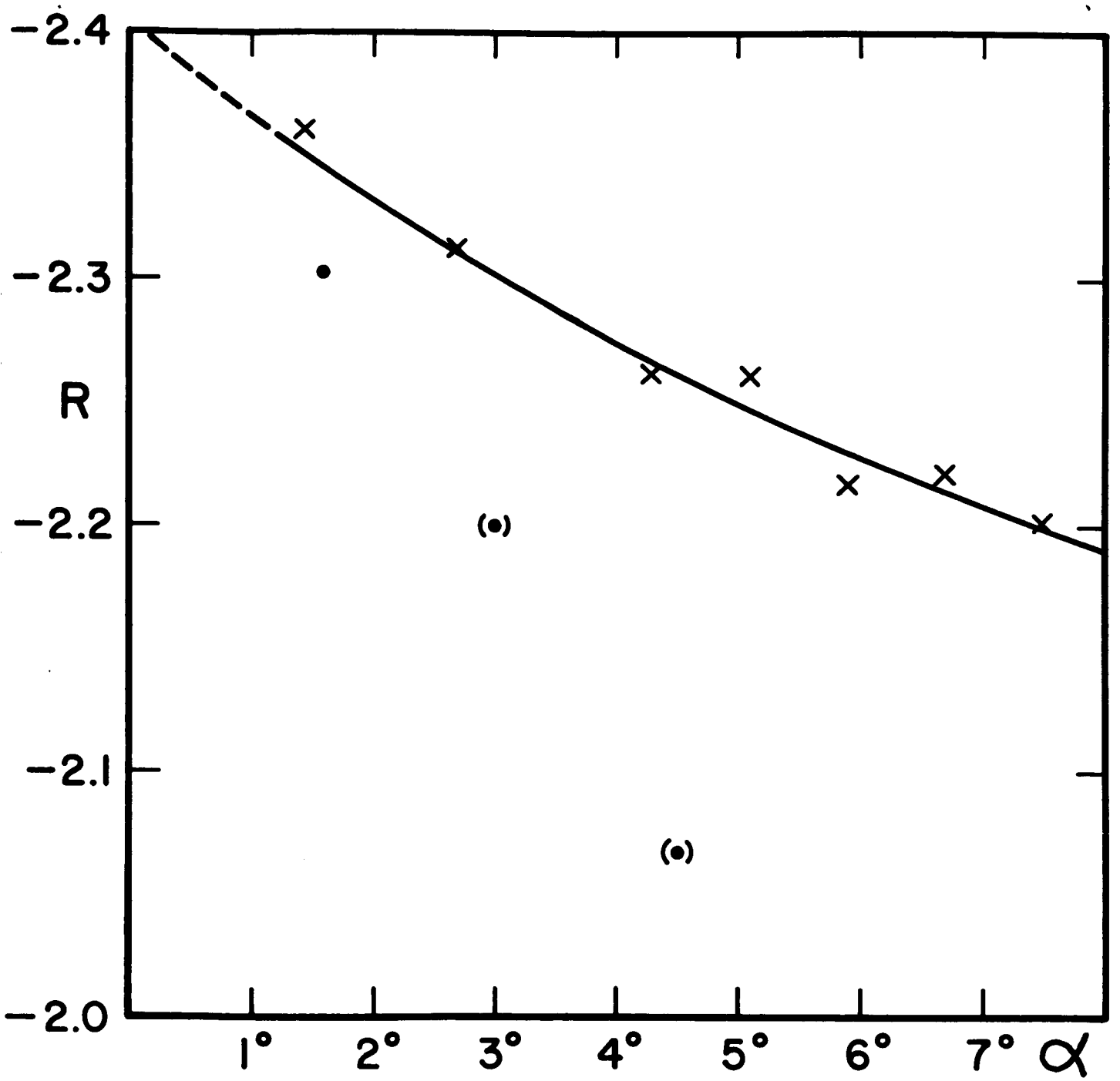

Fig. 17. Same as Fig. 14, except $\lambda = 0.67\ \mu$.

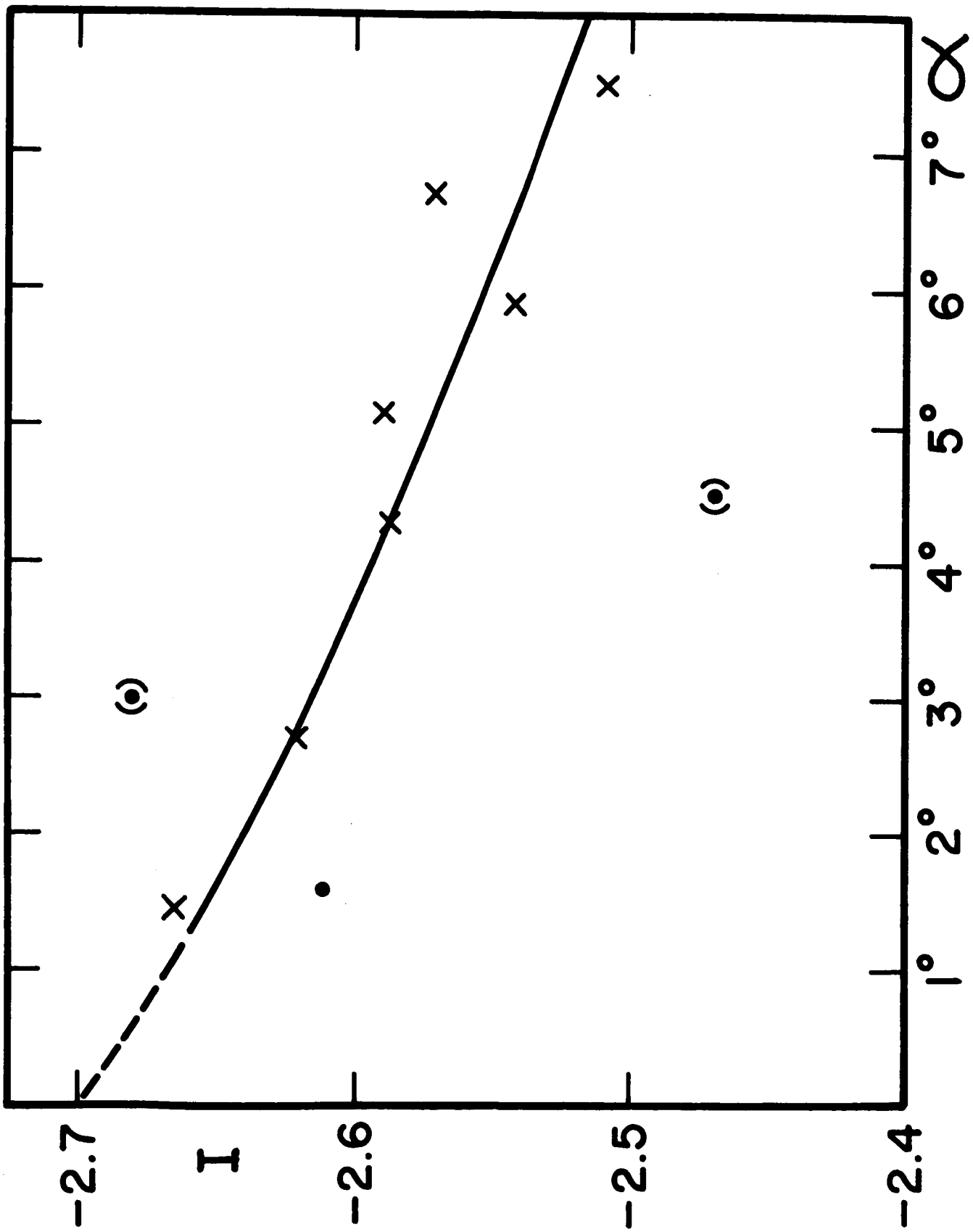

Fig. 18. Same as Fig. 14, except $\lambda = 0.83\ \mu$.

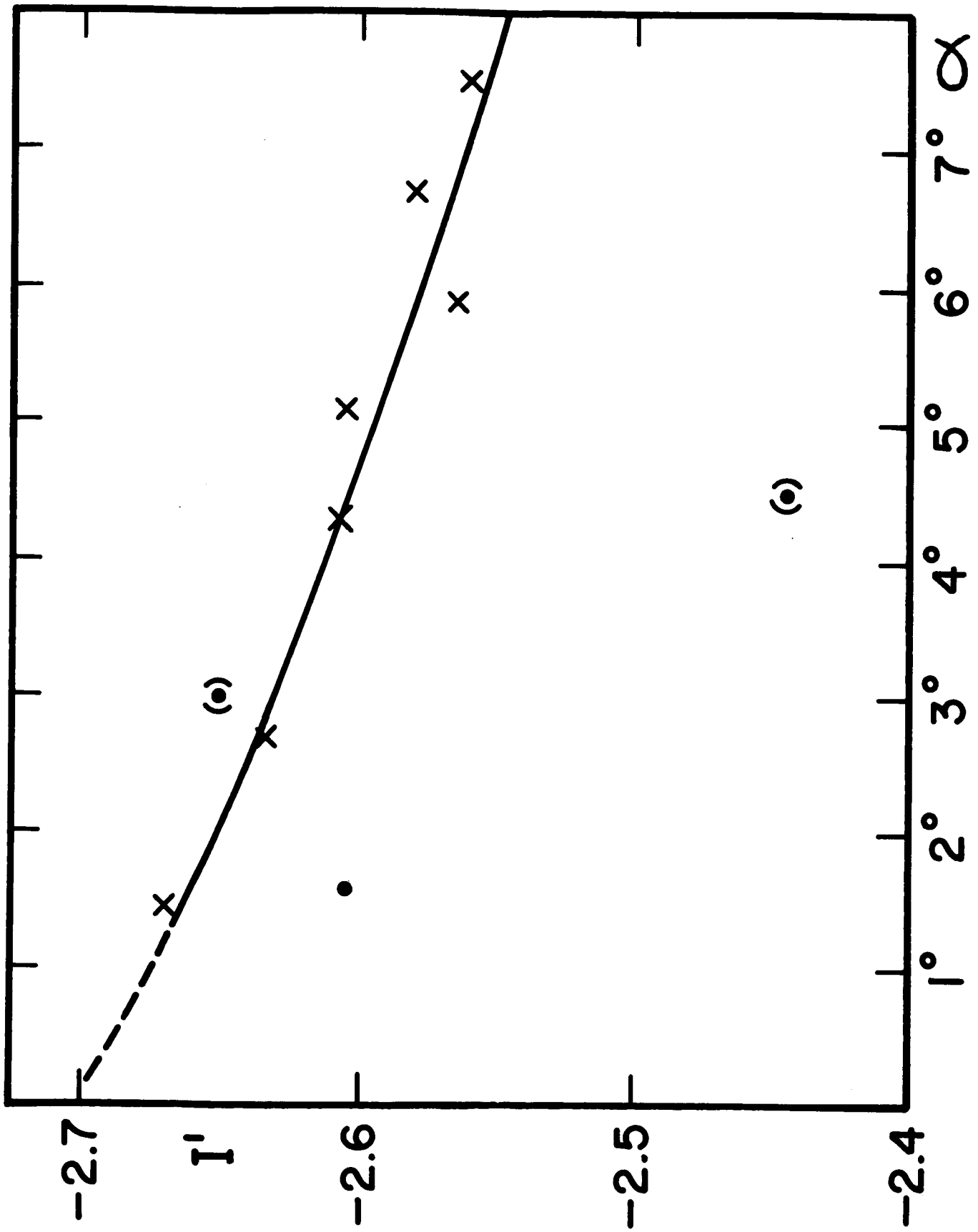

Fig. 19. Same as Fig. 14, except λ = 1.04 μ.

areas. Regardless of the method used for deriving the phase curve, the best fit for a smoothed phase curve is well established in any of Figs. 11, 13, and 16 (each Figure resulting from a different method for deriving V for Mars).

The Chilean data show more error scatter than the Kitt Peak data for two reasons: photomultiplier tube fatigue and fewer observations (only one or two) of Mars per night. However, the error scatter for both sets of data is small enough to define well the shapes of the phase curves.

Extrapolating the curves in Figs. 14 to 19 to $\alpha = 0°$, we have the absolute 1967 opposition magnitudes for Mars. These values in terms of V-magnitude and colors, along with those derived from the Chilean data, are listed in Table IX. For comparison the mean opposition magnitudes and colors af Mars are also listed with the assumption that a linear phase function may be extrapolated to zero phase. This assumption has been invoked in previous evaluations of Martian m_0 (Harris 1961 and de Vaucouleurs 1964).

It is noted from Table IX that the discrepancies in zero-point between the data are large, greater than would be expected in spite of an opposition effect and anticipated seasonal and secular magnitude and color changes on Mars (de Vaucouleurs 1964). The zero-point discrepancies between the Kitt Peak and Chilean data are themselves disturbing.

This problem is obviously due to large transformation errors. Let us say, for example, the value of ψ is in error by 5 per cent, which is very plausible in view of the error scatter in standard star observations. The third expression in eq. (2.2.3) shows three terms in ψ. One involves its product with $\Delta(U - V) = 3.11$ between Mars and Spica. Thus, a 5 per cent error in ψ would mean a 0.15 error in the zero point of my magnitude

TABLE IX

Visual Magnitude and Colors of Mars at Opposition

	V	U-B	B-V	V-R	R-I
Kitt Peak (1967) uncorrected for zero-point errors	-1.65	0.76	1.28	0.76	0.29
Cerro Tololo (1967) uncorrected for zero-point errors	-1.83	0.53	1.41	--	--
Mean of Previous Observations with Extrapolated Linear Phase Function[a]	-1.52	0.63	1.33	1.12	0.38
Present observations, shifted in zero-point to fit previous observations for	-1.73	0.59	1.27	1.04	0.35

[a]From de Vaucouleurs (1964)

system. On the other hand, the other two terms involve products of ψ with the variables k'_{uv}, k''_{uv}, ΔX, and X. These two terms are negligibly small even for the hypothetical 5 per cent error in the transformation coefficient, so problems arise only in the zero point of the magnitude system and not the shape of the phase curve.

Similarly, zero-point errors probably occurred in the Chilean photometry because of the phototube fatigue and the reduced voltage.

Because of thsee zero-point errors and the fact that opposition magnitudes and colors of Mars have been observed to change intrinsically from apparition to apparition (Harris 1961 and de Vaucouleurs 1964), it was decided to fit the Kitt Peak and Chilean observations to the mean data of de Vaucouleurs (1964). This was done in the following way: extrapolate the smoothed Martian phase curves of Figs. 14 to 19 from my data for $\alpha < 8°$ in such a way as to coincide eventually with the quoted linear phase curve (de Vaucouleurs 1964). The resultant phase curves are shown in Fig. 20. The zero points of the magnitudes are then established from de Vaucouleurs' value of m_0, the absolute magnitude of Mars at mean opposition derived from extrapolating the mean linear phase function for $\alpha \gtrsim 10°$ to zero phase.

Unfortunately, the opposition effect of Mars starts at $\alpha > 5°$ unlike the case of the Moon. This discrepancy is especially pronounced at shorter wavelengths. However, the smoothed phase curve for $\alpha < 8°$ closely approximates a curving quadratic expression. Thus the vertical displacement of the assumed linear phase function with which the extrapolated quadratic curve eventually coincides is in doubt by no more than $0^m.01$. This assumes no large anomalies in the Martian phase curves between $\alpha = 8°$ and $15°$. This is not expected since all previously observed Martian phase curves

Fig. 20. The Martian opposition effect in six colors fitted to the linear phase functions for $\alpha \gtrsim 10°$ reported by de Vaucouleurs (1964). Values for the absolute magnitudes (the ordinates on left sides of the figures) of Mars are corrected for transformation errors. Reflectivities normalized to geometric albedoes (derived in text) are shown as the ordinates on the right sides of the figures.

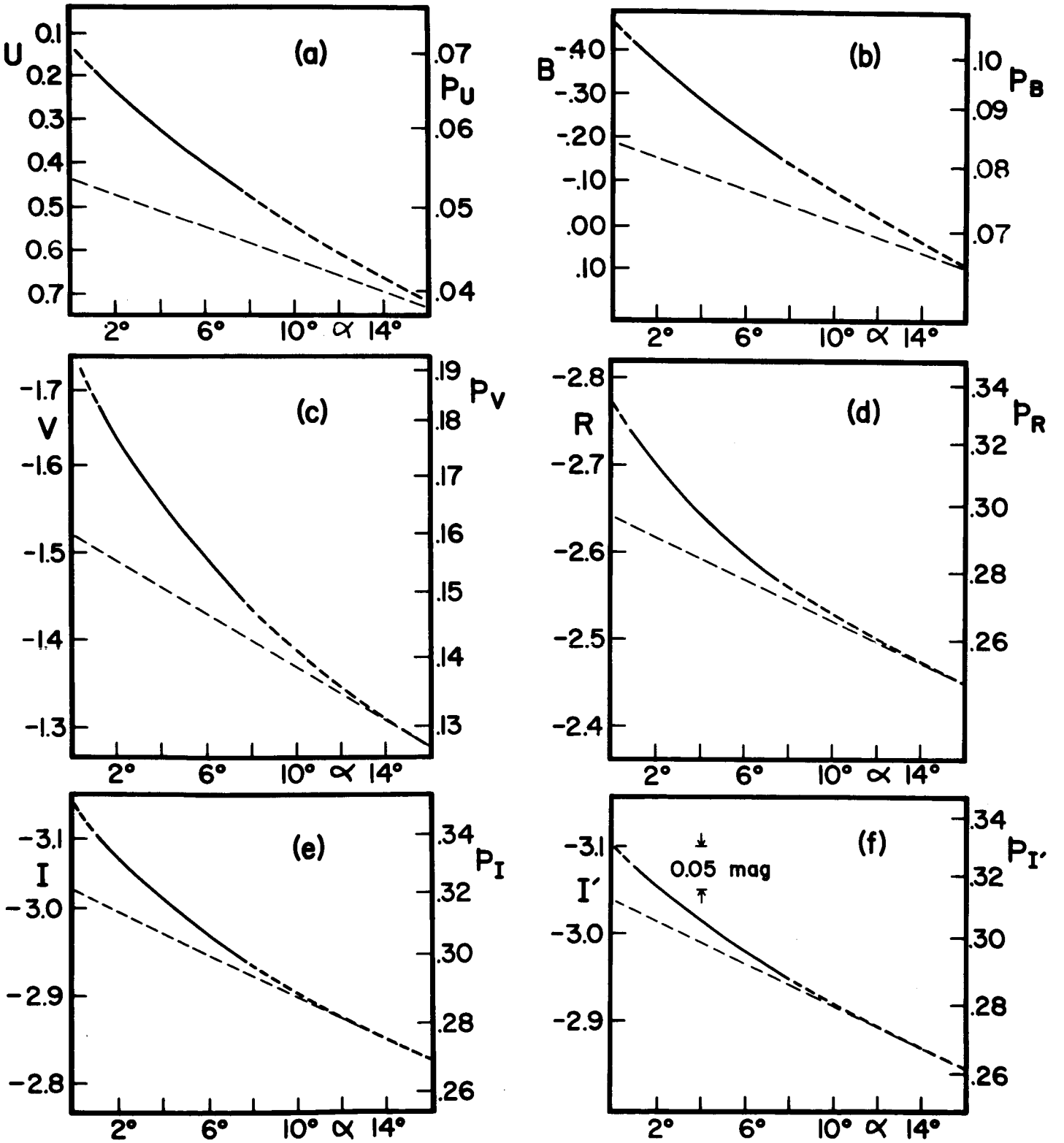
U
0.1
0.2
0.3
0.4
0.5
0.6
0.7
(a)
.07
.06
.05
.04
P_U
2°
6°
10°
α
14°
B
-.40
-.30
-.20
-.10
.00
.10
(b)
.10
.09
.08
.07
P_B
2°
6°
10°
α
14°
V
-1.7
-1.6
-1.5
-1.4
-1.3
(c)
.19
.18
.17
.16
.15
.14
.13
P_V
2°
6°
10°
α
14°
R
-2.8
-2.7
-2.6
-2.5
-2.4
(d)
.34
.32
.30
.28
.26
P_R
2°
6°
10°
α
14°
I
-3.1
-3.0
-2.9
-2.8
(e)
.34
.32
.30
.28
.26
P_I
2°
6°
10°
α
14°
I′
-3.1
-3.0
-2.9
0.05 mag
(f)
.34
.32
.30
.28
.26
$P_{I'}$
2°
6°
10°
α
14°

are approximately linear with slopes not too different from those observed near $\alpha = 8°$ (although U and B still have steep slopes near $\alpha = 8°$).

Another zero point error arises from deviations from the assumed slope, a, of the linear phase function. de Vaucouleurs (1964) reported the observed values for a for wavelengths between $\lambda = 0.36\ \mu$ and $0.7\ \mu$. This error probably does not exceed 0.001 mag./deg., so the resultant error in the zero point should be about $0^m.01$. The value for a at $0.82\ \mu$ and $1.04\ \mu$ was assumed to be $0^m.012$, the value at $0.70\ \mu$. If a varies inversely with albedo, the fact that the Martian albedo changes little for $\lambda > 0.7\ \mu$ probably makes this value for a not unreasonable for $0.82\ \mu$ and $1.04\ \mu$.

One more possible error in the evaluation of the mean Martian opposition magnitude is the assumed extrapolation of the curving phase function for $\alpha < 1°.2$. Again the error in this extrapolation should not exceed $0^m.01$, barring anomalies.

Thus, the zero point errors in the new values for absolute magnitudes for Mars are probably less then $0^m.03$. These magnitudes (m_0) are listed in Table X (with colors listed in the last line of Table IX), and constitute a drastic revision in the opposition magnitudes of Mars. Details of the results will be discussed in the next section.

The next step is the calculation of revised geometric albedoes of Mars. This revision consists of two steps: one regarding more recent values of the Martian radius and of the solar magnitude; the other regarding the opposition effect. The geometric albedo of a planet can be defined by the following expression (Harris 1961):

TABLE X

Corrected Photometric Parameters of Mars[a]

Band $\lambda_e(\mu)$	U 0.355	B 0.450	V 0.555	R 0.70	I 0.82	I' 1.04
m_0	0.13 (0.44)	-0.46(-0.19)	-1.73 (-1.52)	-2.77 (-2.64)	-3.12 (-3.02)	----
m_s	-25.97	-26.11	-26.74	-27.19	-27.48	----
$\underline{a}$ ($\alpha = 1°$)						
$\underline{a}$ ($\alpha = 2°$)						
$\underline{a}$ ($\alpha = 6°$)						
$\underline{a}$ ($\alpha \gtrsim 15°$)						
p	0.071 (0.053)	0.107 (0.084)	0.194 (0.160)	0.334 (0.296)	0.352 (0.321)	~0.342 (0.312)
q	0.692 (0.94)	0.719 (0.94)	0.881 (1.07)	1.152 (1.30)	1.185 (~1.30)	1.230 (~1.30)
A	0.050	0.079	0.171	0.385	0.417	0.406

[a] Values in parentheses are those derived from extrapolation of linear phase functions with slopes $\underline{a}$ ($\alpha \gtrsim 15°$)

$$\log p = 0.4\ (m_s - m_o) - 2 \log R/R_E + 8.741 \qquad (2.3.1)$$

where p is the geometric albedo, or the "ratio of the average luminance of the planet at full phase ($\alpha = 0°$) to that of a perfectly diffusing surface (Lambert surface) at the same distance from the Sun and normal to the incident radiation" (de Vaucouleurs 1964); m_s is the apparent magnitude of the Sun; R is the mean radius of the planet; and R_E is the mean radius of the Earth. The two least known quantities in this expression (besides m_o which we have seen is revised in this work) are R of Mars and m_s.

The Mariner IV occultation experiment (Kliore, Cain, and Levy 1966) produced the following values for the radius of Mars: 3379 km ± 4 km at 60° N latitude (Mare Acidalium) and 3384 km ± 3 km at 50° S latitude (Electris, Mare Chromium). From these observations, we can say that the mean radius of Mars is ~ 3385 km ± 10 km, so $R/R_E = 0.532 \pm 0.001$. This error is very small and will affect the value of p negligibly. I have assumed that the apparent mean radius of Mars does not change with wavelength, i.e., any radius defined by the Martian atmosphere at $\lambda < 0.47\ \mu$ is equal to that defined by the Martian surface in the red. It is not clear yet whether this is true; for example, de Vaucouleurs (1964) adopted a 1 per cent increase in radius from the red to blue after a careful review of the data. Recent measurements by Dollfus (1965), however, show no difference in radii from red to blue. In either case, only small errors in derifed albedoes (~ ± 0.004) would result from adopting the wrong assumption.

The value of m_s is considerably more uncertain. Harris (1961) and de Vaucouleurs (1964) found that V_s (visual magnitude of the Sun) was

- 26.81. On the other hand, a recent review of determinations of V_s by Johnson (1965), including more modern results, gave $V_s = - 26.74 \pm 0.01$ p.e. Using $V_{Mars} = - 1.52$, the visual absolute mean opposition magnitude of Mars deduced from a linear phase function (Harris 1961 and de Vaucouleurs 1964), the derived geometric albedo, p_V, becomes 0.160. The value is 0.011 higher than that derived by de Vaucouleurs, because of the lower solar brightness obtained from more recent data available to me.

As for the other colors, I used the colors of the sun listed by de Vaucouleurs (1964) and Harris (1961): U - B = + 0.14, B - V = + 0.63, V - R = + 0.45, and R - I = + 0.29. These values should not be in error by as much as the V magnitude, since it is expected that the primary error in measuring solar mangitudes is the location of the zero-point in magnitude and not in color for a given instrumental system, provided the transformations to the standard system are well known. Also, my color transformations for Mars are being made to the effective wavelengths listed by de Vaucouleurs.

Resultant values for m_s and p are listed in Table X. The value for p_I, deserves further explanation, since magnitudes for Mars and the Sun at 1.04 μ are not given. Infrared reflectivity curves for Mars have been recently published by Younkin (1966) and Tull (1966). Both authors observed a slight reflectivity drop from 0.82 μ to 1.04 μ such that $p_{I'} \sim 0.97\ p_I$, a relation I assumed in deriving $p_{I'}$.

It is then possible to construct scales of geometric albedoes along the ordinates in Figs. 20 from equation (2.3.1). For example, V = - 1.52 corresponds to $p_V = 0.160$ in the case of extrapolated linear phase function, and V = - 1.73 to $p_V = 0.194$ in the case of the opposition effect (Table IX). It is seen that the geometric albedoes of Mars are considerably higher than

previously thought because of the opposition effect. These new phase curves are redrawn in Fig. 21 in terms of reflectivity, where all reflectivities are referred to the revised values of p at $\alpha = 0$.

Other quantities must also be revised. The spherical albedo (or Bond albedo) $A = p\,q$ is the ratio of the total luminous flux reflected by a sphere in all directions to the total flux intercepted by it in a beam of parallel light, where the phase integral q is defined as

$$q = \int_0^{2\pi} \Phi(\alpha) \sin \alpha \, d\alpha \qquad (2.3.2)$$

or, for a symmetric phase function,

$$q = 2\int_0^{\pi} \Phi(\alpha) \sin \alpha \, d\alpha \qquad (2.3.3)$$

where $\Phi(\alpha)$ is the phase function of Martian brightness normalized to unity at $\alpha = 0$. Since q is difficult to define for a planet whose α does not exceed 47° as seen from earth, only estimates of Martian q are possible. de Vaucouleurs (1964) discussed two methods: (1) direct integration of (2.3.3), which is extrapolated from $\alpha = 47°$ to 180° with the assumptions that the Martian phase function has nearly the same relation as the Earth's phase function in the interval $10° \leq \alpha \leq 40°$ and (2) from the Russell rule which states that $q = 2.20\ \Phi(50°)$, thus requiring only a slight extrapolation of the Martian phase curve. With a linear Martian phase function, the similarity in results from the two methods was reassuring to de Vaucouleurs (1964): $q_V = 1.076$ by method (1) and $q_V = 1.060$ by method (2). The procedure must be repeated in this case, however, since $\Phi(\alpha)$ is not linear for $\alpha \leq 10°$ as de Vaucouleurs had assumed. The new values in V are tabulated in Table XI. Also listed in

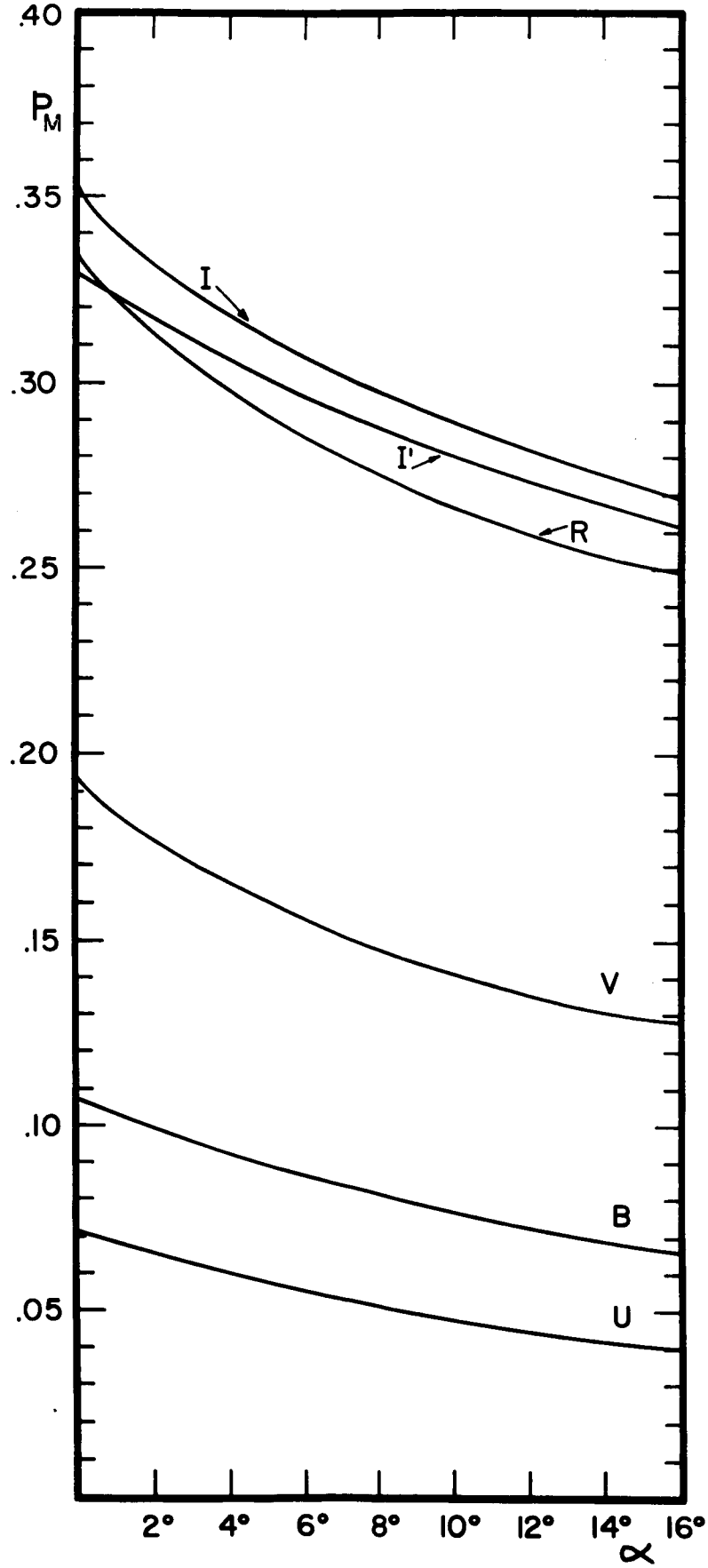

Fig. 21. The Martian opposition effect in six colors in terms of reflectivities normalized to the geometric albedoes.

TABLE XI

Martian Phase Integral in the V Filter [a]

α	ΔV	$\Phi(\alpha)$	$\Phi(\alpha) \sin \alpha$	Φ_0	Φ/Φ_0
0°	0.00	1.000	0.000	1.000	1.000
5°	0.21	0.824	0.072	0.994	0.829
10°	0.34	0.731	0.127	0.985	0.742
20°	0.51	0.625	0.214	0.943	0.709
30°	0.66	0.545	0.272	0.881	0.619
40°	0.81	0.474	0.305	0.800	0.593
50°	(1.00)	(0.398)	(0.305)	0.709	(0.561)
60°	(1.20)	(0.331)	(02.87)	0.591	(0.560)
70°	(1.41)	(0.273)	(0.257)	0.508	(0.537)
80°	(1.64)	(0.221)	(0.218)	0.410	(0.539)
90°	(1.91)	(0.172)	(0.172)	0.318	(0.541)
100°	(2.22)	(0.129)	(0.127)	0.236	(0.547)
110°	(2.55)	(0.095)	(0.089)	0.166	(0.573)
120°	(2.90)	(0.069)	(0.060)	0.110	(0.627)
130°	(3.30)	(0.048)	(0.037)	0.065	(0.738)
140°	(3.76)	(0.031)	(0.020)	0.034	(0.912)
150°	(4.26)	(0.020)	(0.010)	0.015	(1.33)
160°	(4.77)	(0.012)	(0.004)	0.005	(2.40)
170°	(5.3)	(0.008)	(0.001)	0.001	(8.0)

[a] See text for explanation of these values in parenthesis.

2.20 $\Phi(50°) = 0.876$ (Russell Rule)

$$\int_0^{2\pi} \Phi(\alpha) \sin \alpha \, d\alpha = 0.868$$

Table XI is the Martian $\Phi(\alpha)$ relative to the phase function $\Phi_0(\alpha)$ of a purely diffusing (Lambert) surface. I have made the same assumptions as de Vaucouleurs about the extrapolation of the phase curve for $\Phi > 47°$. I obtained $q_V = 0.868$ by direct integration and $q_V = 0.876$ by the Russell rule, in good agreement. The product of q_V and p_V forms the visual bond albedo: $A_V = 0.169$. On the other hand $A_V = 0.171$ from the product of q_V and p_V assuming an extrapolated linear phase function. The values of these quantities are listed in Table X. Their derivation and interpretation are further discussed in the next section.

2.4 Discussion

Thus far, it is evident from the discussion that there is definitely a Martian opposition effect in all colors, that the observed linear phase function for $10° \leq \alpha \leq 40°$ cannot be extrapolated linearly to $\alpha = 0°$, and that many fundamental photometric parameters of Mars must be revised. Table X succinctly summarizes these results.

The opposition effect is the most obvious explanation of the observation reported by Harris (1961, p. 279): ". . . on May 3-4, 1952 ($\alpha = 2\overset{\circ}{.}5$) . . . the ultraviolet magnitude of Mars was 0.3 mag. brighter, the blue magnitude about 0.2 mag. brighter, and the visual magnitude 0.1 mag. brighter than average." My observations show Mars at $\alpha = 2\overset{\circ}{.}5$ to be 0.23, 0.21, and 0.13 mag. brighter than the extrapolated linear phase functions for the U, B, and V filters, respectively (Fig. 20). The opposition effects for the 1952 and 1967 apparitions are thus in good quantitative agreement, affirming its existence and the property of recurrence.

Johnson and Gardiner (1955) noted that the scatter of their observations about a mean phase curve was more than could be explained by

observational errors. Harris (1961) mentioned, "It is probable that variations in the transparency of the Martian atmosphere contributed to this scatter; if the atmosphere is clearer than normal, the observed magnitudes will be fainter than average, while an increase in the 'haze' will make the observed magnitudes brighter." We can be fairly certain that the May 3-4, 1952 anomaly is due to the opposition effect, but there are smaller variations reported by Johnson and Gardiner throughout their phase curve. However, my results indicate a scatter of $\pm 0^{m}.01$ which can most probably be attributed to observational error.

One exceptional observation might be that of April 14, 1967 ($\alpha = 1°.6$), when both the Chile and Kitt Peak data show Mars to be ~ 0.03 (visual) fainter than the mean curve. Otherwise, there seem to be no unusual nights during the 1967 observations. This is fortunate in view of the fact that such scatter would have made it difficult to derive an accurate opposition effect.

Although the revision of the Martian photometric parameters is a significant result of this work, it is also important to analyze the opposition effect in regard to physical interpretations of the surface and atmosphere. Even though Fig. 20 is useful in demonstrating the opposition effect in each color, the slopes of these curves, $\underline{a} = dm_0/d\alpha$ provide additional information. Some values of $\underline{a}(\alpha, \lambda)$ taken from Figs. 14 to 20 are shown in Table XII and drawn in Fig. 22. The slopes near $\alpha = 1°$ are only estimates, since extrapolations are necessary. However, those at $\alpha = 2°$ and $6°$ are probably accurate, since several points are clustered on both sides of each of these phase angles. The slopes at $\alpha \gtrsim 15°$ are taken from de Vaucouleurs (1964) and Table X.

TABLE XII

Slopes, a, of Smoothed Phase Functions of Mars and the Moon, Magnitudes/Degrees

	MARS						MOON[a]
Phase Angle, α / Filter	U	B	V	R	I	I'	V
1°	0.050	0.047	0.047	0.036	0.028	0.024	0.22
2°	0.045	0.042	0.042	0.032	0.025	0.021	0.11
6°	0.039	0.036	0.028	0.021	0.019	0.017	0.030
15°[b]	0.018	0.018	0.015	0.012	0.012	0.012	0.028

[a] From Gehrels et al. (1964)

[b] From deVaucouleurs (1964)

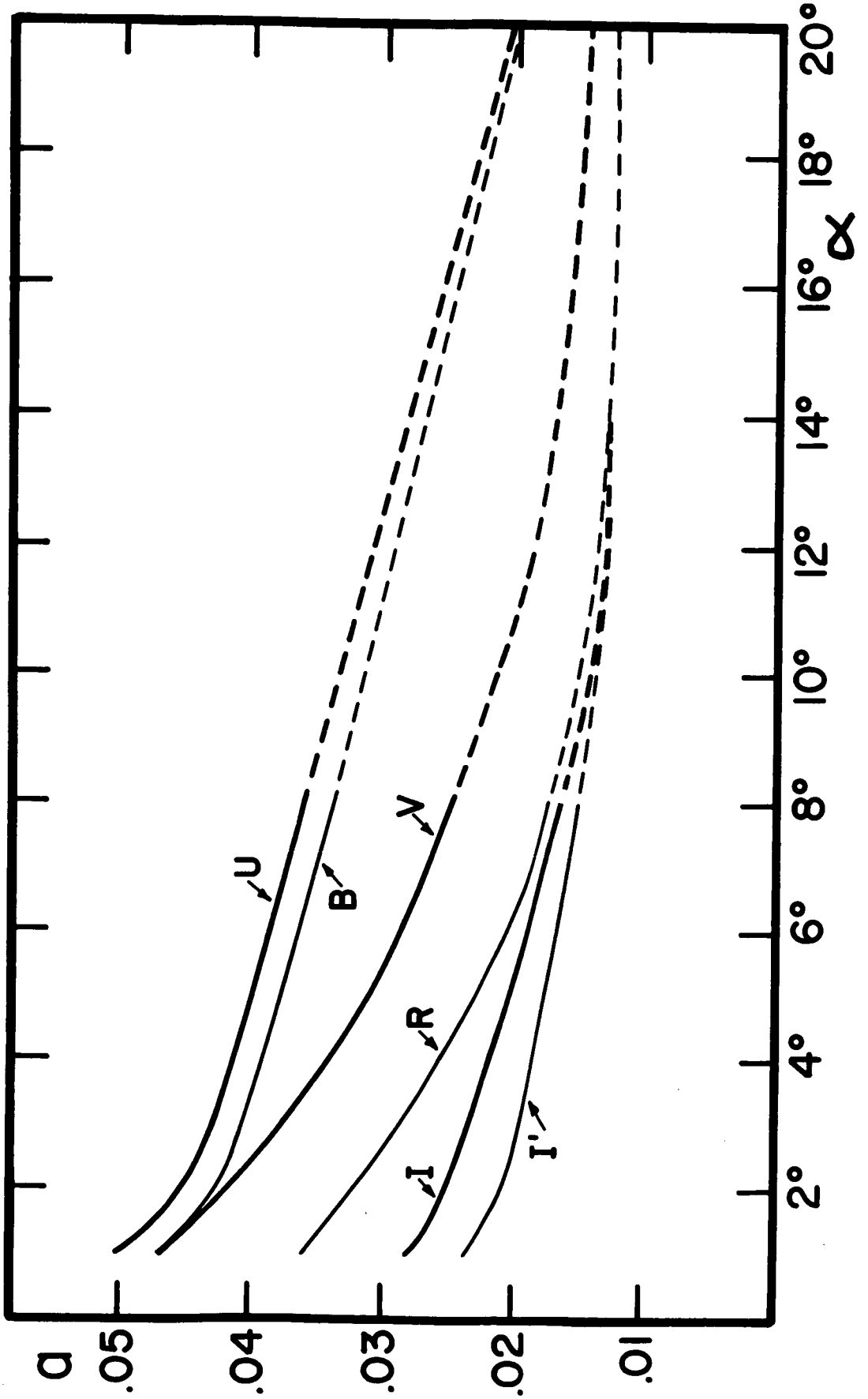

Fig. 22. The slopes a = dm/dα of the Martian phase function versus phase angle in six colors.

It is immediately evident from Table XII and Fig. 22 that the Martian opposition effect is not nearly as strong as the lunar opposition effect, for example, at $\alpha = 1°$ in the visual, $a_{Moon} \sim 5a_{Mars}$. This difference is so pronounced that the mean lunar $p_V = 0.197$ (deduced from Gehrels et al. 1964, using Mag. = - 26.74), whereas the Martian $p_V = 0.194$, taking into consideration the opposition effects of both. This is compared to $A_V = 0.16$ for Mars and $A_V = 0.067$ for the Moon (Harris 1961). In other words, Mars is more than twice as efficient as the Moon in reflecting radiation in all directions in spite of the fact that the two objects are equally efficient reflectors at zero phase.

Another interesting contrast between the Moon and Mars is that the Martian opposition effect in V begins at $\alpha \sim 10°$ (Fig. 20c), whereas the lunar one does not set in until $\alpha \lesssim 5°$ (Gehrels et al. 1964), in spite of the fact that the lunar opposition effect is so much more pronounced. There is thus evidence for large-scale differences in the physical nature of each surface. Oetking (1966) experimentally determined that "differences in the particle size, shape, and opacity of the reflecting materials have an important influence on the opposition effect", so some of these factors combined with compositional differences between Mars and Moon could account for their sharply different opposition effects. A detailed discussion of this in terms of my laboratory results will be presented in Sections 3.3 and 3.4.

Figure 20 indicates that the opposition effect in magnitude units, i.e., per cent change in reflectivity, is more pronounced at shorter wavelengths, i.e., Mars becomes bluer at opposition (Table IX). (The same effect occurs for the Moon (Gehrels et al. 1964).) Since the Martian albedo increases sharply with wavelength from ultraviolet to red (the same

is true of the Moon but to a lesser extent), we have an inverse relation between albedo and the opposition effect for both objects. The Martian results are illustrated in Fig. 23, where Δm_0 is the difference in magnitude between the opposition magnitude from the extrapolated linear phase function with slope $\underline{a}$ and the revised value of m_0, as listed in Table X. For comparison, the lunar value, V_{Moon}, is plotted, and it is seen that it does not fall into the relationship established for Mars. Geometric albedoes p are also plotted as a function of wavelength in Fig. 24 in the case of both the opposition effect and extrapolated linear phase function. The shape of the curve remains the same, but there is a change in displacement. If this curve were plotted in terms of magnitudes rather than albedoes, the tendency for Mars to become bluer at opposition would be more apparent.

In the concluding part of Section 2.3, I mentioned that, because of the Martian opposition effect, p_V increases and q_V decreases in such a way as to leave their product, the Bond albedo (A_V), essentially unchanged; i.e., $A_V = 0.171$ for an extrapolated linear pulse function and $A_V = 0.169$ for the opposition effect. However, since the opposition effect shows that Mars reflects more efficiently for $\alpha < 10°$ (yet no less efficiently for other α) than previously anticipated, one would expect an increase in A_V.

To resolve this question, let us estimate the increase in A_V attributable to the opposition effect. In Fig. 20, curve c, the reflectivity of Mars increases ~ 7 per cent for $0° < \alpha < 10°$. The fraction the solid angle of radius 10° occupies in the entire sphere of reflection is 0.1 Ster./ 4π Ster. = 0.008, so A_V should increase by $0.07 \times 0.008 = 0.0006$.

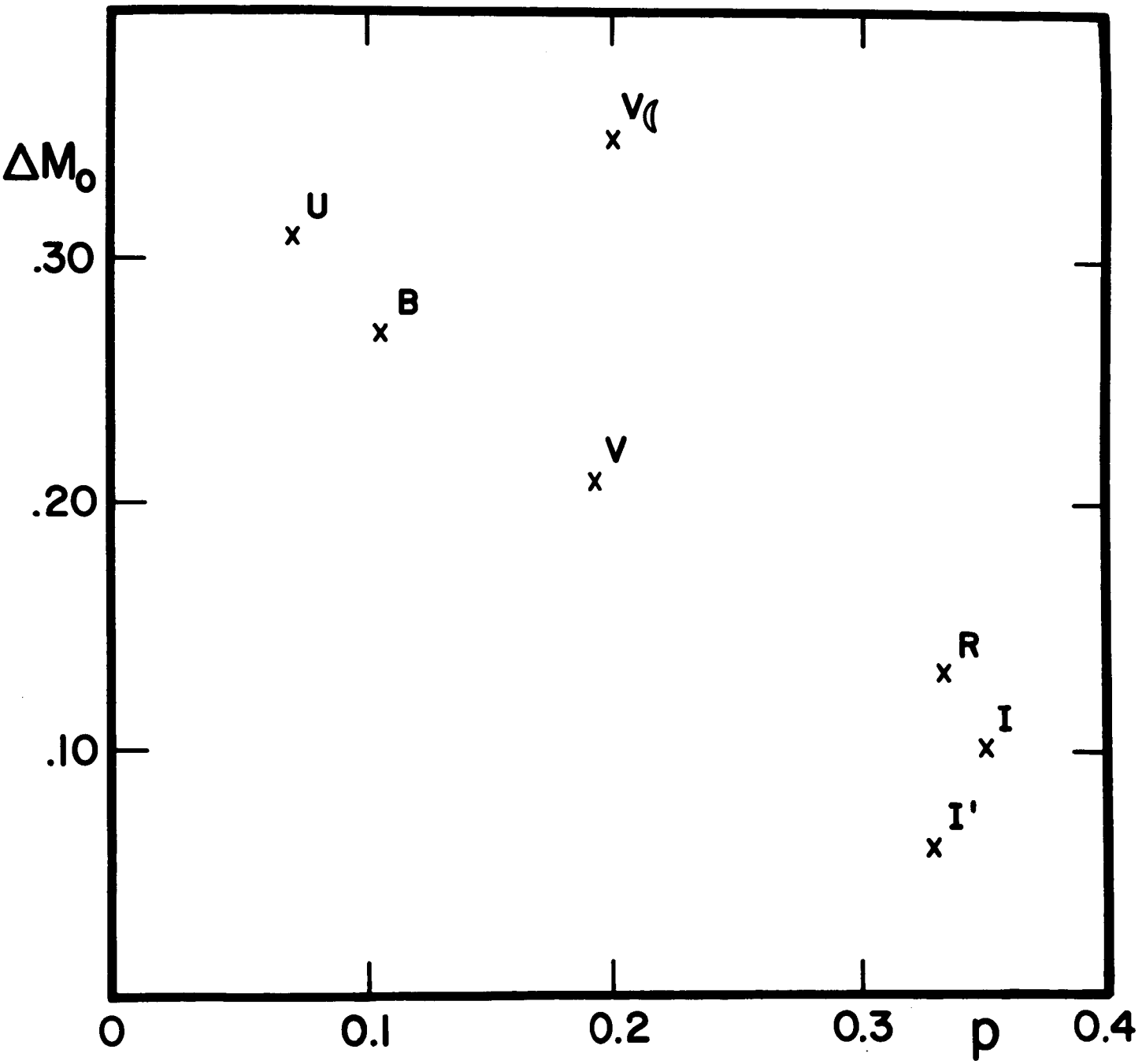

Fig. 23. The difference between Martian brightness from the opposition effect and the Martian brightness from an extrapolated phase function at $\alpha = 0°$, as a function of geometric albedo. Each color filter is denoted by the appropriate symbol defined in Table VI. The point $V_{(}$ denotes the observations of the Moon at 0.56 μ (from Gehrels et al. 1964).

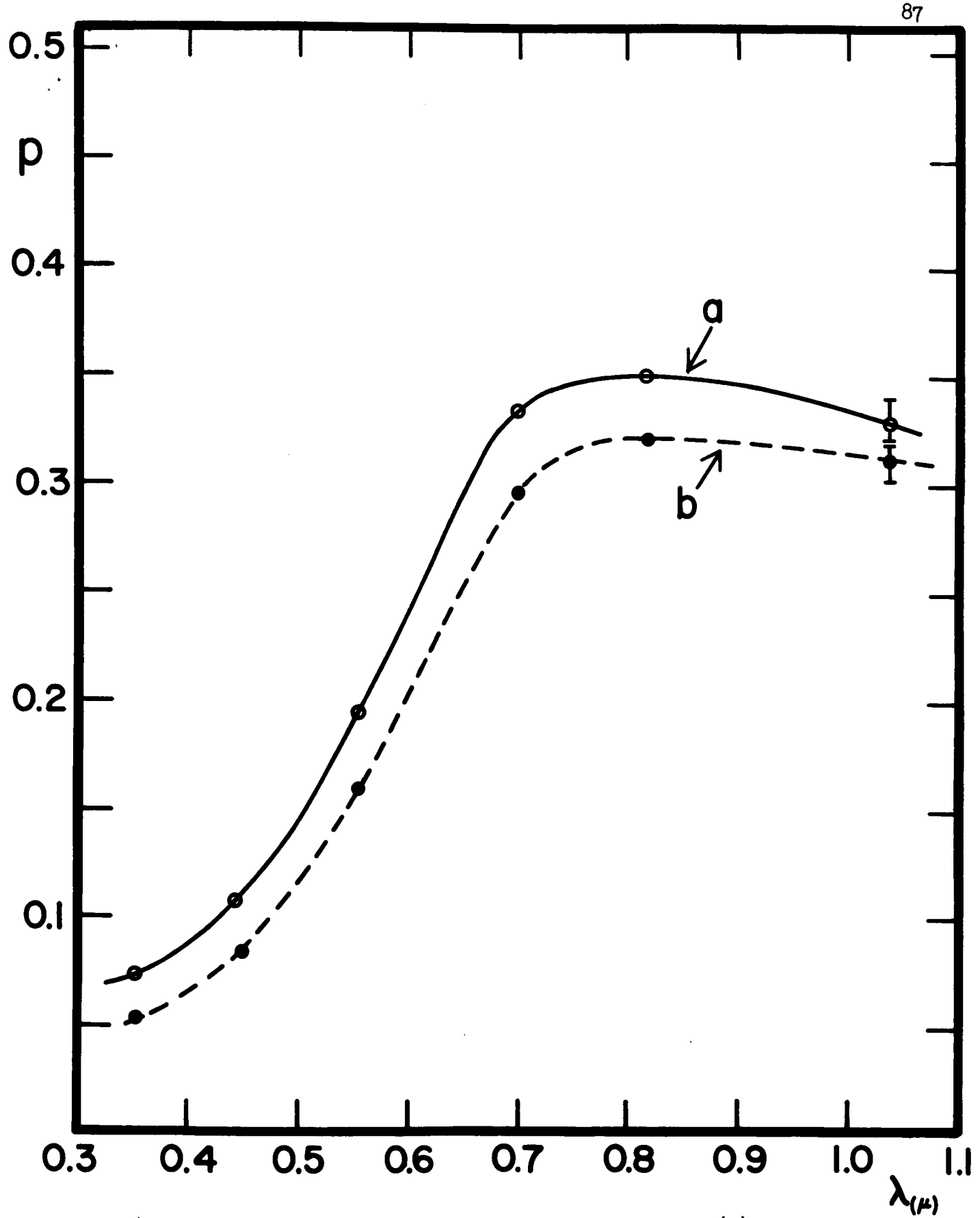

Fig. 24. Spectral variation of Martian geometric albedo: (a) corrected for the opposition effects, and (b) the former values, as derived from extrapolated linear phase functions.

This increase is negligible, so we see that the value of the Bond albedo is unaffected by the opposition effect. The slight discrepancy in A_V can be attributed to a lack of enough significant figures in the calculations. The values for A listed in Table X are calculated as the product of those values for q and p corresponding to an extrapolated linear phase function. The revised values of q from the opposition effect listed in Table X are calculated as the quotient of A (unchanged) and revised p. These values for q are very close to those derived by integration of the phase curve and the Russell rule described in Section 2.3.

Another significant result is the comparison between Martian dark and bright areas. From lunar data of Gehrels et al. (1964) the opposition effect in terms of magnitude change is essentially the same for bright craters and maria, even though their albedoes are different by a factor of two or more. This is rather surprising in view of the dependence of opposition effect on spectral albedo for both the Moon and Mars.

The case of Mars is more difficult to analyze since my small-area photometry failed. However, some of my whole-disk observations are dominated by deserts whereas several others have a large contribution by dark areas. The rotation curve of Fig. 12 shows that Mars is $\Delta V = 0.07$ mag. brighter at $\lambda_c = 135°$, 150°, and 165°, than at $\lambda_c = 195°$, 210°, and 225°. Figure 25 shows phase curves derived for each of these two cases, i.e., crosses represent a mean of the Martian absolute magnitudes at $\lambda_c = 195°$, 210°, and 225°. The plots in U and B show no appreciable rotational effect. This has been reported before (Harris 1961), and is obviously due to the lack of contrast on the Martian disk at $\lambda < 0.47\ \mu$. As for the plots in V, R, I, and I', the slopes of the best line drawn through each set of points (between $\alpha = 2.^{\circ}7$ and 6.7) indicate a negligible

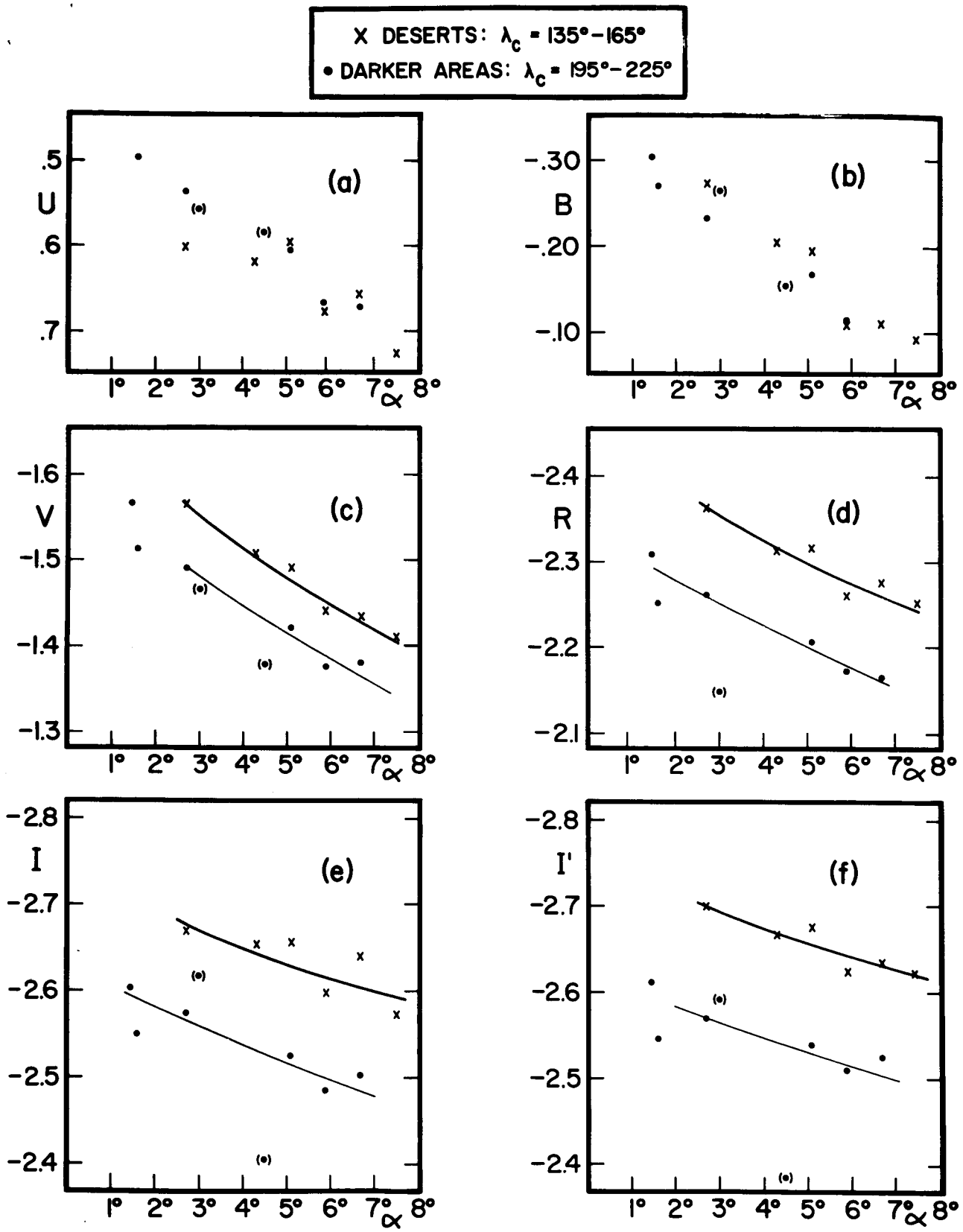

Fig. 25. Comparison between the opposition effects of the dark and bright areas of Mars (uncorrected for transformation errors), from observations of the Martian disk during the 1967 opposition effect. See text for explanation.

difference in the opposition effects in the two cases, and there is an upper limit to the difference in slopes: $\Delta a < 0.0025$ mag./deg. There is only a slight suggestion that $\Delta a \sim 0.005$ in I (0.83 μ) such that the Martian darker areas exhibit a stronger opposition effect.

In any case, it is probably safe to say that $\Delta a < 0.005$ mag./deg. Since the contrast, Γ, between the bright areas and the darkest of the dark areas (e.g., Syrtis Major) is about 2 with the best spatial resolution observed visually and photographically from Earth (Focas 1961), then the sensitivity in my technique is $\Delta V = 0.07$ mag. divided by $\Gamma \sim 0.7$ mag. or one-tenth that obtainable visually or photographically. Thus the upper limit for difference in slope of the opposition effect for bright and dark areas for $\alpha = 3°$ to $7°$ is:

$$\Delta a' < \frac{0.005}{0.1} \text{ mag./deg., or}$$

$$\Delta a' < 0.05 \text{ mag./deg.}$$

and, more likely, $\Delta a' < 0.025$ mag./deg. Since $a_V = 0.031$ at $\alpha = 5°$, then the opposition effect of the dark areas cannot exceed that of the bright areas by more than a factor or two.

It is certain that the Martian deserts are physically different from any area on the Moon, since the opposition effect of the latter is much more pronounced, and the Martian deserts so dominate the disk at $\lambda_c = 135°$, 150°, and 165°.

However, for the dark areas, if a_V were to equal 0.06 mag./deg. at $\alpha = 3.°5$ (approximately the upper limit), this would correspond closely to the lunar case (Gehrels, et al. 1964). Still it is tempting to suggest that even the dark areas of Mars, as observed at the spatial resolution visible from Earth, do not present the same opposition effect as any lunar

areas, even though the Bond albedoes of the Martian dark areas approximate closely the lunar Bond albedo. This suggestion, however, must await more definitive techniques such as photographic photometry of Mars at future oppositions.

Another result obtainable from the Kitt Peak observations is an accurate rotation light curve of Mars. The accuracy is due to the fact that most of the points in Fig. 12 represent the mean of several observations of Mars on several nights. Table XIII compares two extreme points (λ_c = 180° and 270°) on this rotation curve with those in previously published rotation curves. Also listed is D_E, the planetocentric declination of Earth. As the aspect of Mars seen from Earth becomes more northern, the amplitude of variation becomes less. This relation exists because at λ_c = 270° the dark areas Syrtis Major, Mare Cimmerium and Mare Acidalium come into prominence as the Martian South Pole is tilted more toward Earth. Unfortunately, this dependence on D_E complicates any attempt to detect a significant relation between rotation variation and α, yet another method of comparing phase functions of dark and bright areas.

One final datum from the observations is testing for the Martian atmospheric contribution to the opposition effect. It is well known that the Martian atmosphere consists of molecules and perhaps aerosols (Section 1.3). Although there is some uncertainty in the slopes of my phase curves, Table XII and Fig. 22 show a striking difference between observations made in the blue and ultraviolet and those made at longer wavelengths: The slopes of the phase functions of the former are very much greater than those of the latter in the observed range of $4° \lesssim \alpha \lesssim 8°$, i.e., an opposition effect in the U and B filter sets in at much larger α. This anomaly appears well outside the error scatter of the observations.

TABLE XIII

Rotation Magnitude Differences Between Two Selected Martian Longitudes

Reference	D_E	ΔV (λ_c = 180 to 270°)
Lau (1914)[a]	+ 10°	0.11
deVaucouleurs (1939)[a]	- 9°	0.15
Flagstaff (1954)[a]	0°	0.11
Flagstaff (1958)[a]	- 11°	0.12
O'Leary (1967)	+ 20°	0.08

[a] As Presented by deVaucouleurs (1964)

Because of the well known obscuration of Martian detail at $\lambda < 0.47\ \mu$ (e.g., see de Vaucouleurs 1964), the Martian atmosphere might be suspected of causing the anomaly in B and U. To investigate this, we examine the slopes of Rayleigh scattering (by molecules and perhaps small particles) and Mie scattering (by particles whose radii equal approximately the wavelength of observation) phase functions to see how the atmosphere might be playing a role. Finally, these results should be compared to previous observation and interpretation.

The Rayleigh scattering phase function (e.g., see Harris 1961) is simply

$$\Phi/\Phi_0 = 1/2\ [1 + \cos^2\ (180° - \alpha)] \qquad (2.4.1)$$

The brightness decrease for a pure Rayleigh scatterer from $\alpha = 0°$ to 10° is only $\underline{a} = 0.0016$ mag./deg. A Rayleigh scatterer is thus ineffective in producing the observed opposition effect at any wavelength, and alternative origins for both the opposition effect and phase function anomalies must be sought. This is especially important in the case of observations made at shorter wavelengths ($\lambda < 0.47\ \mu$) where Rayleigh scattering might be considered a significant component to the optical properties of Mars. From the above arguments we can say that Rayleigh scattering for small α must play at most a minor role, even at $\lambda = 0.36\ \mu$.

The effect of Mie scattering by atmospheric particles upon a phase function can be considerable, however. For example, Table XIV lists the slopes of the phase functions of 3 ice particle mixtures, called A", B", and C", as calculated by B. M. Herman and cited by Kuiper (1964). The phase functions depend upon: (1) The parameter $x = 2\pi r/\lambda$ where r is the particle radius and λ the wavelength of observation and (2) the complex index of refraction $m = n - ki$, where n is the real part of the refractive

TABLE XIV

Slopes, a, of Phase Functions (Mag./deg.)

Range in α	0°-5°	5°-10°	10°-15°	15°-20°	20°-25°	25°-30°	30°-35°	35°-40°	40°-45°
Mars observed									
U	0.044	0.037	~0.030	~0.023	~0.019	0.018	0.018	0.018	0.018
B	0.041	0.034	~0.028	~0.022	~0.019	0.018	0.018	0.018	0.018
V	0.040	0.026	~0.018	0.015	0.015	0.015	0.015	0.015	0.015
Particle Mixture									
A"	0.004	0.013	0.020	0.027	0.028	0.027	0.021	0.010	0.000
B"	0.008	0.022	0.034	0.036	0.027	0.009	-0.007	-0.013	-0.008
C"	0.021	0.027	0.041	0.020	-0.015	-0.035	-0.003	-0.004	0.002

The Weighting Factors for the Aerosol Mixtures A", B", and C"

x	2.0	2.5	3.0	3.5	4.0	4.5	5.0	5.5	6.0
Mixture									
A"	2	7	10	7	2	0	0	0	0
B"	0	0	2	7	10	7	2	0	0
C"	0	0	0	0	2	7	10	7	2

index and k is the absorption coefficient. For ice m ~ n = 1.31. (This is not to say that ice or these particle size distributions are to be expected on Mars, but merely a demonstration to see if phase functions of Mie scatters can be made to fit the anomalies in the Martian phase function in the blue and ultraviolet mentioned above.) These particular 3 mixtures were considered as "balanced" i.e., neither integral nor half-integral values of x are favored. The weighting factors for Mixtures A", B", and C" are also given in Table XIV.

Table XIV shows that Mixtures B" and C" tend to show a steeper phase curve from $\alpha = 2.^{\circ}5$ to 20°, precisely the tendency observed for Mars in the blue and ultraviolet relative to longer wavelengths (Fig. 22 and Table XII). For example, if aerosol Mixture B" or C" were to contribute about one-fourth of the total amount of reflected radiation from Mars between $\lambda = 0.36$ and $0.43\,\mu$ (with the other three-fourths coming from the surface--we are neglecting the small contribution of Rayleigh scattering by molecules in the Martian atmosphere), the underlying Martian surface would have a phase curve in the blue and ultraviolet similar to that observed at λ 0.55 μ (Table XIV), i.e., the small α opposition effect is retained but the anomalously steep phase curve observed in the U and B filters near for $4^{\circ} < \alpha < 8^{\circ}$ is removed.

At this point it is significant to test the aerosol hypothesis with certain questions: Why would these aerosols not affect observations at wavelengths longer than the blue in a similar way? Why do we suspect that the atmosphere rather than the surface is perturbing the phase function near $\alpha = 6^{\circ}$? Could clouds in the Martian atmosphere affect the observations?

The answer to the first question concerns the wavelength dependence of the fractional contribution of aerosol particle brightness, B_p, to the total Martian brightness $B_s + B_p$, where B_s is the brightness of the Martian surface (for the purposes of this rough calculation, we are neglecting the small molecular component to the total Martian brightness). As far as the aerosols are concerned, a common property of all mixtures is that as most frequent x decreases from 2π (i.e., as λ increases from $\lambda \sim \bar{r}$), B_p decreases (e.g., see Kuiper 1964). For example, at $\alpha = 5°$, Kuiper lists $B_p = 2.87$, 1.92, and 0.84 for ice Mixtures C", B", and A", respectively. Let us assume that for Mars ice Mixture C" applies for observations at $\lambda = 0.36\ \mu$. This means that Mixture B" is applicable to observations at $\lambda = 0.45\ \mu$ and Mixture A" is applicable to observations at $\lambda = 0.61\ \mu$ (Table XIV). Interpolating from these wavelengths, we get $B_p = 2.87$, 2.19, and 1.20 at $\lambda = 0.36$, 0.43, and 0.55 μ, respectively.

On the other hand, $(B_s + B_p)$ increases with λ: Fig. 23 and Table IX show the geometric albedo rising from 0.071 at $\lambda = 0.36\ \mu$, to 0.107 at $\lambda = 0.43\ \mu$, to 0.194 at $\lambda = 0.55\ \mu$.

I have mentioned that $B_p \sim 0.25\ (B_s + B_p)$ at $\lambda \sim 0.39\ \mu$ from the phase slope anomalies, provided we interpret these anomalies to be caused by Mixtures B" or C" in the blue and ultraviolet. In that case, we can derive the ratios $B_p/(B_s + B_p) = 0.35$, 0.18, and 0.05 for $\lambda = 0.36$, 0.43, and 0.55 μ, respectively.

From these numbers we see that aerosols could contribute strongly to the observed brightness of the planet in the blue but very weakly at longer wavelengths. This would thus provide a neat explanation of the abnormally large phase-curve slope observed only in the blue and UV at $\alpha \sim 6°$.

Other explanations are possible, however: in the next chapter we shall see that some substances, e.g., limonite, show a phase function just as steep as the Martian phase function in the blue near $\alpha \sim 6°$. But in such cases, the sample's phase function becomes steeper than the Martian phase function at longer wavelengths. The aerosol explanation is still preferred unless a substance can be found to have this particular idiosyncrasy observed on Mars.

One other explanation could be the influence of clouds present over the Martian disk. While this is possible, certain objections may be raised to this: (1) the low scatter in my photometric data points from night to night and from hour to hour during Martian rotation indicate no abnormal variations in cloud content either in area or in time, and (2) the effect I have observed would have to be due to clouds which scatter considerably more strongly in the blue and UV than at longer wavelengths. These objections would imply that a phenomenon akin to the "blue haze" would be required to produce the effect of the steep phase-curve slope. But this would essentially be the same explanation as my aerosol model, only the nomenclature has been changed from "aerosol" to "haze" or "clouds."

However, C. Capen and A. Binder visually observed some clouds on the planet at the time of my observations. Capen kindly sent to me a detailed description of these observations along with some color photographs and drawings. Capen's disk drawings are shown in Fig. 26. They were obtained from visual observation and photographs in violet- and blue-light, and they show the extent and position of the equatorial clouds and limb haze (dashed lines) and the white, bright, and surface-dependent areas (dotted lines). Although the extent of these clouds were certainly

not of the proportion of a major, planet-wide dust storm, they could still influence the opposition-effect measurements. The alteration would probably be small, however, because of the consistency of my observations.

As mentioned before, the essential points of these observations of the Martian opposition effect are given by O'Leary (1967). However, neither the reference nor this chapter has presented the comparison between these observations and measurements of laboratory samples. This will be discussed in the next chapter.

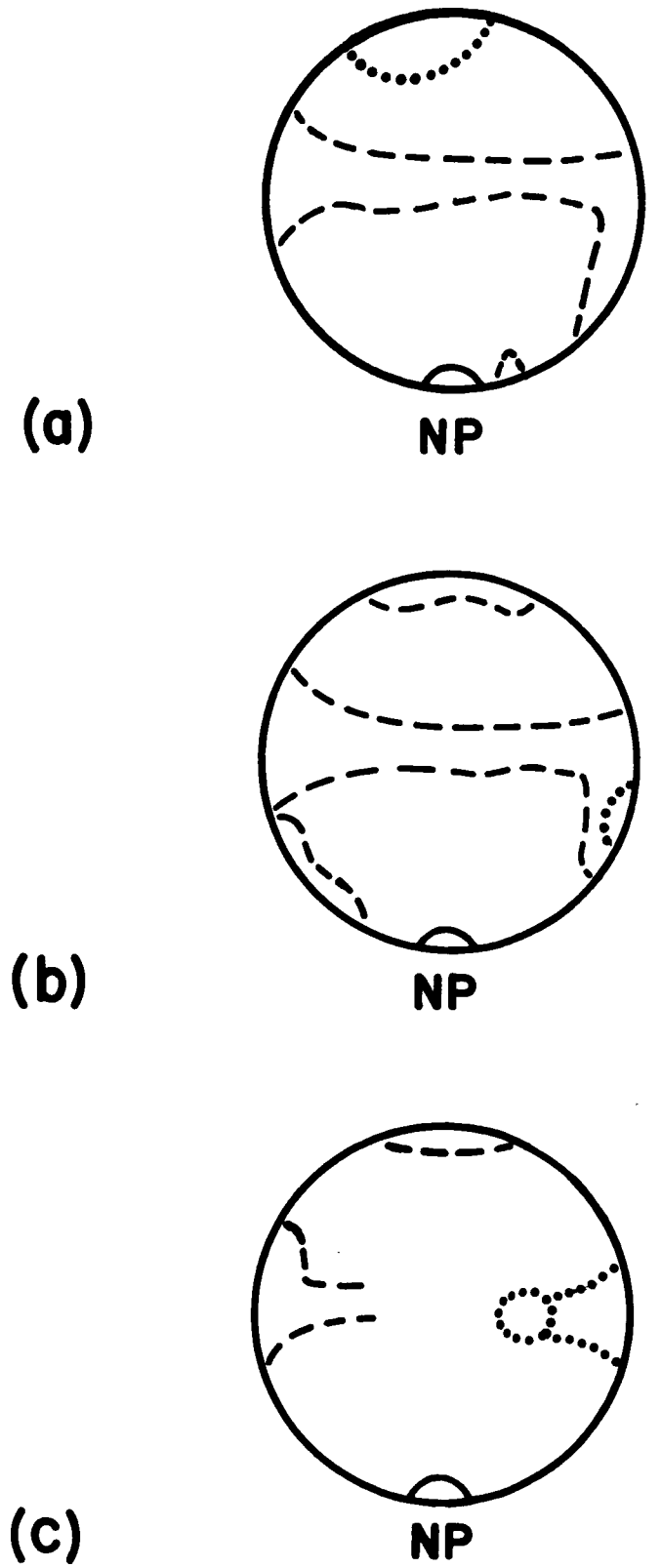

Fig. 26. Drawings of Mars by C. Capen during the 1967 apparition. NP denotes the North Polar Cap, dashed lines denote clouds, and dotted lines frost: (a) 3-9 April 1967, λ_c from 56°-252°; (b) 13-18 April 1967, λ_c from 134°-324°; and (c) 22-25 April 1967, λ_c from 100°-252°.

CHAPTER III. LABORATORY REFLECTIVITY MEASUREMENTS

3.1 Design, Construction, and Calibration of the Reflectometer-Polarimeter

The term reflectometer-polarimeter is defined as a photoelectric photometer assembly which can measure reflectivities and polarizations of surface samples as functions of incidence and reflection angles of light. Such a device has been designed and constructed at the Space Sciences Laboratory at the University of California. (See Fig. 27 for photograph and Fig. 28 for drawing).

The basic design has been adapted from that of Coulson, Bouricius, and Gray (1964, 1965) with a few significant differences: our instrument is smaller scale, thus permitting smaller samples; the divergence of the incident light is small (~ 1/2°); the optics can be adjusted to accept a small spread of phase angles at the receiving aperture; the receiving aperture always "sees" an area larger, not smaller, than the spot of light on the sample; measurements can be made at phase angles as small as 3/4°; and the pulse-counting technique was used in the electronics.

The instrument has been designed for maximum adaptability for both intensity and polarization measurements. There are certain requirements for both types of measurements: in the case of measuring intensities in the range of the opposition effect, we are concerned with minimizing the divergence in the incident beam, minimizing the half-cone angle accepted by the receiving aperture, and minimizing the phase angle at which the incident beam is occulted by the photometer assembly. This procedure is necessary as pointed out by Oetking (1966), since, otherwise, the large range of phase angles received at the photomultiplier tube would smear out any non-linear opposition effect. This procedure is not as important in the case of polarization measurements, since the polarization of all

Fig. 27. Photograph of author operating the reflectometer-polarimeter (from the March 27, 1967, issue of Product Engineering).

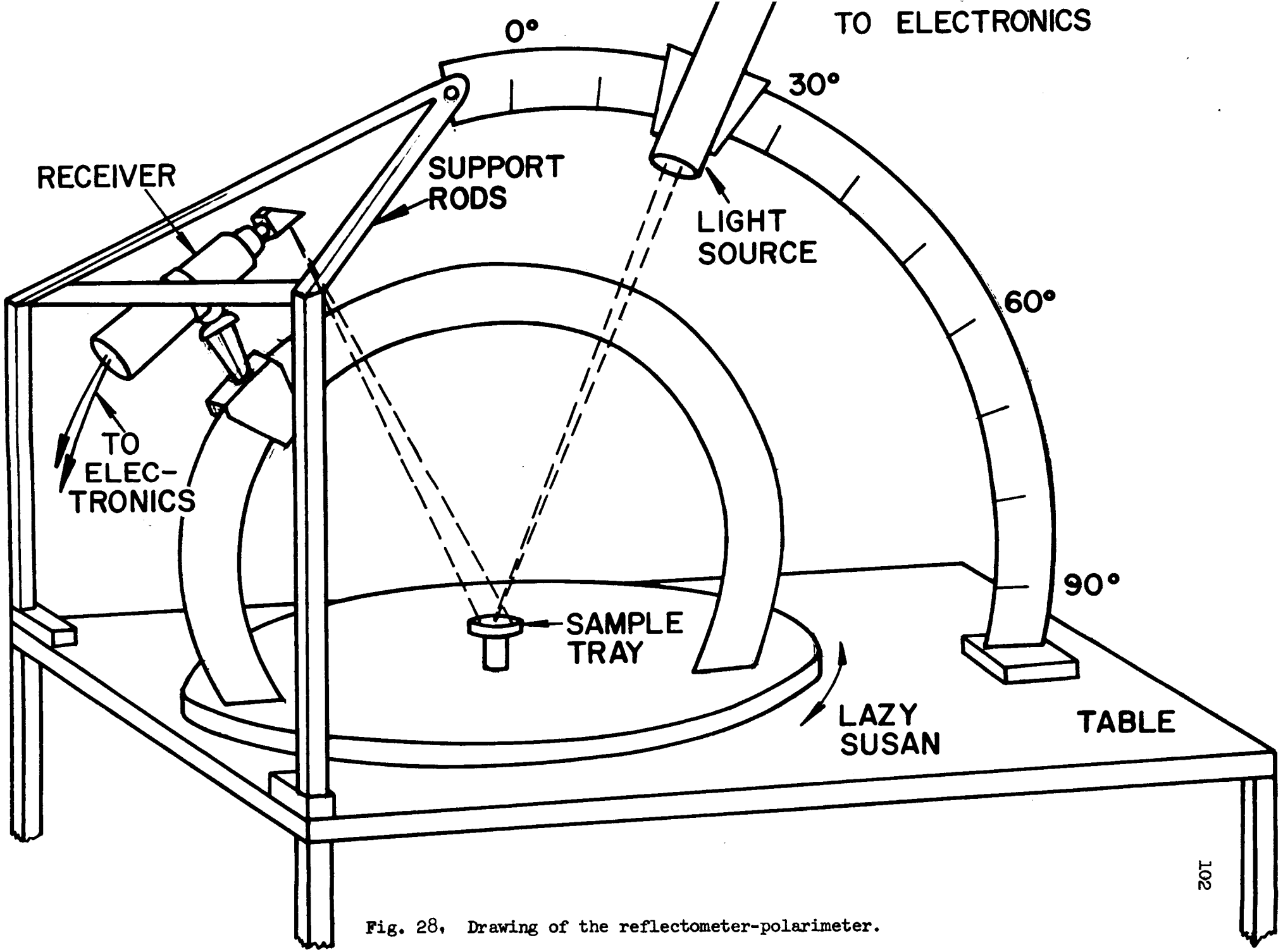

Fig. 28. Drawing of the reflectometer-polarimeter.

substances is zero at zero phase, and it changes with phase angle in such a way as to yield fairly accurate results, even if a spread of a few degrees in phase angle (rather than ~ 1/2° required for the opposition effect) is received by the phototube. For example, the aperture is the instrument of Coulson et al. (1964, 1965) received by half-cone angle of 2°.5, sufficient for polarization measurements and for intensity measurements well away from opposition.

On the other hand, a polarization experiment requires greater internal accuracy, since we are concerned with deriving from measured I_1 and I_2 the value $P = (I_1 - I_2)/(I_1 + I_2)$, where $P < 0.02$ for most samples. A small error in either I_1 or I_2 would result in a relatively large error in $I_1 - I_2$. To minimize statistical error in the pulse counting, larger intensities of light are desirable in measuring the polarization than is obtainable with the small apertures used in measuring the opposition effect. The obvious solution is to change the apertures between the opposition effect and polarization experiments to satisfy each requirement.

Because of the separate requirements, both in light level and in geometry, between the opposition effect and polarization experiments, it was decided to perform them at different times. Only the opposition effect results are described herein, because the electronic system is presently incapable of rendering the accuracy required for the polarization measurements. Furthermore, it is my opinion that at this time the photometric results are of more interest than the polarization results since: (1) I have mentioned in Sec. 1.3 that there is a wide range of possible Martian surface polarizations because of the enormous uncertainty in the atmospheric contribution to Martian brightness; (2) there have already been some polarization experiments performed on candidate substances for the

surface of Mars, whereas the opposition effect measurements have not been attempted on such substances. This is not to say that it is not worthwhile to measure polarizations in the laboratory, since progress in the field might require an accurate catalogue of polarizations of samples suitable for the Martian surface. Furthermore, the experiments to date have been far from complete or definitive. The discussion to be presented about this reflectometer-polarimeter in this section will encompass the instrument's ability to measure both intensity and polarization.

As explained in Section 1.2 and shown in Fig. 2, it is desirable to design in the experiment every possible geometry which could occur at a point on Mars: θ can be varied by moving the goniometer along the semicircular ring, Φ can be varied by rotating the lazy susan, and θ_0 can be varied by moving the light source along its 90°-ring (Fig. 28). Each ring is offset such that the light is always beamed on the center of the sample tray and the receiver is always looking at the center of the sample tray.

The light source assembly is shown schematically in Fig. 29. The source is a General Electric No. 1183 tungsten filament 50 candlepower searchlight lamp. The transfer lens optimizes the useful light per unit area from the filament and projects a light spot on the pinhole aperture (0.030 inches in diameter), which is at the focal point of the collimating lens (focal length of 3.4 inches). The resulting divergence in the collimated beam is 1/2°, twice the value of the diameter of the Sun as seen from Mars. This discrepancy is not expected to alter the results in any appreciable way. An aperture next to the collimating lens is used to define the diameter of the beam (1/4 inch in the case of the intensity measurements). The sample tray is about 30 inches from the collimating lens. Any component is easily removable and replacable so that other beam intensities, widths, and divergences are possible.

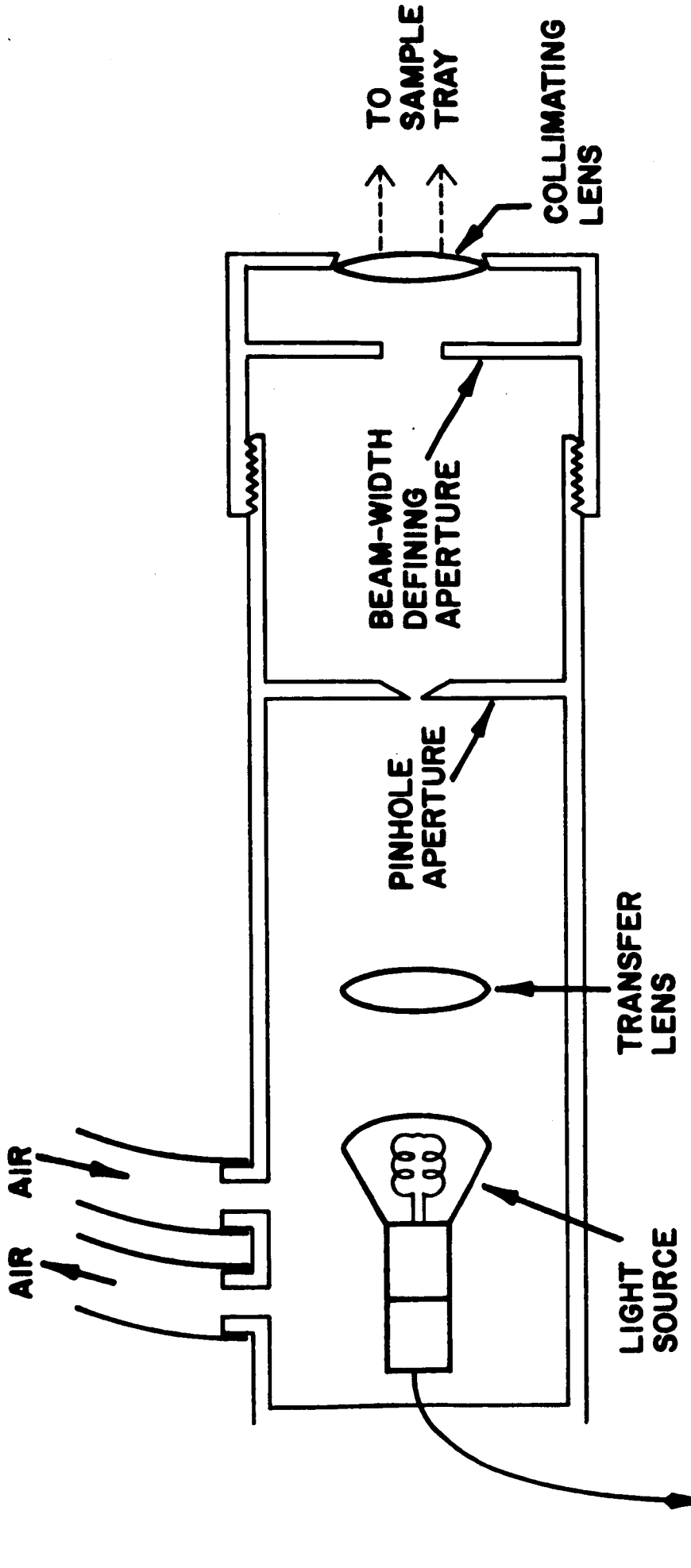

Fig. 29. Schematic drawing of the light source assembly.

A schematic drawing of the receiver is shown in Fig. 30. The light enters a right-angle prism near its tip end, such that the prism does not occult the incoming beam until a phase angle of 3/4° is reached. The receiving aperture (1/8-inch diameter for the intensity measurements) is imaged by a lens upon the photocathode. The half-cone angle of radiation received by the detector depends on the size of the aperture and on the apparent size of the light spot on the sample tray as seen by the receiving aperture. This is so because the photometer is always looking at an area larger than the light spot. For example, at a phase angle of 0° (but where $\theta = \theta_0$ can be any value), the aperture "sees" a 1/4-inch spot. Thus, the half-cone angle for an 1/8-inch aperture 30 inches from the spot is ~ 1/3°. When the incident beam is elongated to 1 inch (i.e., grazing incidence) while the receiving aperture is along the normal to the surface, the half-cone angle becomes ~ 1°. But this latter case occurs only for large phase angles, where the half-cone angle is not a critical factor. In the case of opposition effect measurements, the half-cone angle is always ~ 1/3°. For all geometries, the half-cone angle accepted by the 1/8-inch receiving aperture for radiation coming from one point on the sample surface is ~ 1/6°.

Also in the optical path of the receiver (Fig. 30) is a rotating Glan Thompson polarizing prism (removed from the apparatus during the opposition effect measurements). The prism is made of calcite, carefully prepared by the Karl Lambrecht Company. The prism is mounted in a cylinder and can be attached by belt either to a synchronous motor or any other device. The intensity components I_1 and I_2, as well as the position angle of the plane of polarization, χ, can be measured by rotating the prism.

The photomultiplier tube used was an RCA 4463 housed in a PM-101 Electro Optics coldbox. The advantage of this tube is its S-20 spectral

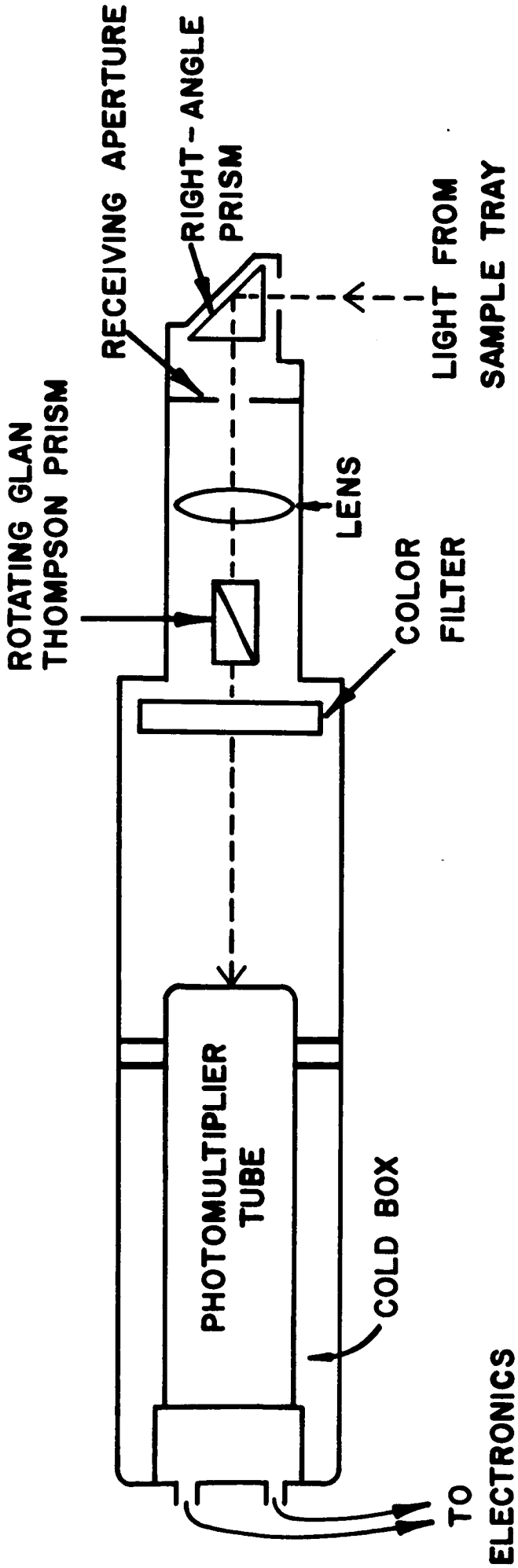

Fig. 30. Schematic drawing of the receiver.

response, where the quantum efficiency is high at maximum response in the blue, yet adequately high in the red. The tube is cooled with dry ice, improving the measured signal-to-dark count by a factor of ~ 20.

The sensitivity curves for the color filter-phototube-lamp combinations used in the experiment are shown in Fig. 31. They were obtained by taking the products of the sensitivities of each of the three components of the system. The methods for obtaining the spectral response for each component is described in the figure caption. The resulting effective wavelengths for each combination were 0.44 μ (blue), 0.56 μ (green), and 0.69 μ (red). These wavelengths are reasonably close to those of B, V, and R filters used in the Martian opposition effect observations (see Table VI).

A flow chart of the electronic system is shown in Fig. 32. The photomultiplier tube was operated by a Power Designs, Inc., voltage regulated DC power supply. The voltage level was 1650 V., the rated voltage for the RCA 4463 phototube. After amplification the output signal passed through a variable threshold pulse height discriminator. The discriminator was set at such a level to optimize linearity in the system. If the discriminator were set to count only the largest pulses, then deviations from linearity would occur because of an excessive number of large pulses in the dark current. On the other hand if the threshold is set to count the smallest pulses as well, deviations from linearity would result from system noise.

The pulses were counted by a Computer Measurements Company Model 7058 frequency-period counter. All counts were made with a 1-second integration time. Each count was printed on a Hewlett Packard Model 562A Digital Recorder. The light source was operated by a Hewlett Packard 6286A DC power supply. The rated voltage on the lamp was 5.5 V., but I ran it at ~ 4.5 V., for reasons to be given later.

Fig. 31. Relative transmission profiles for the 3 lamp-color filter-phototube combinations used in the reflectivity measurements. The spectral distribution curves of the various components were obtained as follows: (1) the lamp from a color temperature of 2527°K at 4.5 V measured on an optical pyrometer at the Department of Ceramic Engineering, U.C. Berkeley; (2) the color filters from transmission curves run on the U.C. Space Sciences Laboratory Cary 14 RI double-beam spectrophotometer; and (3) the phototube from the S-20 curve in the RCA catalogue.

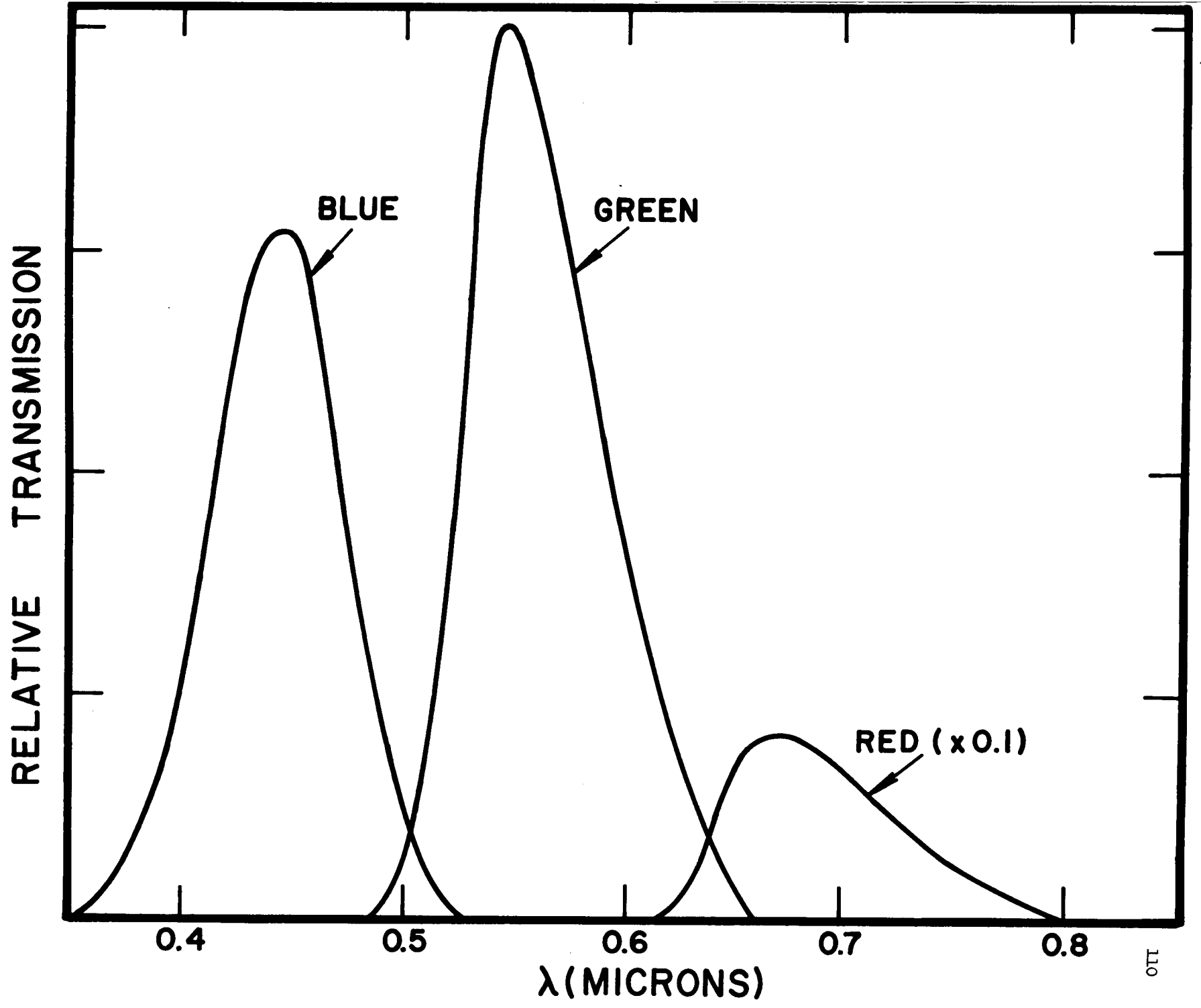
RELATIVE TRANSMISSION
BLUE
GREEN
RED (x 0.1)
0.4
0.5
0.6
0.7
0.8
λ (MICRONS)

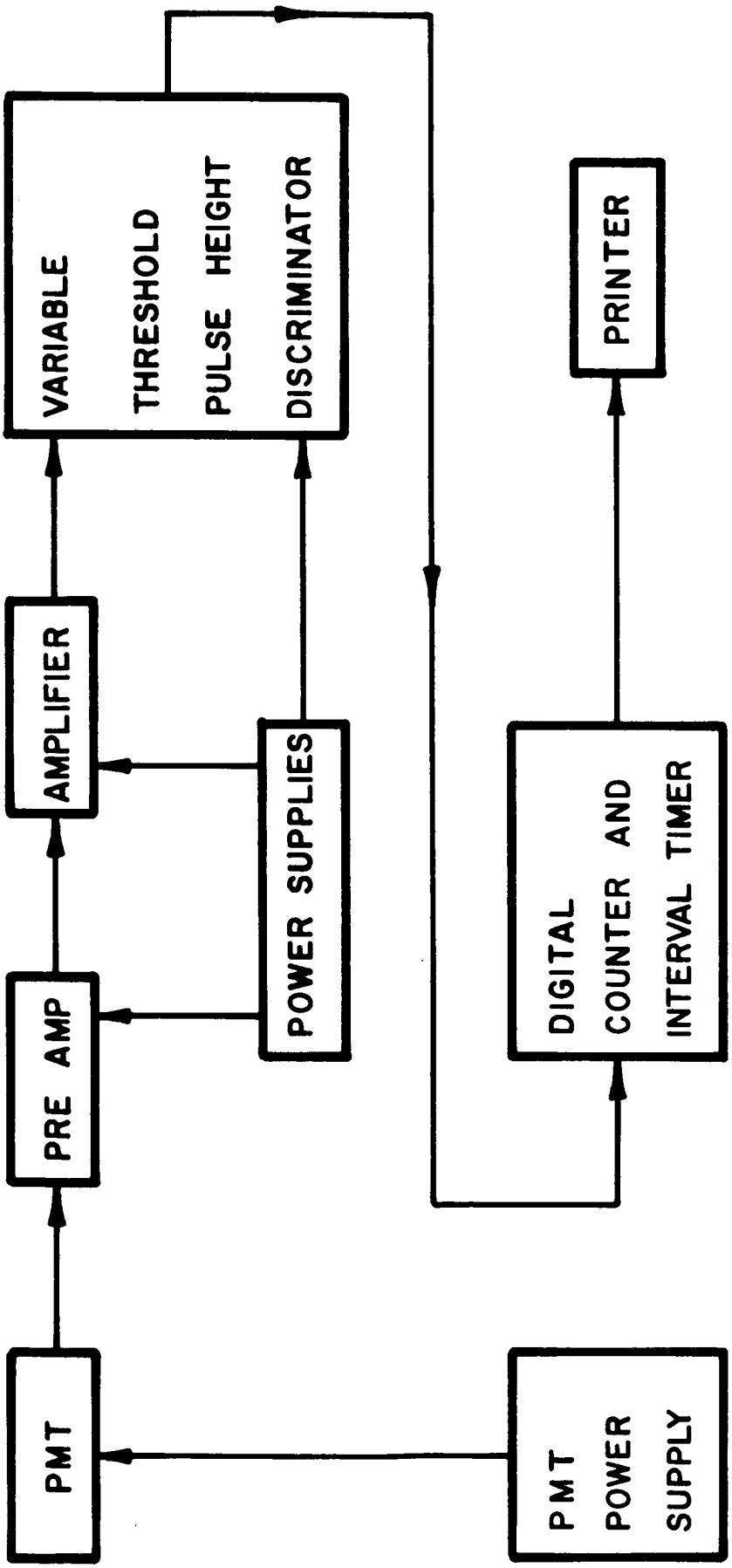

Fig. 32. Flow chart of the electronic system for the reflectometer-polarimeter.

The linearity of the system was calibrated with the use of two lamps: if the system were linear, then the number of counts from both lamps together should equal the sum of counts from each individual lamp. The voltage on the lamps was varied in such a way that the total counts from the lamp combination varied from 1,000 to 100,000 counts-per-second. The dark count was monitored and subtracted from each measurement (a typical value for the dark count was 100/sec.). Table XV shows the results of the linearity test. We see that deviations from linearity occurred for the higher counts. These deviations were always in the direction that the larger counts are underestimated, and are due to coincidence loss in the counting system. It was decided to make 100,000/sec. the maximum count for any sample during the experiment. An appropriate correction factor was applied to the higher counts. It turned out that magnesium oxide with the red filter produced the most counts in the experiment, so the voltage on the light source was set to a voltage (4.5 V.) corresponding to 80,000 counts in this situation.

There were serious drifts and oscillations in the electronics with unknown origin. However, in all but one or two of the many photometric measurements to be presented herein, these drifts were not beyond the tolerance limits of the experiment as long as the standard surface was measured often (at least once a minute).

3.2 Preparation of Samples and Experimental Procedure

The photometric phase functions and spectral reflectivities of eleven samples were measured. The samples selected have been of interest in the study of the Martian surface, as discussed in previous literature and in Section 1.3. The properties of these samples are summarized in Table XVI, and detailed mineralogical and chemical descriptions of some of the samples

TABLE XV

Linearity Test of the Electronic System, Using Two Lamps

Lamps 1 and 2 together (counts/sec.)	(Counts/sec. of Lamps 1 and 2 together) ÷ (Counts/sec. of Lamp 1 + Lamp 2 separately)
10,000	1.01
20,000	1.00
50,000	0.98
100,000	0.95

TABLE XVI

Properties of Mineral Samples Investigated[a]

Sample Number	Identification	Source	Particle Radii	Washed?	Comments
MS-1	Goethite ($FeO \cdot OH$)	Biwabik, Minn.	< 19 μ	No	See Appendix I
			125-250 μ	Yes	
MS-2	Yellow-ochre Limonite (Mostly $FeO \cdot OH$)	Tuscaloosa County, Ala.	< 19 μ	No	Mineralogical analysis should closely resemble that of goethite
MS-3	Hematite (Fe_2O_3)	Ishpeming, Mich.	< 19 μ	No	Apparently homogeneous in hand sample
			250-500 μ	Yes	
MS-4	Siderite ($FeCO_3$)	Roxbury, Conn.	< 19 μ	No	See Appendix I
			250-500 μ	Yes	

[a] Adamcik's four synthetic samples are described in Appendix II

are presented in Appendices I and II. Seven of the samples were pulverized and sieved from hand samples of goethite, yellow ochre limonite, hematite, and siderite. The other four samples are synthetic mextures which were kindly loaned to me by J. Adamcik.

The larger samples were washed in distilled water or acetone in order to remove any smaller particles which might be coating the surfaces of the larger grains. The washing process was found to be especially significant in the cases of the goethite and limonite samples: before washing, the albedo and color of the larger particles are about the same as those of the fine powder, but after washing, the samples darken considerably. The mineralogical analysis of the goethite sample carried out by J. T. O'Connor indicates the presence of small fibers a few microns in diameter which are responsible for the higher albedo and yellow ochre color that is so characteristic of this mineral (see Appendix I). The larger sized particles ($r \gtrsim 50\ \mu$) are made up largely of aggregates of these fibers. When these samples are washed, the small fibers disappear. The result is a lower albedo in washed samples than in unwashed samples. The important point to bear in mind is that the albedo of unwashed, larger particles is essentially the same as that of the finely divided particles, and washing is an important process in sample preparation. Otherwise, the particle-size parameter would lose any meaning.

The hematite and siderite samples were mineralogically unchanged by washing, but a darkening was again noted.

Two optical experiments were performed with these samples: reflection spectra were recorded from $\lambda = 0.4$ to $2.6\ \mu$ and intensity measurements were recorded with the reflectometer. Prior to both experiments, the samples were sifted through sieves onto the sample trays. This was done in such a

way that the samples were horizontal. Heavily smoked magnesium oxide (MgO) was used as the reference sample in each experiment and was prepared by burning strips of magnesium, the smoke from which was deposited upon a sample tray with a buffed-aluminum surface.

The reflection spectra were taken on the Space Sciences Laboratory Cary 14 RI double-beam spectrophotometer. The results are shown in Figs. 33 to 37 along with plots of the spectral dependence of the Martian Bond albedoes reported by Tull (1966). In each case MgO was used in the reference beam. The 100% line in the spectra was determined by running MgO in both the sample and reference beams. This line drifted by ~ 2%, so this should be the maximum error in the spectra in Figs. 33 to 37. The angles of incidence and reflection for both the reference and experimental samples were 15° (from the normals to the surfaces). The spectral slit widths ranged between 0.002 and 0.005 microns.

There is good agreement between my spectra and spectra sent to me by Adamcik on his samples, indicating reliable results and lack of contamination of the samples. The infrared reflectivities for the coarser samples were systematically lower than those of the finer samples, in agreement with spectra of similar samples presented by Hovis (1965). There are small dips beyond 2.0 μ in some of the spectra in Figs. 33 to 37 which might be spurious, however. These dips do not enter any of the interpretations of the spectra discussed in the next section.

We next discuss the experimental procedure with the reflectometer. Coulson et al. (1964, 1965) obtained their data by keeping the light source fixed at some angle θ_0 and moving the detector through various values of θ. Then θ_0 was changed and the procedure repeated. The reason for their doing this was that the light spot on the photocathode was limited in size by the

Fig. 33. Visible and near-infrared spectra of laboratory samples from 0.4 to 2.6 microns compared to a plot of the spectrum of the Bond albedoes of Mars, as reported by Tull (1966).

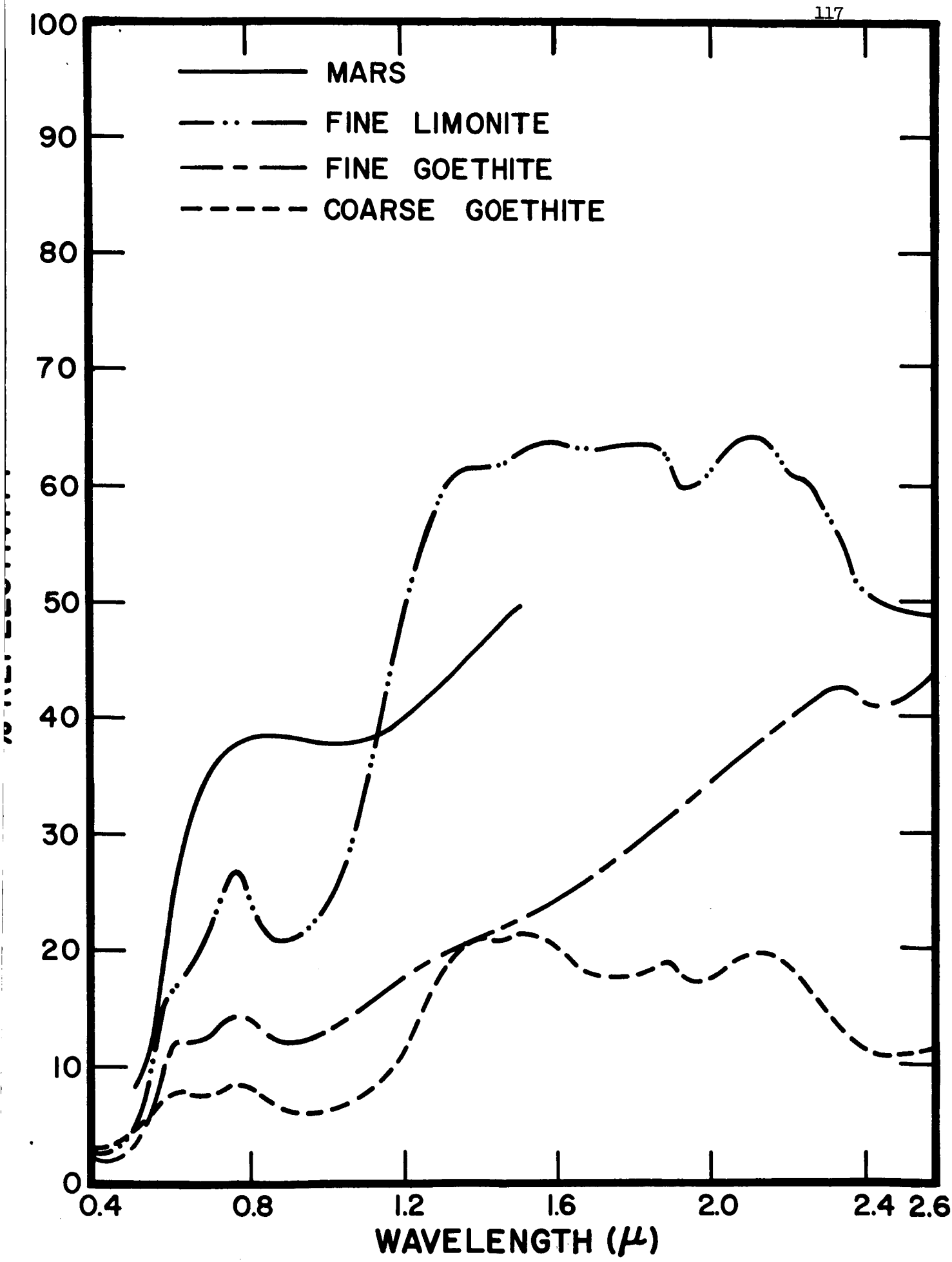
MARS
FINE LIMONITE
FINE GOETHITE
COARSE GOETHITE
100
90
80
70
60
50
40
30
20
10
0
0.4
0.8
1.2
1.6
2.0
2.4
2.6
WAVELENGTH (μ)

Fig. 34. Same as Fig. 33.

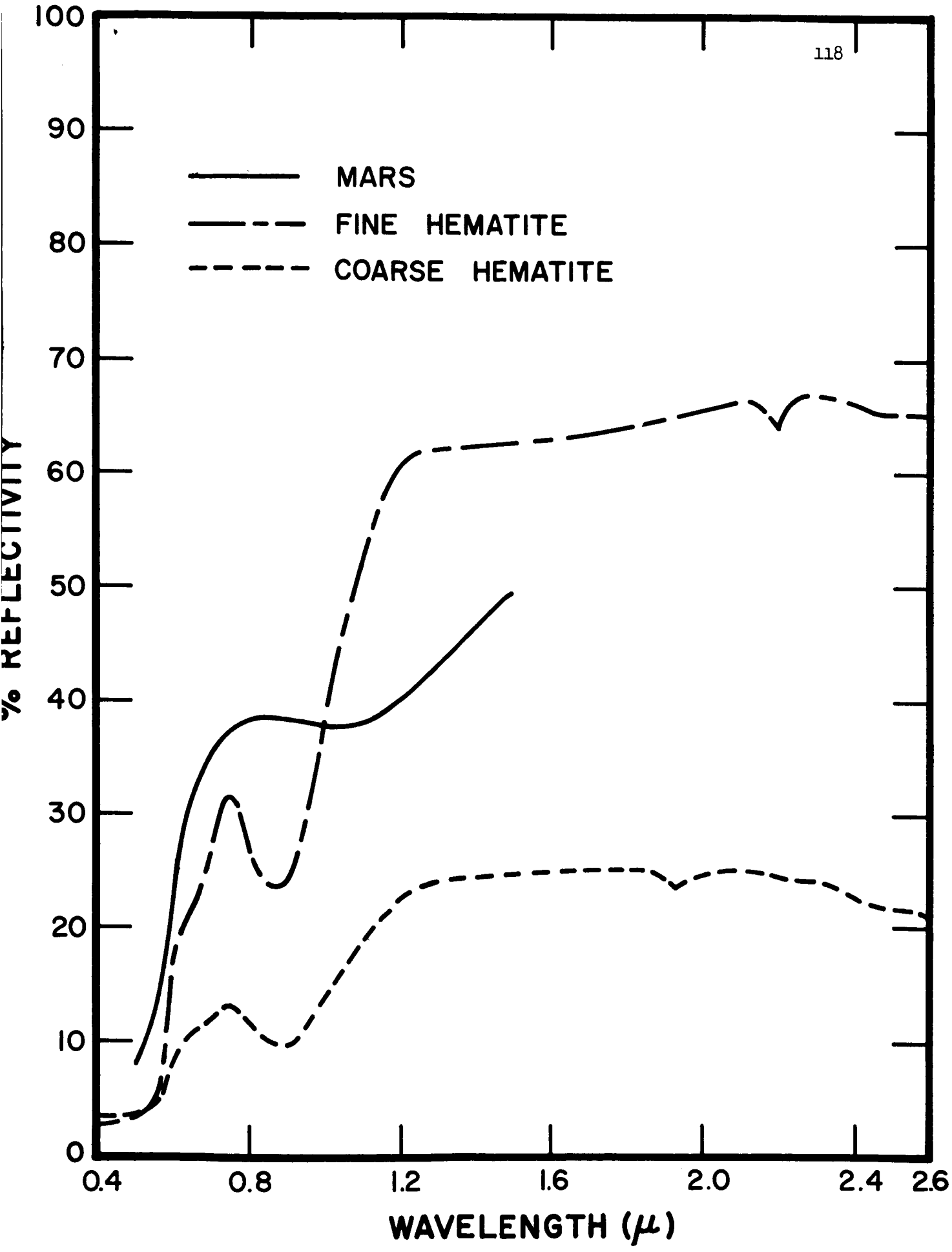
MARS
FINE HEMATITE
COARSE HEMATITE
% REFLECTIVITY
100
90
80
70
60
50
40
30
20
10
0
0.4
0.8
1.2
1.6
2.0
2.4
2.6
WAVELENGTH (μ)

Fig. 35. Same as Fig. 33.

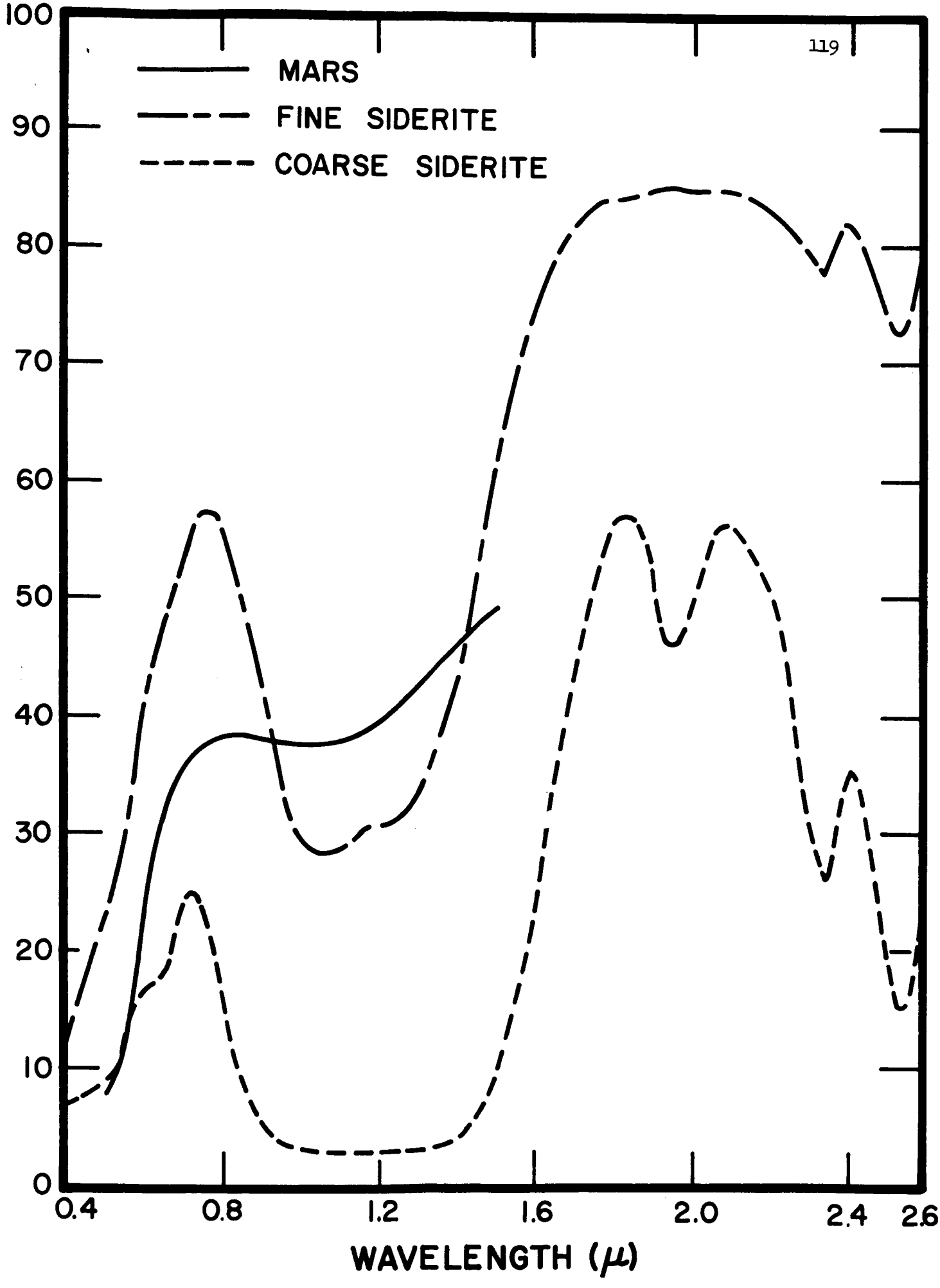
MARS
FINE SIDERITE
COARSE SIDERITE
100
90
80
70
60
50
40
30
20
10
0
0.4
0.8
1.2
1.6
2.0
2.4
2.6
WAVELENGTH (μ)

Fig. 36. Same as Fig. 33.

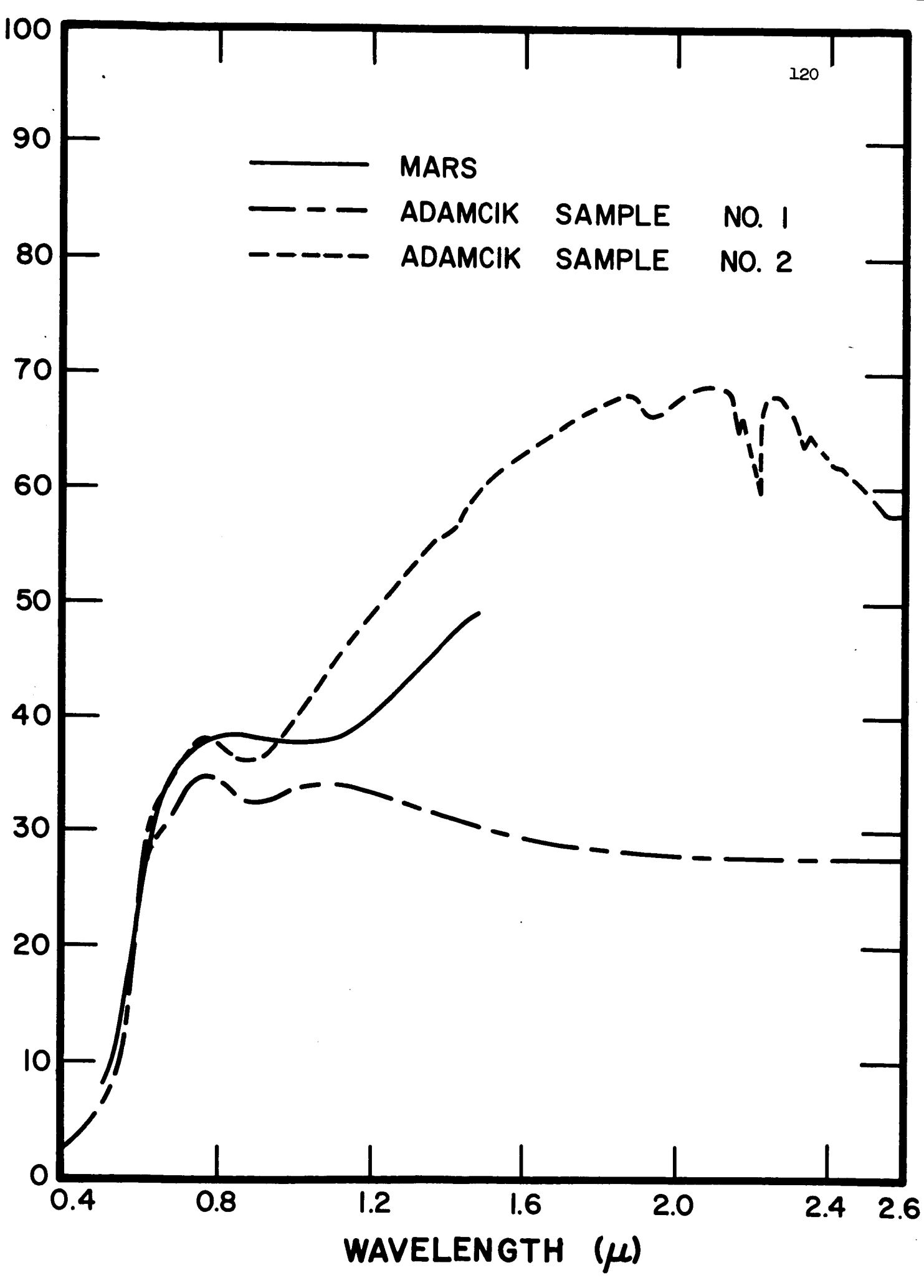
MARS
ADAMCIK SAMPLE NO. 1
ADAMCIK SAMPLE NO. 2
100
90
80
70
60
50
40
30
20
10
0
0.4
0.8
1.2
1.6
2.0
2.4
2.6
WAVELENGTH (μ)

Fig. 37. Same as Fig. 33.

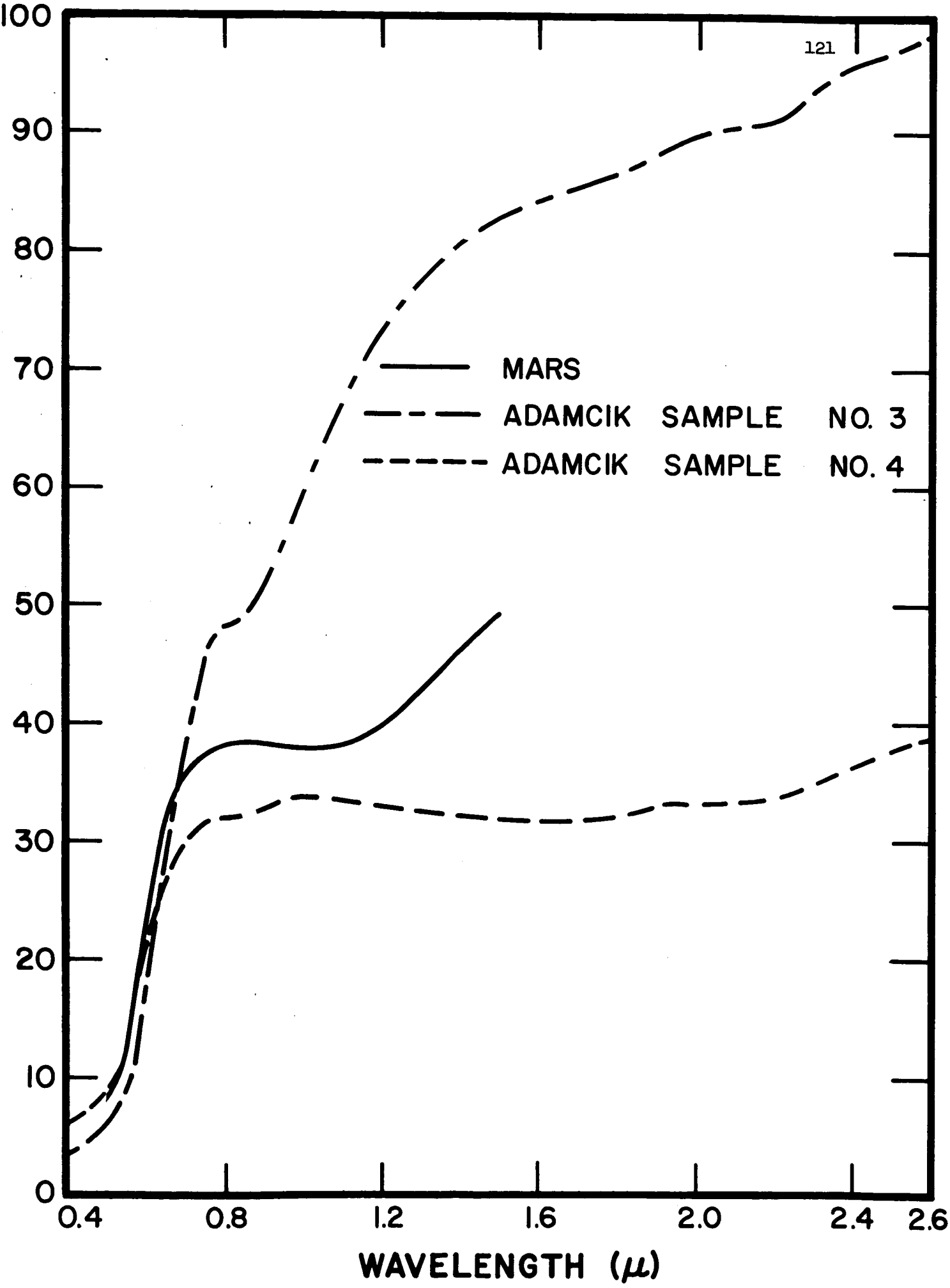
100
90
80
70
60
50
40
30
20
10
0
0.4
0.8
1.2
1.6
2.0
2.4
2.6
WAVELENGTH (μ)
MARS
ADAMCIK SAMPLE NO. 3
ADAMCIK SAMPLE NO. 4

receiving apertures, so that the photocathode always looked at an area smaller than the light spot on the sample. We recall from Sec. 1.2 that the reflectivity for a Lambert surface is independent of direction, i.e. the scattered intensity per unit solid angle coming from a unit projected area is independent of the scattering angle. Thus, in the case of Coulson et al. and observations of parts of the Martian disk with a small-aperture diaphragm, we find for a Lambert surface that the brightness, or flux, is proportional to cos θ_0 but does not depend on cos θ or cos ϕ. Thus, keeping the light source fixed and moving the photometer requires no correction in the data reduction due to projection factors.

In Oetking's cases and mine, however, the photocathode "sees" an area larger than the light spot. Hence, the brightness is proportional to cos θ but does not depend on cos θ_0, and keeping the photometer fixed and moving the light source would require no geometric adjustments in the data reduction. This was the procedure I followed.

As mentioned in the previous section, the instability of the electronics system was sufficient to warrant frequent measurements of the standard-magnesium oxide. It was found desirable, except under the most stable circumstances, to measure the magnesium oxide at about 30-second intervals. Since it often takes that long to move the apparatus in angle and/or to change a color filter, it was decided to measure MgO for each angle and filter. The sequence of measurements for a given angle and filter was: MgO, 2 or 3 samples (quickly rotated), MgO. About 5 to 8 one-second integrations were allowed for each sample. The filter was then changed and the sequence MgO-samples-MgO was repeated. After the third color filter was used, the position of the light source was moved to another angle, and the above procedure repeated.

One difficulty arises from the procedure of measuring MgO at each value of θ_0. Although I mentioned that the measured brightness of a Lambert surface with this apparatus should be independent of θ_0, the MgO is unfortunately not an ideal Lambert surface, as pointed out by Oetking (1966). A good calibration curve for MgO is thus needed. This is not a simple matter since the angle of the light source must be switched rapidly back and forth between an experimental and standard θ_0. This calibration was performed a few times, with the resulting curve taken at $\lambda = 0.56\ \mu$ shown on Fig. 38. The curve was drawn for $\theta = 0°$ and various values of θ_0, with the reflectivity, ρ, normalized to unity at $\theta_0 = 10°$, that value adopted as the standard θ_0 for the calibration. The position $\theta = 0°$, $\theta_0 = 10°$ was also used as the primary standard ($\rho = 1.00$) during the experiment. Thus, each individual MgO measurement at a given θ_0 was divided by the appropriate value of ρ shown on the calibration curve in Fig. 38.

The curve on Fig. 38 confirms completely Oetking's finding that heavily smoked MgO is not an ideal Lambert surface; rather it shows an opposition effect. The close quantitative agreement with Oetking's curve, also shown on Fig. 38, indicates no serious systematic errors in the $\rho(\alpha)$ measurements and a close correspondence between our MgO samples.

One more adjustment was necessary in the MgO measurements: for the very high counting rates (as obtained with MgO in the red and green filters), there is deviation from linearity due to coincidence loss in the pulse-counting system. From the data showing the calibration for linearity, it was possible to multiply these high-count intensity measurements by an appropriate factor, Δ($\Delta = 1.02$ for MgO in the green filter, corresponding to ~ 50,000 counts/sec.; and 1.04 for MgO in the red filter, corresponding to ~ 85,000 counts/sec.). In any case, these adjustments are small in view

Fig. 38. Calibration curve of the magnesium oxide samples at $\lambda = 0.56\ \mu$. Normalized to unity reflectivity at $\alpha = 10°$.

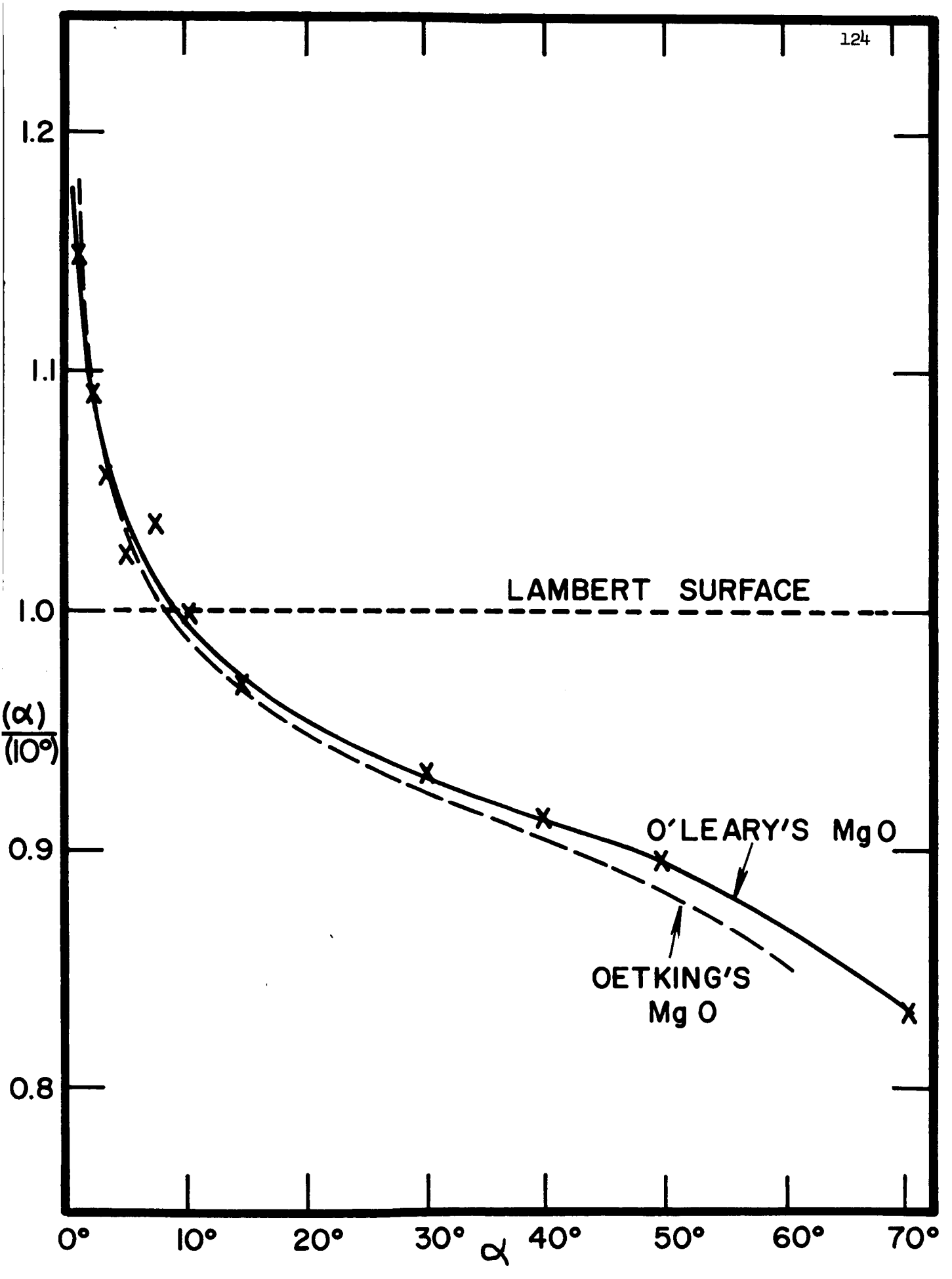
1.2
1.1
1.0
0.9
0.8
(α)/(10°)
LAMBERT SURFACE
O'LEARY'S MgO
OETKING'S MgO
0°
10°
20°
30°
α
40°
50°
60°
70°

of the fact they don't introduce any systematic errors in the slopes in percent change in reflectivity of the derived phase curves. (Note that hereafter the term "slope of the phase curve" refers to the percent change in reflectivity per unit phase angle.)

There is also a few percent uncertainty in the definition of unit reflectivity in the experiment. Uncertainties in the reflectivities of Mars (e.g. atmosphere, heterogeneity) and their correspondence to the laboratory situation are also to be expected. A more complete discussion of the Mars-laboratory normalization will be given in the next section. Again, though, all these factors should not change the slopes of the phase curves, but merely their normalization.

From the above discussion, the reflectivity of each sample can be derived from this expression:

$$\rho(\alpha)_{sample} = \frac{B(\alpha)_{sample}}{B(\alpha)_{MgO}\rho(\alpha)_{MgO}\Delta}$$

where each value of B is equal to a measured count minus the dark current count.

There is one more difficulty about the interpretation of the data: the measurements of Mars made in Chapter II refer to the light reflected from the whole disk, so an exact simulation of the Martian situation would require integration over all possible θ_0, θ, and Φ's for a given α. Such a procedure is cumbersome in practice, and should be adopted only in the case of materials particularly well-suited for the Martian surface. In the general survey analysis of materials presented herein, only data for $\theta = 0^\circ$ (corresponding to the sub-earth point) are shown.

That the $\theta = 0°$ situation is applicable to the measurements of the whole Martian disk can be demonstrated from both observational and laboratory data. In the case of the observational data, we take Dollfus and Focas' brightness measurements along the equator of the Martian disk for $\alpha = 10°$ and $30°$ (see Fig. 29 of Dollfus and Focas, 1966). First they were replotted in terms of annuli of equal area over the disk. The integration of these curves yields $B(\text{disk}, \alpha = 30°)/B(\text{disk}, \alpha = 10°) = 0.82$. These values are corrected for defect of illumination of the disk, i.e. a gibbous disk. On the other hand, recalling that observations of the Martian disk at constant θ_0 require no correction for projection factors, $B(\theta_0 = 0°, \alpha = 30°)/B(\theta_0 = 0°, \alpha = 10°) = 0.87$, reasonably close to that derived for the disk. In other words, the slope of the phase curve for the case of the whole Martian disk is probably similar to that for the sub-solar point. The laboratory data of Coulson et al. (1965) also show a close match between the two cases of whole disk vs. sub-light-source point for a sample of limonite.

It seems, then, that the assumption that $\theta = 0°$ in my laboratory data yields the same phase curve slope as that integrated over the disk is a good one, but further verification would be desirable. I have adopted this assumption, but must admit that any serious error in the assumption might dilute some of the comparisons between Mars and the laboratory samples discussed in the next section.

3.3 Opposition Effect: Results and Discussion

Figs. 39 to 48 show plots of the reflectivity of the samples versus phase angle between $\alpha = 1°$ and $30°$. As mentioned in the previous section each plot applies to $\theta = 0°$, or the sub-earth point, while θ_0, and thus α, varies.

Fig. 39. The opposition effects and phase curves for $1° \leq \alpha \leq 39°$ of laboratory samples compared to those of Mars, $\lambda \sim 0.43\ \mu$ (see text for explanation and Table XVI for sample identification).

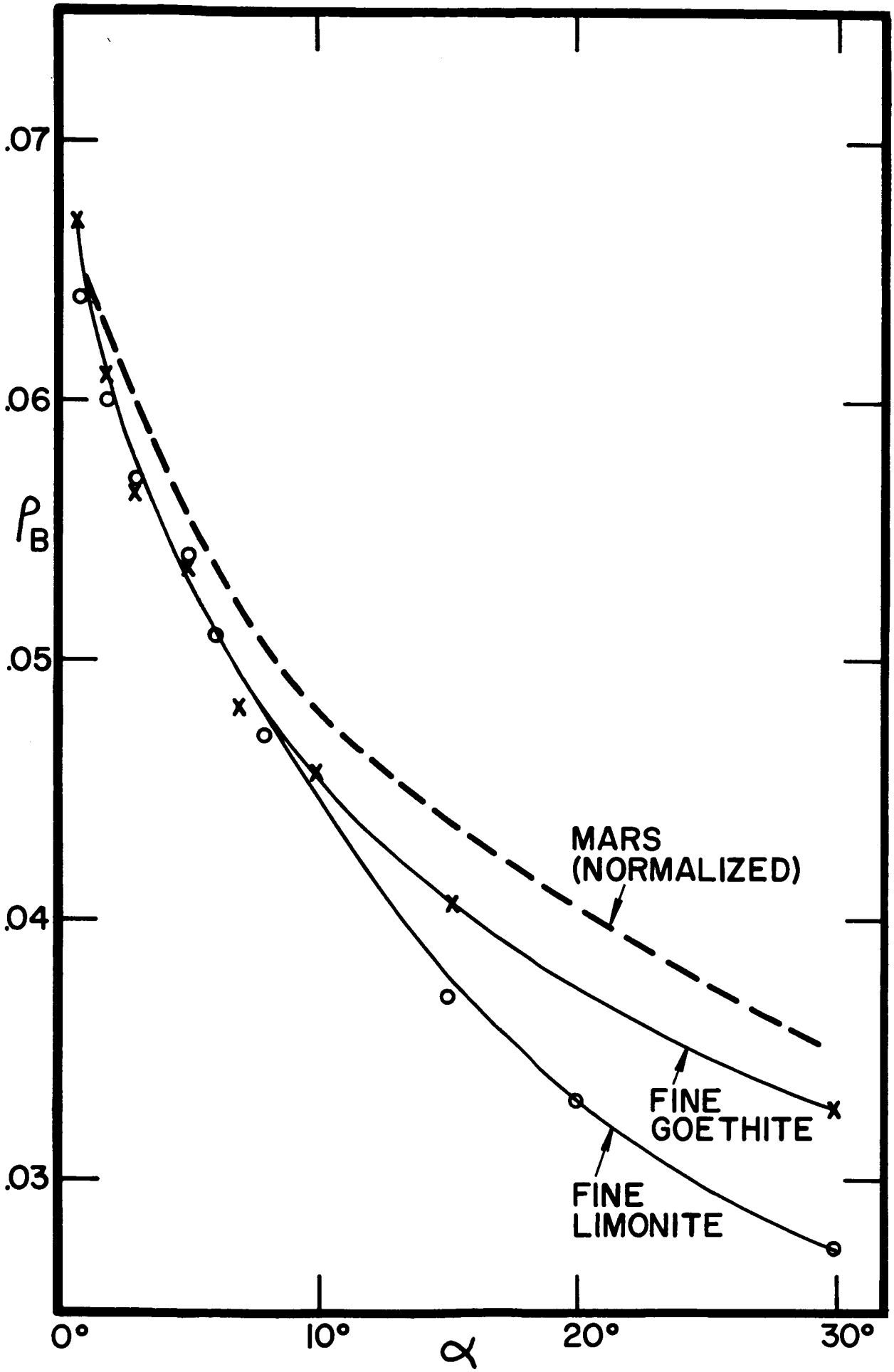
.07
.06
.05
.04
.03
ρ_B
0°
10°
20°
30°
α
MARS
(NORMALIZED)
FINE
GOETHITE
FINE
LIMONITE

Fig. 40. Same as Fig. 39, except $\lambda \sim 0.56\ \mu$.

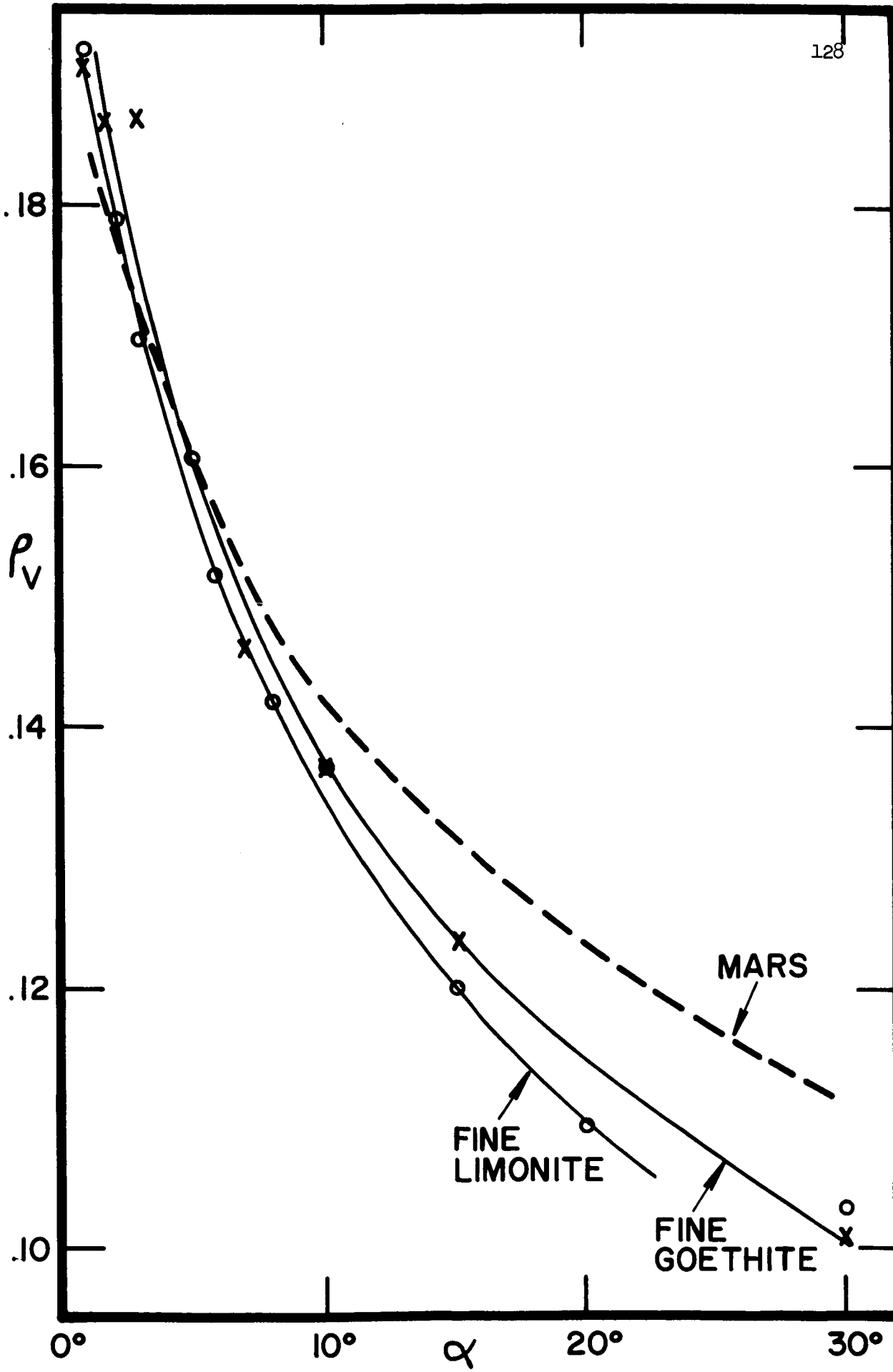
.18
.16
ρ_V
.14
.12
.10
0°
10°
α
20°
30°
MARS
FINE
LIMONITE
FINE
GOETHITE

Fig. 41. Same as Fig. 39, except $\lambda \sim 0.68\ \mu$.

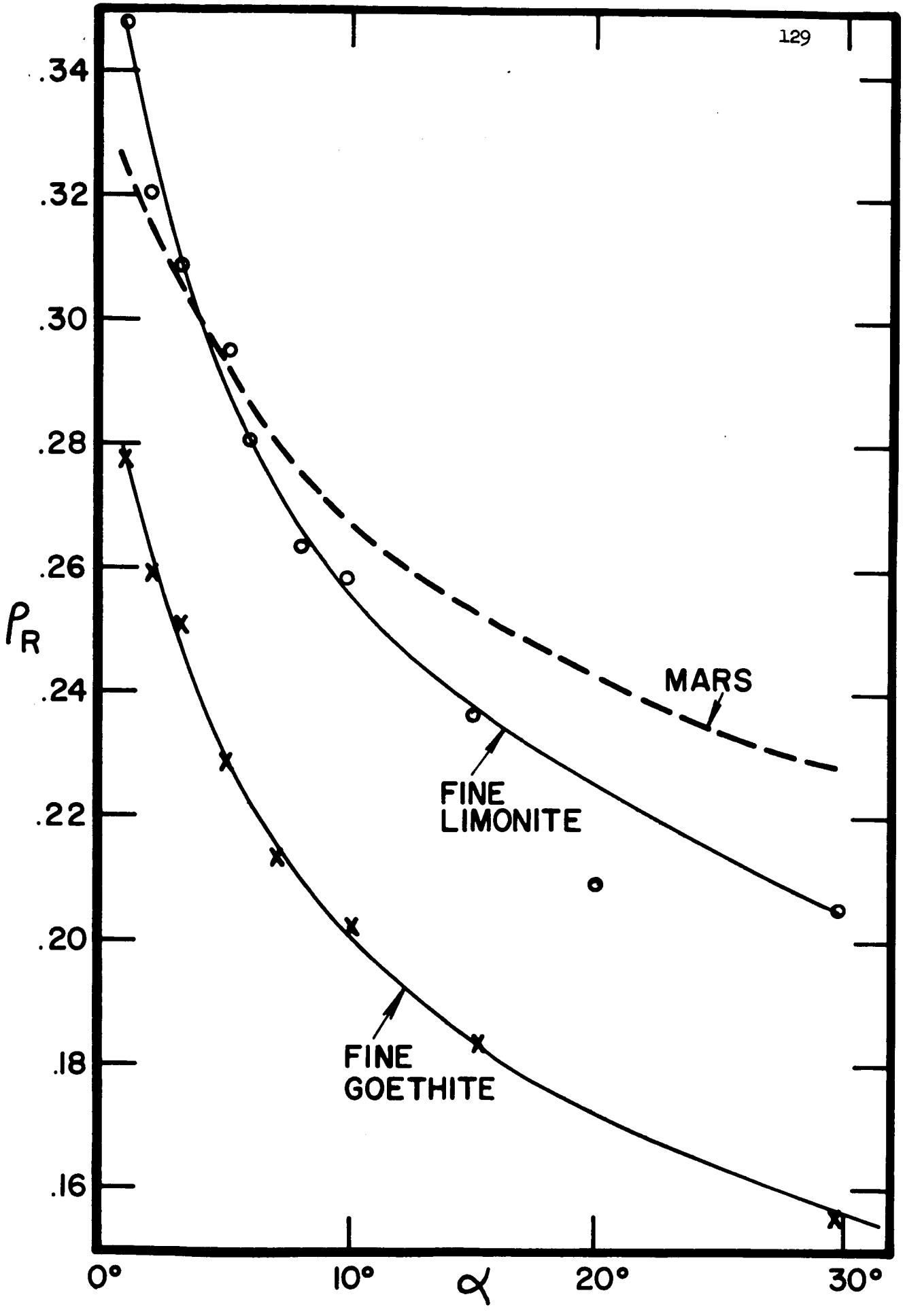
.34
.32
.30
.28
.26
.24
.22
.20
.18
.16
ρ_R
MARS
FINE
LIMONITE
FINE
GOETHITE
0°
10°
α
20°
30°

Fig. 42. Same as Fig. 39.

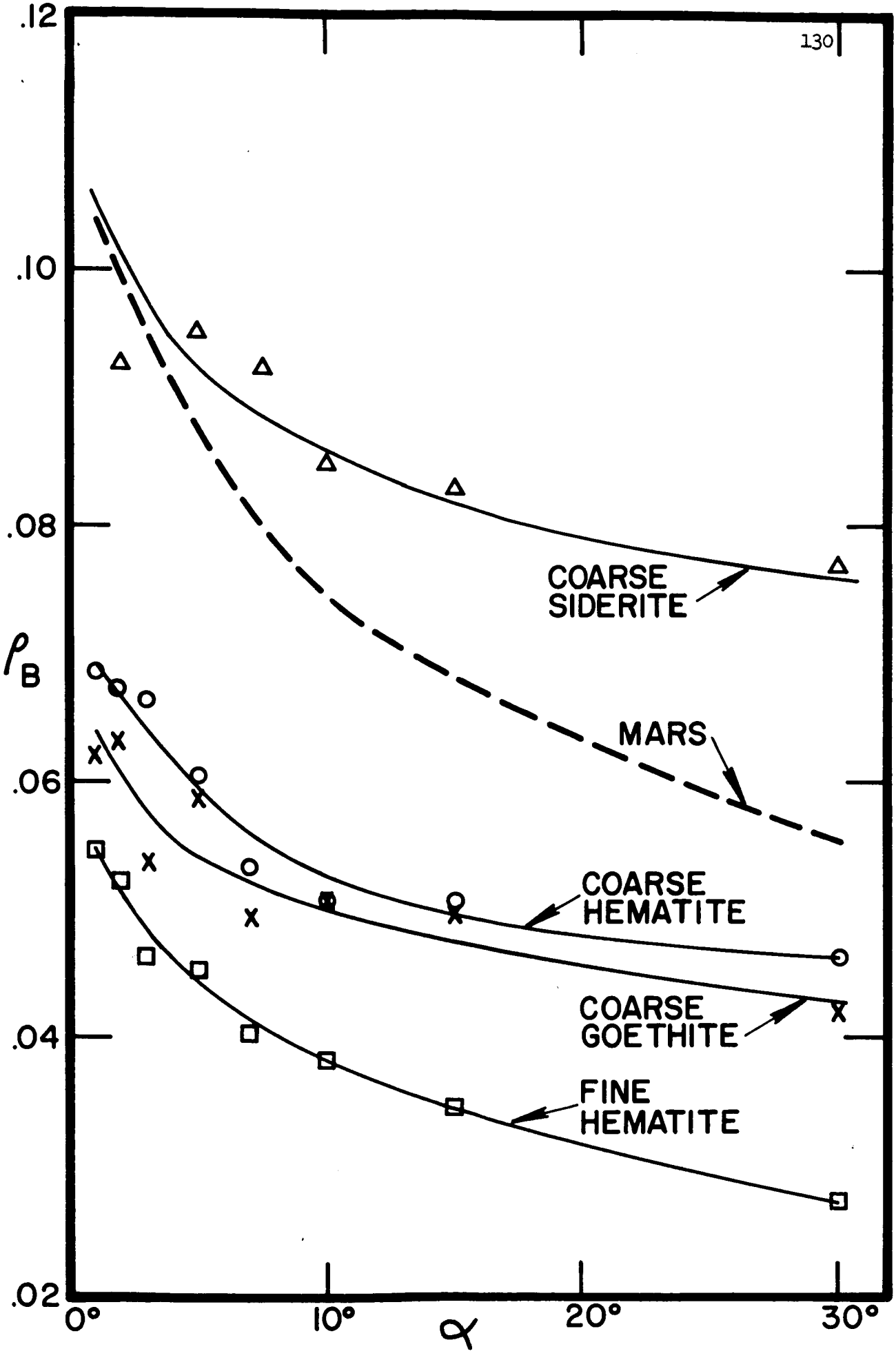
.12
.10
.08
.06
.04
.02
ρ_B
0°
10°
20°
30°
α
COARSE SIDERITE
MARS
COARSE HEMATITE
COARSE GOETHITE
FINE HEMATITE

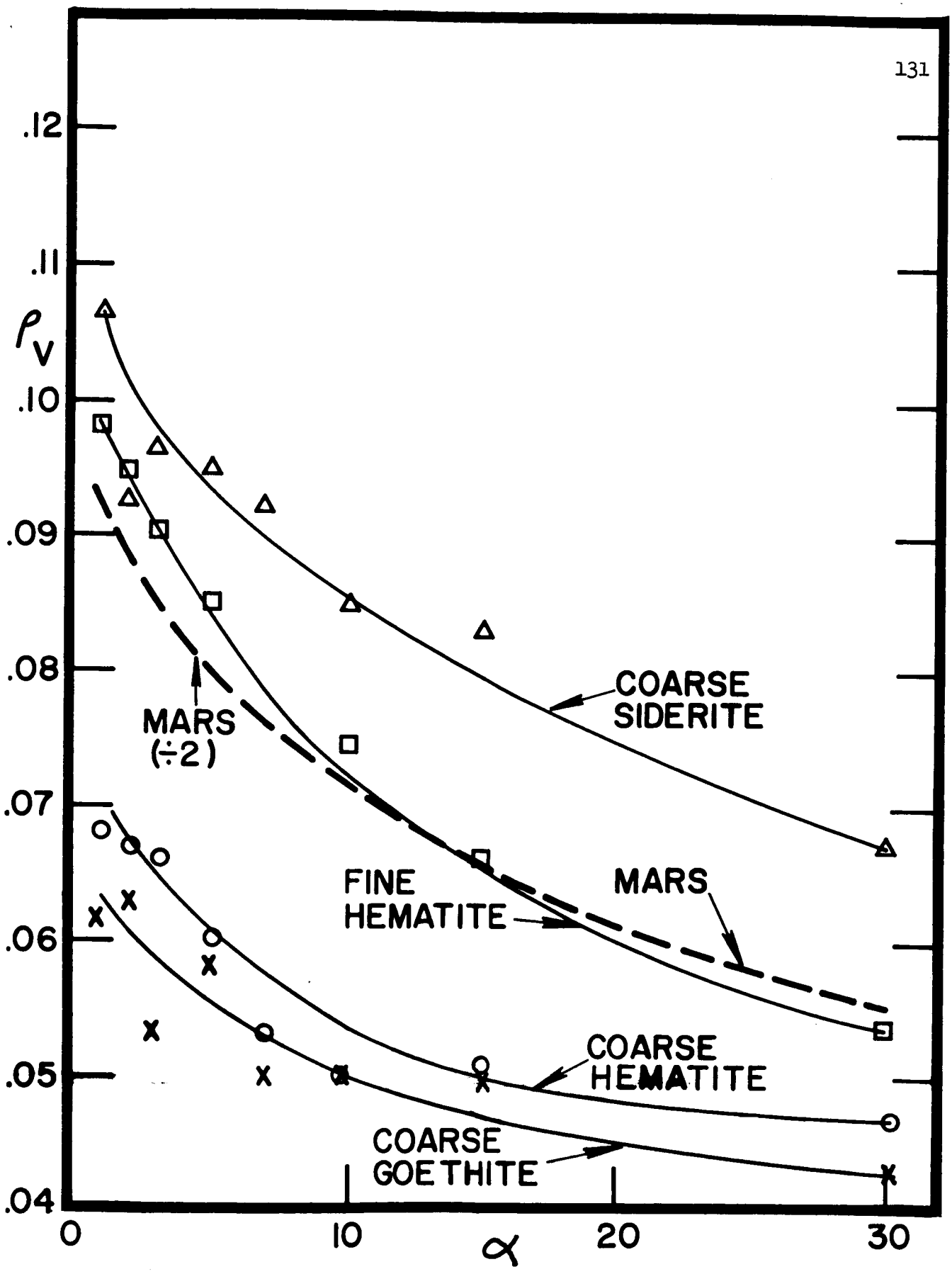

Fig. 43. Same as Fig. 39, except $\lambda \sim 0.56\ \mu$.

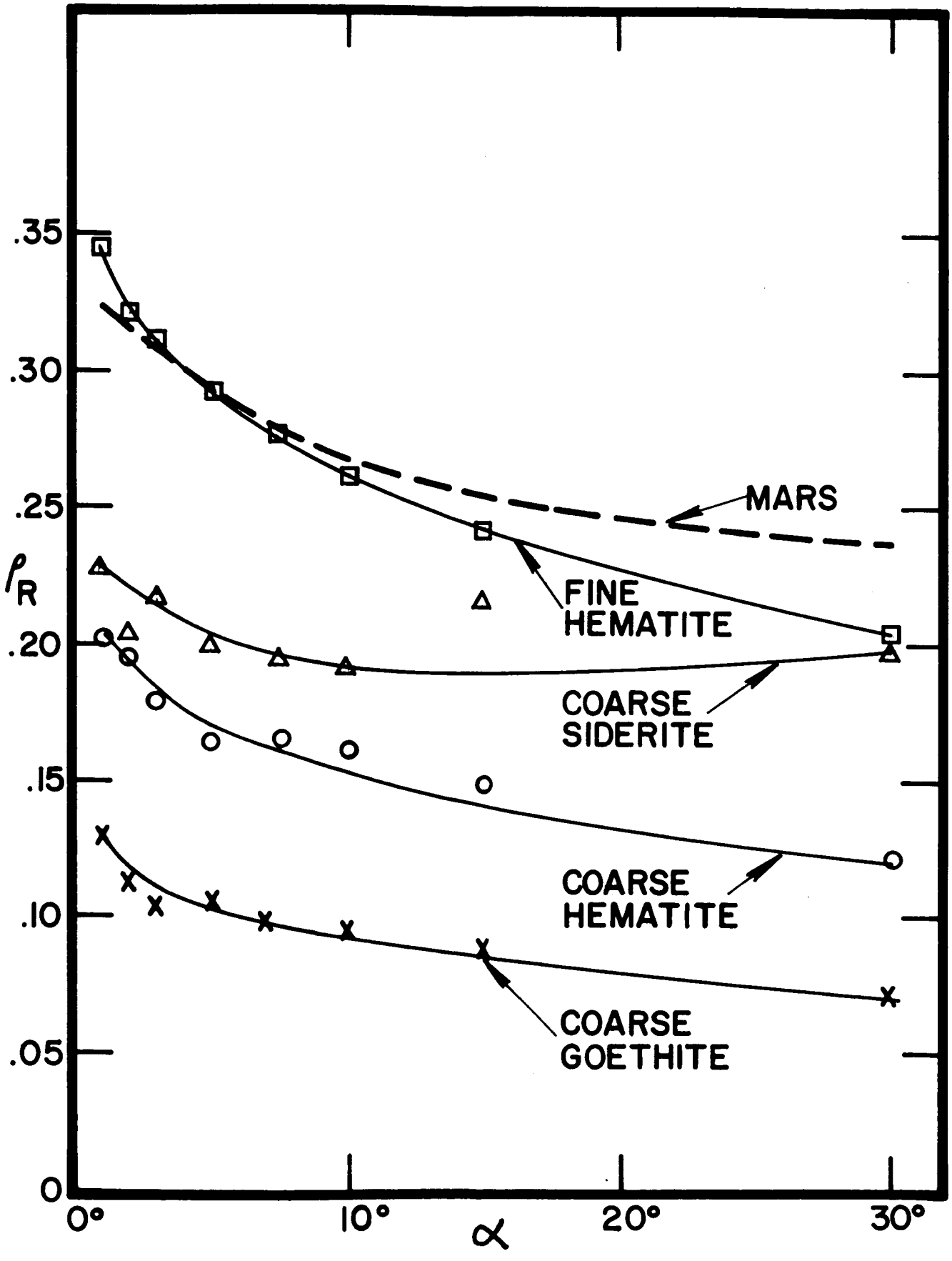

Fig. 44. Same as Fig. 39, except $\lambda \sim 0.68\ \mu$.

Fig. 45. The opposition effects and phase curves of the fine siderite sample, $\lambda \sim 0.43\ \mu$, $\sim 0.56\ \mu$, and $\sim 0.68\ \mu$ (see text for explanation).

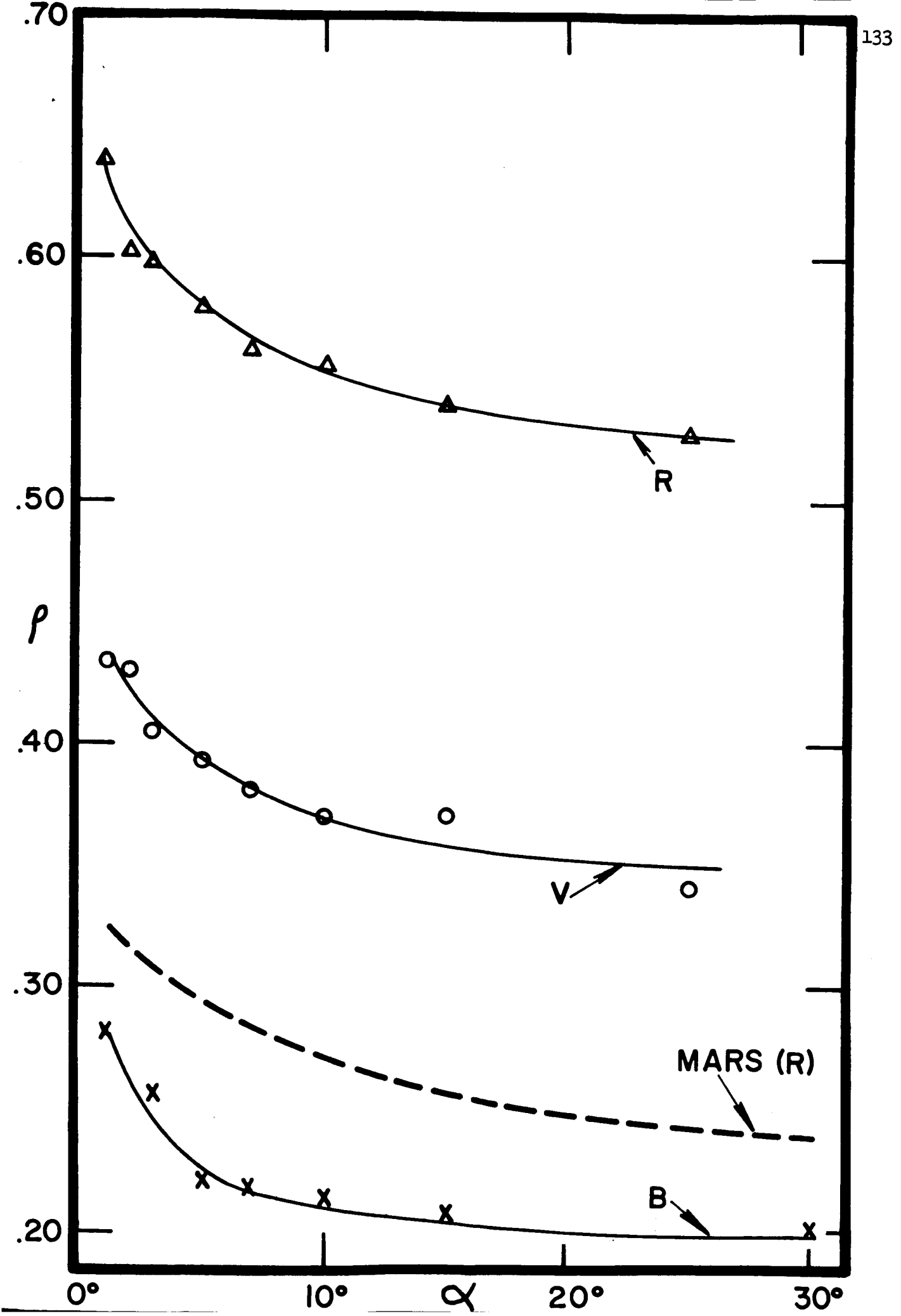
.70
.60
.50
ρ
.40
.30
.20
R
V
MARS (R)
B
0°
10°
α
20°
30°

Fig. 46. Same as Fig. 39.

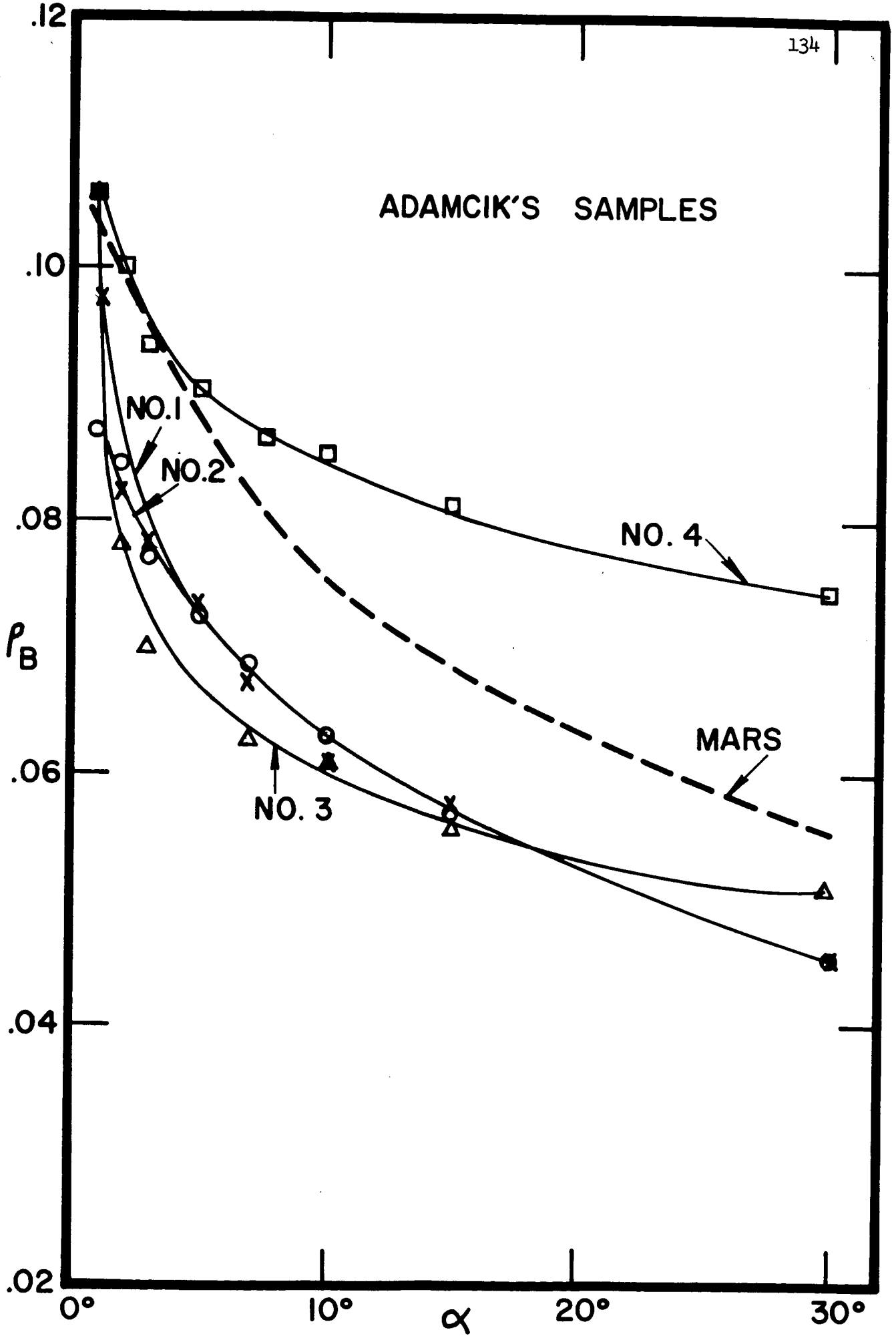
ADAMCIK'S SAMPLES
NO.1
NO.2
NO. 4
MARS
NO. 3
ρ_B
.12
.10
.08
.06
.04
.02
0°
10°
20°
30°
α

Fig. 47. Same as Fig. 39, except $\lambda \sim 0.56$ μ.

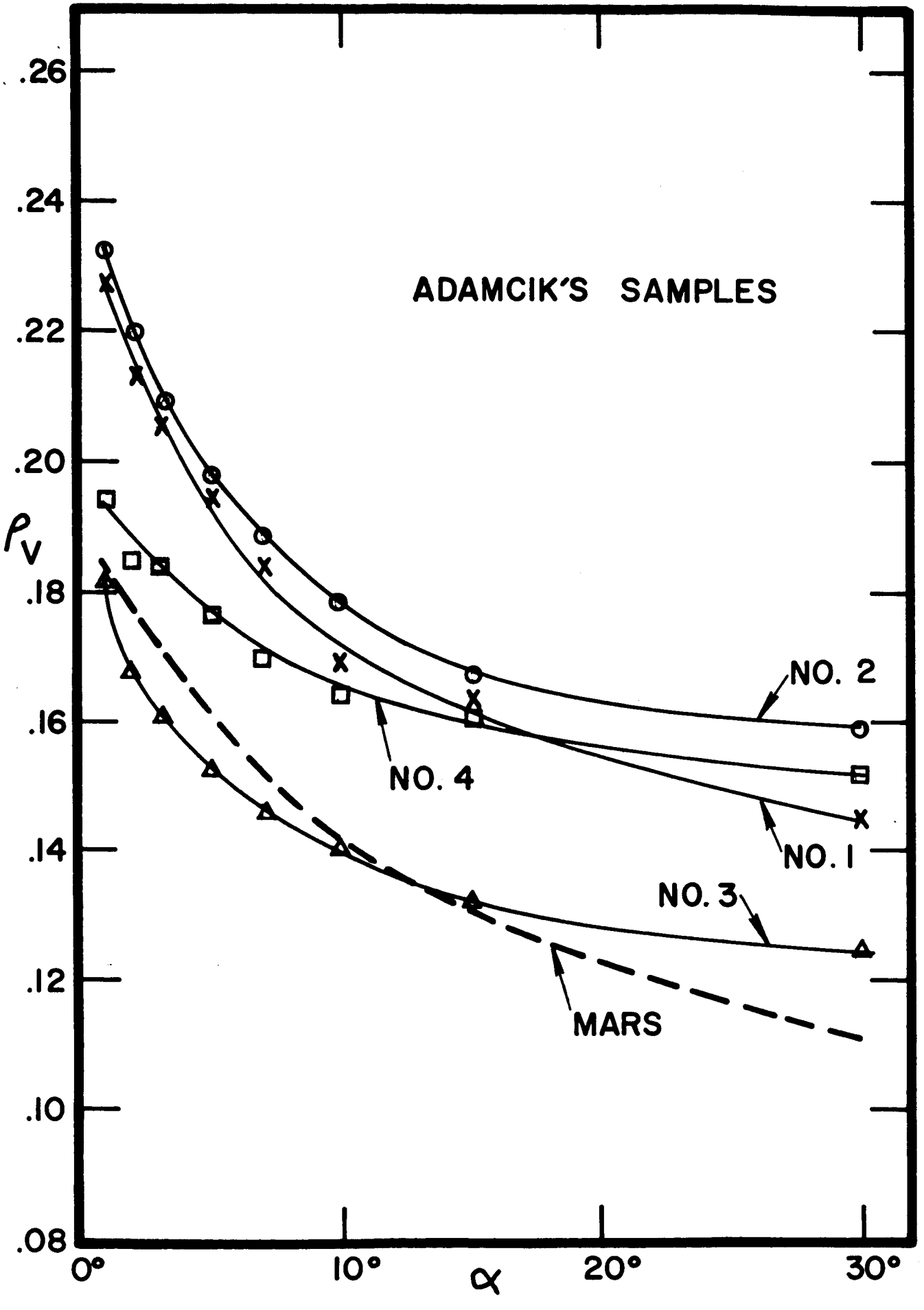
ADAMCIK'S SAMPLES
.26
.24
.22
.20
.18
.16
.14
.12
.10
.08
ρ_V
0°
10°
20°
30°
α
NO. 2
NO. 4
NO. 1
NO. 3
MARS

Fig. 48. Same as Fig. 39, except $\lambda \sim 0.68\ \mu$.

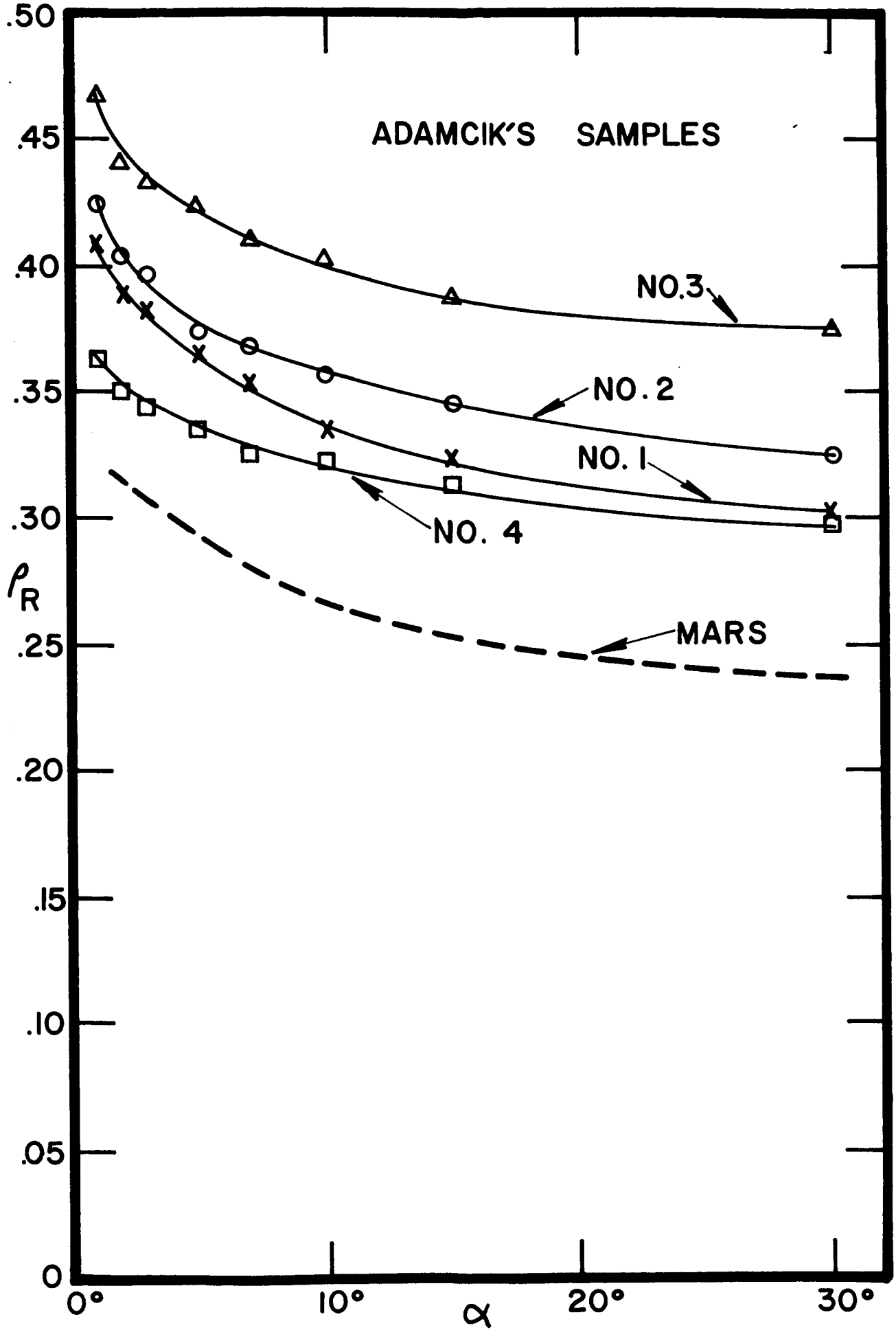
ADAMCIK'S SAMPLES
NO.3
NO. 2
NO. 1
NO. 4
MARS
ρ_R
.50
.45
.40
.35
.30
.25
.20
.15
.10
.05
0
0°
10°
20°
30°
α

On the other hand, the dashed curves in these figures correspond to my observations of the whole Martian disk (from Fig. 20), which have been normalized to the appropriate geometric albedos at $\alpha = 0°$. The Martian curves in Figs. 39 to 48 have been corrected for defect of illumination of the disk. This in effect means that the reflectivity of a gibbous planet is compared to that of a Lambert surface of a flat disk having the same area as the projected illuminated portion of the planet. Limb darkening would add a slight error to this correction, but the error is insignificant for the range of phase angles considered herein.

In order to check the correspondence in reflectivity between the disk and the sub-earth point, we first examine the definition of geometric albedo: the ratio of the average luminance of a planet at $\alpha = 0°$ to that of a Lambert surface of unity albedo at the same distance from the Sun and normal to the incident radiation. But since the observed portion of Mars is actually a hemisphere rather than a disk, all points on the surface are not normal to the incident radiation except for the sub-earth point. There would be equality between the reflectivity of a hypothetical Martian "disk" normal to the incident radiation and that of the observed Martian hemisphere only if there is no limb darkening or no limb brightening.

If Mars were to reflect as a Lambert surface, then the limb darkening law (in terms of brightness per unit area on the "disk") would be $\rho(\theta_0) = \rho(0) \cos \theta_0$ from the definition of a Lambert surface.

There is in fact limb darkening reported for Mars (Dollfus and Focas 1966, Koval 1964, Opik 1966), which is nearly as pronounced as the case of the Lambert surface. For example, Table XVII lists the ratios, b, of reflectivities between $\theta = 45°$ and $0°$ for a Lambert surface and for Mars.

TABLE XVII

Limb darkening of Mars and of various substances, $\lambda = 0.56\ \mu$.

All laboratory measurements apply to $\alpha = 1°$.

Sample	$b = \frac{\rho(\theta_0 = 46°,\ \theta = 45°)}{\rho(\theta_0 = 1°,\ \theta = 0°)}$
Lambert Surface	0.71
Mars[a]	0.78
Smoked Magnesium Oxide	0.65
MS-1: Goethite ($r < 19\ \mu$)	0.96
Goethite ($125\ \mu < r < 250\ \mu$)	0.96 (?)
MS-2: Yellow Ochre Limonite ($r < 19\ \mu$)	0.98
MS-3: Hematite ($r < 19\ \mu$)	0.93
Hematite ($250\ \mu < r < 500\ \mu$)	0.85 (?)
MS-4: Siderite ($r < 19\ \mu$)	0.91
Siderite ($250\ \mu < r < 500\ \mu$)	0.83 (?)
Adamcik Samples:	
No. 1	0.94
No. 2	0.95
No. 3	0.89
No. 4	0.81

[a]From observations by Koval (1965) and Dollfus and Focas (1966) performed for $\alpha \lesssim 10°$.

Thus, in order to derive a value for $\rho(\theta = 0°)$ in terms of the measured (disk), it is necessary to recover $\rho(\theta = 0°)$ from the integration. Consider an element of area dA on the hemisphere at angular distance θ from the sub-earth point and at azimuthal position ϕ. In that case,

$$\rho(\text{disk}) = \frac{\int_{\text{hemisphere}} \rho(\theta,\phi) \cos\theta_0 \cos\theta \, dA}{\int \cos\theta \, d\, A} \tag{3.3.1}$$

But

$$dA = \sin\theta \, d\theta \, d\phi, \tag{3.3.2}$$

and at $\alpha = 0°$, $\theta = \theta_0$, so

$$\rho(\text{disk}) = \frac{\int_{\theta=0°}^{\pi/2} \int_{\phi=0}^{2\pi} \rho(\theta,\phi) \sin\theta \cos^2\theta \, d\theta \, d\phi}{\int_{\theta=0°}^{\pi/2} \int_{\phi=0°}^{2\pi} \sin\theta \cos\theta \, d\theta \, d\phi} \tag{3.3.3}$$

For a Lambert surface,

$$\rho(\text{disk}) = \rho(\theta = 0°) \int_{\theta=0°}^{\pi/2} \int_{\phi=0°}^{2\pi} \sin\theta \cos^2\theta \, d\theta \, d\phi \tag{3.3.4}$$

$$= \frac{2}{3} \rho(\theta = 0°).$$

From the data in Table XVII we can say from the rough correspondence between Mars and a Lambert surface that the reflectivity of the visible Martian hemisphere is ~ 0.7 times the reflectivity of Mars at $\theta = 0°$. It would thus seem advisable to adjust the Martian disk observations to the

$\theta = 0°$ observations in order to establish correspondence with the laboratory situation.

However, it was first worthwhile to measure the limb darkening for the experimental samples. Table XVII lists values of $b = \rho(\theta_0 = 46°, \theta = 45°)/\rho(\theta_0 = 1°, \theta = 0°)$ for the samples. These values of b then denote the limb darkening at $\theta = 45°$ for $\alpha = 1°$. Note the high values of b for the laboratory samples relative to those values for Mars, MgO, and a Lambert surface. This effect is especially pronounced for the finely divided substances.

The point to make here is that the reflectivities of most samples investigated, especially finely divided goethite and limonite, behave in such a way as to give very small limb-darkening for a planet covered with these substances. I decided to retain the values of Martian ρ integrated over the disk without correcting for limb-darkening, since there is only slight limb-darkening in the laboratory cases. In other words, the reflectivities measured for a given sample correspond roughly to those reflectivities which would be obtained from integration over a ficticious planet, covered with that sample. Although this correspondence--and thus the correspondence of the laboratory reflectivities with the Martian reflectivities--is far from perfect, the uncertainties in the actual Martian reflectivities mentioned above (e.g. atmospheric component, heterogeneity of the surface), are sufficient so as not to be concerned with an exact relationship between the Martian and laboratory reflectivities. What is important in Figs. 39 to 48 is a match in slopes of the phase curves, not a match in the actual values of the reflectivities between Mars and the samples.

The large apparent discrepancy between the limb darkening of Mars and that of limonite powder was mentioned to me by E. Gray (private communication), as a result of his experiments conducted with Coulson and Bouricius (Coulson et al. 1964, 1965). He suggested it could be resolved by asserting the Martian surface does not darken toward the limb. He mentioned some observations showing no Martian limb darkening, reported to him by Sinton at Flaggstaff and the Southern Hemisphere.

However, it would certainly be worthwhile to get a better understanding of Martian limb darkening. The fact that it seems so pronounced, yet repeatable, from Koval's, Opik's, and Dollfus and Focas' observations (as well as some I made at Kitt Peak during the 1967 opposition, and the fact that it is not very different from the Lambert case (the similarity is especially striking toward longer wavelengths), make it difficult to explain the limb darkening by transient phenomena such as clouds near the limb. Furthermore, any clouds or haze concentrated toward the limb should result in limb brightening, not limb darkening, since all observed Martian clouds seem to be bright or brighter than the bright areas; i.e., the bright areas have never been reported to have been obscured by darker features. Perhaps those observations of no Martian limb-darkening were made at times of clouds or haze near the limb, whereas those observations of Martian limb darkening were made at times of atmospheric transparency. In that case the limb darkening would almost certainly have to be attributable to the surface.

If the discrepancy between Martian limb darkening and laboratory limb darkening is real, then the theory of the widespread yellow ochre limonite powder over the Martian bright areas might be in serious trouble. It would be worthwhile to check this problem further by performing detailed photometry of existing photographs of Mars. If limb-darkening appears to be firmly established from these analyses, then it would be fruitful to

attempt to prepare a form of limonite which will give the Martian limb darkening. As to whether such a form were to exist is not known now. Since the tendency toward limb darkening is greater for the coarser samples, perhaps a mixture of larger limonite particles (but with the fine grains adsorbed on the surfaces to preserve the yellow-ochre color and the required opposition effect) with a variety of orientations of the surface slopes either due to roughness or to the particles themselves, would produce the limb darkening. Limonite "stain" on larger particles or rocks, suggested by Binder and Cruikshank (1966) is another possibility. Likewise, very small particles might result in a tendency toward limb darkening, presumably because a fine powder would better approximate a Lambert Surface.

However, the large range of particle sizes considered make the possibility for considerable limb darkening very slim from the limonite and goethite samples so far investigated: Coulson et al.'s pulverized samples have a mean radius of 7 μ, and my two samples had radii of less then 19 μ and ~ 200 μ, respectively. All samples showed negligible limb darkening.

Until a more thorough analysis is performed on this important limb darkening test, it would be premature to completely eliminate yellow ochre limonite as the predominant substance covering the Martian bright areas. However, this discrepancy seems to be a significant objection for the time being.

We now turn our attention to the interpretation of the opposition effects of Figs. 39 to 48. Again I emphasize that the correspondence in percent reflectivities between Mars and samples is not the significant factor, as there are too many uncertainties to be able to establish an accurate match. What is significant is the correspondence in the slopes of the phase curves (in terms of percent change in reflectivity per unit

interval in phase angle). A better ordinate in Figs. 39 to 48 might have been magnitude rather than reflectivity, but reflectivity was preferred for easier reading of the laboratory values.

The phase curves in Figs. 39 to 48 generally show consistent results with small error scatter in spite of the instabilities in the electronics. This is due to the fact that the MgO standard was frequently run, and its calibration curve (Fig. 38) well known. The error scatter for the powder samples was $\sim \pm 1\%$, about the same amount as that obtained from the photometry of Mars described in Chapter II. However, the coarser samples showed a higher error scatter, presumably because of the large sizes of the particles relative to the quarter-inch spot of light in the sample tray. There are bound to be some specular reflections in various isolated directions from the sides of these larger particles.

Phase angles of up to 70° ($\theta = 0°$, $\theta_0 = 70°$) were reached in the laboratory photometry. However, they are not presented in Figs. 39 to 48 because of the importance of showing the known portions of the Martian phase curve next to the laboratory curves. Most samples generally showed a minimum in reflectivity at $\alpha = 40°$ to 50° and an increase at larger phase angles such that $\rho(70°) \sim \rho(20°)$.

We now discuss the interpretation of the results, one sample at a time. Note that the phase curves measured in the blue (0.44 μ) might be quite different from the observed Martian phase curve because of the uncertain atmospheric component. The conclusions reached about each substance essentially ignore the polarization results, since the possible range in $P(\alpha,\lambda)$ of Mars is expected to tolerate large quantities of these samples on the Martian surface (see Sec. 1.3). Of course, further investigations might find this assumption to be inapplicable.

Figs. 33 and 39-41 show the spectra and phase curves, respectively, of the finely pulverized limonite and goethite from samples MS-1 and MS-2 described in Table XVI. The Martian phase curve at λ 0.44 μ (Fig. 39) is arbitrarily normalized to a reflectivity of 0.065 at $\alpha = 1°$ in order to make a closer comparison between Mars and laboratory. This systematic reduction of reflectivities of Mars from those observed is expected for the surface, since the Martian atmosphere at this wavelength probably contributes a significant component to the total brightness. Note the fairly good agreement between the samples and Mars, both in spectra and phase curve slopes at 0.44 and 0.56 μ (the opposition effects of the limonite and goethite are slightly steeper than those of Mars). But in the red and near infrared the limonite and goethite are not as bright as Mars and the phase-curve slopes are considerably steeper than the Martian one. Furthermore, the 0.87-μ band present in the limonite and goethite spectra is missing in the Martian spectrum (Younkin 1966; Tull 1966; and Sinton 1967). From all these data it is highly suggestive that the finely pulverized limonite and goethite from samples MS-1 and MS-2 cannot cover a major portion of the Martian bright areas. A more quantitative statement about this will follow a discussion of the other samples.

The spectra and phase curve of the coarse goethite is shown in Figs. 33 and 42-44. It is immediately obvious that this sample is too dark to cover the Martian bright areas, but it is conceivable that it might be plentiful over the dark areas. The visible reflection spectrum of the dark areas is similar to that reported by Dollfus, and the opposition effects and phase curves are not unlike those of Mars. The opposition effect of these coarse samples is generally stronger than that of the Martian disk, but the phase curve for $\alpha > 5°$ is not as steep. If photometry of the Martian dark areas near opposition can be performed accurately, it would be

interesting to look for these effects. Of course, the idea that larger particles cover the Martian dark areas is not a new one (Rea 1965). He suggested that this variation in particle size "may result from a combination of a range of surface elevations with a size fractionation in altitude of the dust raised from the surface by winds." Presumably, the particle size distribution in elevated areas would depend on the atmospheric circulation, and would be skewed toward larger particles (the dark areas).

In spite of the possibility that goethite or limonite with larger particle sizes may cover the dark areas, there is the problem of the lack of the 0.87-μ band in the spectrum of both the Martian dark areas as well as the bright areas (Younkin 1966).

The spectra and phase curves of fine and coarse hematite from samples MS-3 are shown in Figs. 34 and 42-44. We first discuss the fine hematite. A significant atmospheric component (~ 50%) at 0.55 μ must be postulated for hematite to be the major constituent of the Martian surface, since that material is too dark at wavelengths shorter than the red. We recall that, on the contrary, the limonite and goethite samples were not bright enough in the red to match Mars but were sufficiently bright at shorter wavelengths. A mixture of goethite and hematite might alleviate matters, but there is still the 0.87-μ band present in the spectra of all these iron oxides but absent in Martian spectra to contend with. The opposition effects of the hematite are slightly stronger than the Martian one at 0.44 and 0.56 μ, but considerably stronger in the red. One cannot help but arrive at a similar conclusion about the fine hematite as the fine goethite and limonite: it is highly suggestive that hematite cannot cover a major portion of the Martian bright areas.

The spectra and phase curves of the coarse hematite from sample MS-3 are also shown in Figs. 40 and 42-44. All properties of the coarse hematite are remarkably similar to those of the coarse goethite (except that the latter is "darker" in the red and infrared), and similar conclusions can be made: it is conceivable for coarse hematite to cover the dark areas from the points of view of the opposition effect and visible and near infrared reflectivities. However, the lack of the 0.87-μ band in the Martian spectrum remains as a serious objection.

The spectra and phase curves of the fine siderite from sample MS-4 are shown in Figs. 35 and 45. From the spectra, we see that the fine siderite is much too bright in the visible to exclusively cover even the brightest Martian bright areas. There is also the problem of the broad, deep 1.05-μ absorption band in the siderite. It is interesting to note, however, that the slight 1.05-μ minimum in the Martian spectrum reported by Tull (1966) and Sinton (1967) do not report a 1.05-μ minimum in the Martian spectrum, but this is not inconsistent with Tull's data, since Younkin and Sinton did not observe at wavelengths greater than 1.1 μ. Fig. 35 shows that neither Mars nor the siderite samples start to increase in reflectivity until wavelengths of greater than 1.1 μ are reached.

This possibility of the presence of siderite on the Martian surface is also interesting in view of the 3.45-μ minimum in Martian spectra reported by Sinton (1957, 1959) and reanalyzed by Rea, O'Leary, and Sinton (1965). This minimum might be attributable to carbonates, perhaps siderite, on the Martian surface.

In regard to the thermodynamic equilibrium of siderite and other carbonates, O'Connor (1967) mentioned, "It should be of interest to note that the equilibrium conditions for the Martian surface indicate a probability

of the presence of a family of minerals with known infrared absorption bands--the carbonates." If Tull's absorption does in fact exist, then the siderite and carbonate matter should certainly be pursued further. Initially, polarizations of siderite samples should be measured.

The opposition effect and phase curve slopes of the fine siderite (Fig. 45) are close to those of Mars; only the visible albedos in the two cases are very different.

The coarse siderite shows an even stronger 1.05-μ absorption band (Fig. 35) than the fine siderite. The reflectivities of the coarse siderite are similar to those of Mars at 0.44 and 0.56 μ, but are considerably lower than those of Mars in the red (Figs. 42-44). The opposition effects of coarse siderite and Mars match well in the green and red filters, but Mars has a considerably steeper phase function than the siderite at 0.44 μ and $5° < \alpha < 30°$. An explanation for this behavior might be a significant contribution to the observed Martian brightness in the blue by aerosols having steep phase functions in the range $\alpha \gtrsim 5°$, as discussed in Chapter II. But the fact that the 1.05-μ band is not prominent in the Martian spectrum again rules out the predominance of any siderite covering the Martian surface.

We finally come to Adamcik's four synthetic samples consisting of various mixtures of limonite, hematite, hornblende, magnetite, kaolin, etc., described in Appendix II. The composition of these samples was deliberately set to match the visible and near infrared reflectivities in most portions of the Martian reflection spectrum (e.g. see Draper, Adamcik, and Gibson 1966). For example, we can see from Fig. 36 that if his sample No. 1 were combined with his sample No. 2 in about equal parts, then the Martian reflection spectrum would be well-matched. The same principle applies to his samples No. 3 and No. 4 (Fig. 37). There is one

notable exception to this: the 0.87-μ iron oxide band remains prominent in his samples No. 1 and No. 2, and a trace of it remains in his samples No. 3 and No. 4. Incidentally, it was Adamcik's sample No. 1 which, when mixed with Dollfus and Focas' yellow ochre limonite powder sample D_0 in a mosaic (32% sample No. 1 and 68% sample D_0), yielded for Dollfus and Focas (1966) their mixture M_4, a mixture they have reported to match so well the Martian bright areas in $P(\alpha,\lambda)$ and $\rho(\lambda)$.

At 0.44 μ (Fig. 46) the opposition effects (for $\alpha < 5°$) of samples Nos. 1, 2, and 3 are considerably steeper than that of Mars. There is again the possibility of aerosols contributing significantly to the total Martian brightness such that the observed phase curve is flattened at $\alpha < 5°$. This could be done by either Rayleigh or Mie scatters. Sample No. 4 on the other hand matches well the observed opposition effect in the blue, but the phase curve of the sample for $\alpha > 5°$ is much flatter than the Martian phase curve. Again, aerosols could explain the discrepancy, but this time it would be Mie scatterers with a steep phase function for $\alpha > 5°$. An exact interpretation of the behavior of the phase curves in the blue is obviously ambiguous.

The situation at 0.56 μ(Fig. 47) is perhaps clearer: samples 1 and 2 match well the observed Martian phase curves at all phase angles, but samples 3 and 4 show considerably flatter phase curves for $\alpha > 5°$. Furthermore, sample 3 shows a slightly greater opposition effect and sample 4 a slightly flatter opposition effect than does Mars.

The phase curves in the red (Fig. 48) for Adamcik's samples are all reasonably compatible with the Martian phase curve.

Table XVIII concisely summarizes the results discussed in the last few paragraphs as well as the entire work. This Table will be discussed in the next, and concluding, chapter.

TABLE XVIII

Comparisons of the samples with observations of Mars[a]

Sample	Spectral Features	Reflectivity and Color in Visible (0.5-0.8 μ)	Infrared Reflectivity (0.8-1.5 μ)	Opposition Effect Slope ($\alpha < 5°$)	Phase Curve Slope ($\alpha > 5°$)	Polarization $P(\alpha, \lambda)$	Thermodynamic Stability Under Martian Conditions[b]	Tentative Verdict	Probable Limb Darkening in Visible
MS-1: fine goethite	0.87-μ band not found on Mars	fairly good except lower in red	lower	slightly steeper	fairly good	fairly good	probably unstable		considerably less
MS-1: coarse goethite	0.87-μ band not found on Mars	lower except for Martian dark areas	lower	fairly good	fairly good	possible	probably unstable		considerably less
MS-2: fine yellow-ochre limonite	0.87-μ band not found on Mars	fairly good	fairly good	slightly steeper	fairly good	fairly good	probably unstable		considerably less
MS-3: fine hematite	0.87-μ band not found on Mars	fairly good except lower in green	fairly good	somewhat steeper	slightly steeper	possible	?	might be present in small quantities but cannot be the predominant covering for the Martian surface	somewhat less
MS-3: coarse hematite	0.87-μ band not found on Mars	lower except for Martian dark areas	lower	fairly good	fairly good	possible	?		slightly less
MS-4: fine siderite	strong 1.05-μ band, and 3.45-μ band found marginally on Mars	considerably higher	fairly good except in 1.0 μ region	fairly good	fairly good	?	stable		slightly less
MS-4: coarse siderite		fairly good except lower in red	lower	fairly good	somewhat less	?	stable		slightly less
Adamcik No. 1	0.87-μ band not found on Mars	good	slightly higher	fairly good	fairly good	fairly good	probably unstable		considerably less
Adamcik No. 2	0.87-μ band not found on Mars	good	slightly lower	fairly good	fairly good	fairly good(?)	probably unstable		considerably less
Adamcik No. 3	weak 0.87-μ band not found on Mars	good	slightly higher	somewhat steeper	somewhat less	fairly good (?)	probably unstable		somewhat less
Adamcik No. 4	weak 0.87-μ band not found on Mars	good	slightly lower	somewhat steeper	somewhat less	fairly good (?)	probably unstable		slightly less

[a] "slightly," "somewhat," and "considerably" are subjectively determined gradations denoting the extent of the difference between the sample and Mars.

[b] cf. O'Connor (1967).

CHAPTER IV: CONCLUSION

Table XVIII summarizes the investigations carried out in this work and in previous works. From all the evidence presented the verdict on all eleven samples investigated must necessarily be: "Might be present in small quantities but cannot be the predominant covering for the Martian surface." This one phrase could well summarize the investigation of all materials tested to date.

The main reasons for such a conclusion are: (1) the 0.87-μ absorption band, which has been found in the near infrared spectrum of all the limonites, hematites, and goethites investigated so far, has not been found in the Martian spectrum (Younkin 1966; Tull 1966; and Sinton 1967); and (2) the very strong band of siderite at 1.05 μ appears, at most, very weak in the Martian spectrum.

On the other hand, wide-band photometric and polarimetric investigations are necessarily ambiguous. For even if the Martian surface were covered predominantly with, say, yellow ochre limonite, there are always other possibilities to satisfy the presently known polarimetric and photometric requirements. Thus, Dollfus and Focas (1966) were correct in saying that the bright areas of Mars are "similar" to a mixture of fine yellow ochre limonite (at least insofar as the photometric and polarimetric properties are concerned). That is as far as one can go in the interpretation, and I emphatically warn any investigator against stating that any form of limonite is in fact the major constituent of the Martian surface, either bright areas or dark areas, from the presently available evidence. Such a statement would be false, because: (1) the 0.87-μ band is absent in the Martian spectrum; (2) all available evidence from this work shows that one could do nearly as well--perhaps even better--in

finding another substance or mixture of substances to satisfy the known $P(\alpha,\lambda)$ and $\rho(\alpha,\lambda)$ properties of Mars; (3) if the reported limb-darkening of Mars is correct and indicative of the Martian surface, then neither goethite nor limonite can be the dominant material since both show negligible limb darkening; (4) the assumption that one substance in a certain range of particle sizes dominates the surface bespeaks a homogeneous planetary surface--this is probably an oversimplification; and (5) goethite, the major component of limonite, is probably thermodynamically unstable under conditions at the Martian surface.

So I would like to conclude by re-opening entirely the question of the composition of the Martian surface. Since the Voyager Mars-landing mission will probably not be performed until 1975 or later, we must look forward to many more years of discussion about the composition of the Martian surface. It is thus worthwhile to think of what research should be directed toward answering this question from the standpoint of remote sensing.

In my opinion, the first and foremost need is a complete, low-resolution infrared spectrum of the planet from outside the Earth's atmosphere. No polarimetry or wide-band photometry would be able to replace a spectrometer in yielding diagnostic information about the presence or absence of a substance either in the atmosphere or on the surface. It is hoped that the spectrometer aboard Mariner Mars '69, or one aboard either an earth-orbiting satellite or a balloon, will give us some valuable information.

More work needs to be done on the thermodynamic stability question. What is most interesting is the probable stability of carbonates under Martian conditions, following with the suggestion of the presence of the 1.05-μ and 3.45-μ bands in the Martian spectrum and the high abundance of

CO_2 in the atmosphere. Conversely, the extent of instability of goethite should be further investigated. Such efforts are underway now by J. T. O'Connor and D. G. Rea at the University of California, Space Sciences Laboratory.

Polarimetry and photometry should not be ignored either: The atmospheric contribution to the observed brightness of Mars must be known better to diminish the possible range in $P_s(\alpha,\lambda)$. A better feeling is also needed in assessing the aerosol composition of the Martian atmosphere. This is a difficult chore, since so many parameters are involved. There is considerable evidence that aerosols are in fact present and that they might not obey the simple Rayleigh law of scattering. Future investigations should not quickly dismiss this important problem. Better observations of $\rho(\alpha,\theta,\lambda)$ and $P(\alpha,\theta,\lambda)$, perhaps from outside our atmosphere, are desired and Mie scattering models constructed for a better understanding of the aerosols.

The observed opposition effect of Mars unfortunately encompasses many of the samples investigated, so it cannot be relied upon as a definitive tool. However, there are some substances whose opposition effects differ from the Martian opposition effect sufficiently to be wary of their predominance. This factor should be included in the future tests of any minerals or mixtures of minerals potentially considered to be abundant on the Martian surface.

The limb-darkening test might turn out to be an important one, once the extent of limb darkening of the Martian surface is well established. This is true because nearly all substances investigated showed <u>much</u> less limb darkening than Mars apparently does, especially in the case of limonite.

In spite of a potentially interesting future in remote observations of Mars, I frankly believe that even the most dominant surface constituents

will not be known until a well-equipped laboratory is landed on the planet, just as in the case of the Moon. However, every step in knowing more about the surface is significant; without efforts such as those of Lyot, Dollfus and others, we might just as well expect earth, air, fire, water, and people to compose the surface of Mars.

If I may venture a guess, I think that some carbonates along with small quantities of iron oxides might be found on Mars.

ACKNOWLEDGEMENTS

Without the efforts of certain people, this research could not have gotten far. I am particularly indebted to D. G. Rea for his attentive advice and flow of ideas throughout the work.

The observations described in Chapter II were made possible through the generosity and attention of A. A. Hoag and J. Graham of the Kitt Peak staff, who allotted me three weeks' observing time at their No. 2 36-inch telescope. I am particularly thankful to N. Sanduleak and D. J. MacConnell at the Cerro Tololo Observatory, La Serena, Chile, for making and reducing UBV observations of Mars and Spica during four crucial nights near the Martian opposition, when skies over Kitt Peak were cloudy. These Chilean observations resulted from a last-minute short-wave radio contact between A. A. Hoag, N. Sanduleak, and myself. I am also grateful to I. King for his advice on the technique and reduction of my photometric observations.

I am thankful to D. Coffeen for sending me his recent polarization data of Mars prior to publication; and to C. Capen for sending me some excellent color photographs of Mars along with a detailed description of his observations.

The apparatus described in Chapter III required a great deal of attention from many individuals. The perseverance of R. Dorr, W. Daniel, and D. G. Rea, especially during those final critical states of trouble-shooting the electronics, is very deeply appreciated. Thanks also go to R. Laurie, who did an excellent job in constructing, machining, and improving the apparatus. Some of the ideas underlying the design and performance of the experiment were generously communicated to me by K. L. Coulson, G.M.B. Bouricius, and E. L. Gray.

The mineral samples were prepared with J. T. O'Connor, who in turn performed and wrote the mineralogical and chemical analyses of Appendix I. J. A. Adamcik sent me four of his samples, the analyses of which are described (in his words) in Appendix II. Such careful sample preparations and descriptions were carried out thanks to the efforts of Drs. O'Connor and Adamcik.

I am thankful to D. Nyman and my wife, Joyce, for efficiently getting through the large tangle of clerical work.

I am finally grateful to the following individuals, with whom talks and correspondences have contributed to many of the ideas discussed in this work: W. J. Welch, A. B. Binder, D. P. Cruikshank, C. Capen, and J. Pollack.

REFERENCES

A'hearn, M. (1966, Ph.D. Thesis, Department of Astronomy, University of Wisconsin.

Barabashev, N. P. (1922), Bestimmung der Erdalbedo und des Reflexionsgesetzes für die Oberflache de Mondmeere Theorie der Rillen, Astron. Nachr., 217, 445-452.

Binder, A. B., and D. P. Cruikshank (1966), Lithological and minerological investigation of the surface of Mars, Icarus, 5, 521-525.

Cann, M. W. P., W. O. Davies, J. A. Greenspan, and T. C. Owen (1965), A review of recent determinations of the composition and surface pressure of the atmosphere of Mars, NASA Contractor Report CR-298, Illinois Institute of Technology, Research Institute, Chicago, Illinois.

Chamberlain, J. W., and D. M. Hunten (1965), Pressure and CO_2 content of the Martian atmosphere: A critical discussion, Reviews of Geophysics, 3, 299-317.

Chandrasekhar, S. (1950) Radiative Transfer, Oxford Clarendon Press.

Clarke, D. (1965), Studies in Astronomical Polarimetry III. The wavelength dependence of the polarization of light reflected by the Moon and Mars, Monthly Notices of the Royal Astron. Soc., 130, 83-94.

Coulson, K. L., G. M. B. Bouricius, and E. L. Gray (1964), Effect of surface properties on planet-reflected sunlight, Technical Information Series Report R64SD74, General Electric Co., Missile and Space Div., Space Sciences Laboratory.

Coulson, K. L., G. M. B. Bouricius, and E. L. Gray (1965), Effects of surface reflection on radiation emerging from the top of a planetary

atmosphere, Technical Information Series Report R65SD64, General Electric Co., Missile and Space Div., Space Sciences Laboratory.

Deirmendjian, D., and R. J. Clasen (1962), Light scattering on partially absorbing homogeneous spheres of finite size, U. S. Air Force Project Rand Report R-393-PR, The Rand Corp., Santa Monica, Calif.

Dollfus, A. (1955), Etude de planètes par la polarisation de leur lumière, Thesis, University of Paris; also in Ann. Astrophys. Suppl. 4 (1957), English translation in NASA Report TTF-188 (1964).

Dollfus, A. (1957), Propriétés photométriques des contrées désertiques sur la planète Mars, Comptes Rendus, 244, 162-164.

Dollfus, A. (1961), Polarization studies of the planets, in "Planets and Satellites" (G. P. Kuiper and B. M. Middlehurst, eds.), Chap. 9, Univ. of Chicago Press, Chicago, Illinois.

Dollfus, A., and J. H. Focas (1966), Polarimetric study of the planet Mars, Final Scientific Report under Contract AF-61 (052)-508, through the European Office of Aerospace Research and the U. S. Air Force Cambridge Research Laboratories.

Draper, A. L., J. A. Adamcik, and E. K. Gibson (1964), Comparison of the spectra of Mars and a goethite-hematite mixture in the 1 to 2 micron region, Icarus, 3, 63-65.

Egan, W. G. (1967), Polarimetry of a limonite surface as a function of wavelength and particle size, Grumman Research Department Memorandum RM-371J, and presented at the 48th Annual Meeting of the American Geophysical Union, Washington, D. C., April 17-20, 1967.

Egan, W. G. and K. M. Foreman (1967), A new perspective on Martian polarimetric measurements, Grumman Research Department Memorandum RM-366J, and presented at the 1967 National Technical Symposium of the American Astronautical Society, Huntsville, Alabama, June 11-14, 1967.

Evans, D. C. (1965), Ultraviolet reflectivity of Mars, Science, 149, 969-972.

Gehrels, T., and T. M. Teska (1962), Communications of the Lunar and Planetary Lab., 1, 173.

Gehrels, T., T. Coffeen, and D. Owings (1964), Wavelength dependence of polarization III. The lunar surface, Astron. J., 69, 826-852.

Gray, L. D. (1966), Transmission of the atmosphere of Mars in the region of 2 μ, Icarus, 5, 390-398.

Guthnik, P. and R. Prager (1914), Veröffentl. K. Sternev., Berlin-Babelsberg, I (Heft 1), 53.

Hapke, B. W. (1966), Comments on paper by Phillip Oetking, 'Photometric studies of diffusely reflecting surfaces with applications to the brightness of the Moon', J. Geophys. Res., 71, 2515.

Hapke, B., and H. Van Horn (1963), Photometric studies of complex surfaces, with applications to the Moon, J. Geophys. Res., 68, 4545-4570.

Hardie, R. H. (1962), Photoelectric reductions, In "Astronomical Techniques" (W. A. Hiltner, ed.) Chap. 8, Univ. of Chicago Press, Chicago, Illinois.

Harris, D. L. (1961), Photometry and colorimetry of planets and satellites, In "Planets and Satellites" (G. P. Kuiper and B. M. Middlehurst, eds.) Chap. 8, Univ. of Chicago Press, Chicago, Illinois.

Hovis, W. A., Jr. (1965), Infrared reflectivity of iron oxide minerals, Icarus, 4, 425-430.

Johnson, H. L. (1963), Photometric systems, In "Basic Astronomical Data" (K. Aa. Strand, ed.), Chap. 11, Univ. of Chicago Press, Chicago, Illinois.

Johnson, H. L. (1965), The absolute calibration of the Arizona photometry, Comm. Lunar and Planetary Lab., 3, 73-77.

Johnson, H. L., and A. J. Gardiner (1955) Publ. Astron. Soc. Pacific, 67, 74.

Kaplan, L. D., G. Munch, and H. Spinrad (1964), An Analysis of the spectrum of Mars, Astrophys. J., 139, 1-15.

Kliore, A., D. L. Cain, and G. S. Levy (1965), Occultation experiment: results of the first direct measurement of Mars' atmosphere and ionosphere, Science, 149, 1243-1248.

Kliore, A., D. L. Cain, and G. S. Levy (1966) Radio occultation measurement of the Martian atmosphere over two regions by the Mariner IV space probe, presented to the Seventh International Space Science Symposium, Committee on Space Research (COSPAR), Vienna, Austria, May 11-17, 1966.

Kohan, E. K. (1962), Investigation of the polarization properties of the surface of the Moon, In "The Moon" (Z. Kopal and Z. K. Mikhailov, eds.) Academic Press, London and New York, pp. 469-474 (I.A.U. Symposium No. 14).

Koval, I. K. (1964), Distribution of brightness in the edge zone of Mars, In "Life Sciences and Space Research" II (Florkin and Dollfus, eds.) North-Holland Publ. Co., Amsterdam, Interscience Publ., a division of John Wiley and Sons, Inc., New York, N. Y., pp. 246-249.

Kuiper, G. P. (1964), Infrared Spectra of Stars and Planets, IV: The spectrum of Mars, 1 - 2.5 microns, and the structure of its atmosphere, Comm. Lunar and Planetary Lab., 2, 79-112.

Luyten, W. J. and E. Ebbinghausen (1935), On the apsidal motion in a Virginis, Astrophys. J., 81, 305-311.

Lyot, B., (1929), Recherches sur la polarasation de la lumière des planètes et de quelques substances terrestres, Ann. Observatoire de Paris, 8, no. 1; English translation in NASA TTF-187 (1964).

Moroz, V. I. (1964), The infrared spectrum of Mars (λ 1.1 - 4.1), Soviet Astron., AJ, English Transl., 8, 273-281.

Moroz, V. I., and A. V. Kharitonov, (1957), ibid., 1, 874-890.

Muller, G. (1893), Publ. Potsdam Astrophys. Obs., 8, 326.

O'Connor, J. T. (1967), Mineral stability at the surface of Mars, submitted to J. Geophys. Res.

Oetking, P. (1966), Photometric studies of diffusely reflecting surfaces with applications to the brightness of the Moon, J. Geophys. Res., 71, 2505-2513.

O'Leary, B. T. (1967), The opposition effect of Mars, Astrophys. J., Letters to the Editor (in press: Sept. 1967 issue).

Opik, E. J. (1966), The Martian Surface, Science, 153, 255-265.

Owen, T. C. (1967), presented at the "Physics and Chemistry of Space" session, Gordon Research Conferences, Tilton, N. H., July 10-14, 1967.

Pollack, J. B. (1967), Rayleigh scattering in an optically thin atmosphere and its application to Martian topography, Icarus, 7, 42-46.

Rea, D. G. (1964), The darkening wave on Mars, Nature, 201, 1014-1015.

Rea, D. G. (1966), The atmosphere and surface of Mars--a selective review, in Proceedings of the Caltech-JPL Lunar and Planetary Conference, Pasadena, Calif., Sept. 13-18, 1965, pp. 209-238.

Rea, D. G., B. T. O'Leary, and W. M. Sinton (1965), Mars: The origin of the 3.58- and 3.69-micron minima in the infrared spectrum, Science, 147, 1286-1288.

Sagan, C., J. P. Phaneuf, and M. Ihnat (1965), Total reflection spectrophotometry and thermograviometric analysis of simulated Martian surface materials, Icarus, 4, 43-61.

Schorn, R. A. and L. D. Gray (1967), The Martian surface pressure, Astrophys. J., 148, 663-664.

Sharonov, V. V. (1961), A lithological interpretation of the photometric and colorimetric studies of Mars, Soviet Astron., -AJ, 5, 199-202.

Sinton, W. J. (1957), Spectroscopic evidence for vegetation on Mars, Astrophys. J., 126, 231-239.

Sinton, W. M. (1959), Further evidence of vegetation on Mars, Science, 130, 1234-1237.

Sinton, W. M. (1967), On the composition of Martian surface materials, Icarus, 6, 222-228.

Stebbins, J. (1914), Photometric tests of spectroscopic binaries, Astrophys. J., 39, 475-478.

Struve, O., J. Sahade, S. S. Huang, and V. Zebergs (1958), The spectroscopic binary Alpha Virginis (Spica), Astrophys. J., 128, 310-326.

Tull, R. G. (1966), The reflectivity spectrum of Mars in the near-infrared, Icarus, 5, 505-514.

Van Diggelen, J. (1965), The radiance of lunar objects near opposition, Planet. Space Sci., 13, 271-279.

de Vaucouleurs, G. (1964) Geometric and photometric parameters of the terrestrial planets, Icarus, 3, 187-235.

Wells, R. A. (1967), Ph.D. Thesis, Dept. of Astronomy, University of London.

Wildey, R. L., and H. A. Pohn (1964), Detailed photoelectric photometry of the Moon, Astron. J., 69, 619-634.

Wright, F. E., F. H. Wright, and H. Wright (1963), The lunar surface: Introduction, Chapter I in "The Moon, Meteorites, and Comets" (G. P. Kuiper and B. M. Middlehurst, eds.), Univ. of Chicago Press, Chicago, Illinois.

APPENDIX I

Petrographic Examination of the Goethite and Siderite Samples

MS-1 Goethite

Physical properties:

Acicular prisms in fibrous bundles and massive aggregates. Prisms are mostly 2 μ to 6 μ in diameter with length to diameter ratios of 2:1 to 20:1. Irregular areas largely obscured by very fine grained < .1 μ dark red, brown, and orange material probably clay minerals, hematite, and finely divided goethite. Goethite is yellow to yellowish brown in transmitted light, dark brown in reflected light if particles are greater than ca 1 μ in diameter, yellow-brown if much smaller.

Composition (Necessarily by estimation)

Goethite plus inclusions 100%. Inclusions are irregularly distributed and so small as to be impossible to count by standard petrographic techniques. They appear to be 5% to 10% of the total mass of the sample.

MS-4 Siderite

Physical Properties:

Massive cleavage rhombs veined with quartz. Growth zoning visible in reflected light; zones are apparently due to abundance of inclusions (very fine grained opaques possibly clay minerals, hematite (not red), or magnetite) zones are sharper on one side than the other. Many inclusions seem to lie at rhomb (or grain) borders. Some inclusion areas yellow brown--may be goethite. Cleavage rhombs are several cm in diameter. The mineral is grey in transmitted light with scarce brown patches of inclusion and stain.

Compositions: (Standard point count analysis, 1500 points, 1 thin section)

Siderite	93.3%
Quartz	1.9%
Inclusions	4.8%

APPENDIX II

Composition of Adamcik's Samples

Sample No. 1 is a mixture containing 99.3% U-135 with 0.65% magnetite (Fe_3O_4) added to reduce the reflectance so that it agrees approximately with the Bond albedo of Mars at about 0.8 μ. The composition of U-135 is: 75% of a mixture of: 75% of a material made by chemically depositing 16.4% goethite ($Fe_2O_3 \cdot H_2O$) on silica sieved to pass a 62 μ screen and 25% of the same material heated to change the goethite to hematite (Fe_2O_3). 25% of a mixture of: 75% of a material made by depositing 16.3% goethite on commerical kaolin and 25% of the same material heated to change goethite to hematite.

Sample No. 2 is a mixture containing 78% U-135 plus 22% powdered hornblende to reduce the reflectance to agree approximately with the Bond albedo of Mars at about 0.8 μ.

Sample No. 3 consists of 99.80% of a material prepared by depositing 2.4% goethite on -62 μ silica followed by heating to change the goethite to hematite and 0.20% magnetite.

Sample No. 4 consists of 99.78% of a material prepared by depsoiting 17.5% goethite on -62 μ silica followed by heating to change the goethite to hematite (resulting in a hematite content of 15.8%) and 0.30% magnetite.

Visible and infrared reflection spectra of Adamcik's samples are shown in Figs. 36 and 37.